ABSTRACT

GRIMES, HARTLEY RAY. The Longitudinal Shear Behavior of Carbon Fiber Grid Reinforced Concrete Toppings. (Under the direction of Dr. Rudolf Seracino.)

Precast double-tee (DT) floor systems with cast-in-place concrete toppings reinforced with welded wire fabric (WWF) often suffer from durability problems along the longitudinal joints of adjacent DTs. The high strain demand along these joints leads to cracking of the concrete topping, exposing the steel reinforcement to an aggressive environment resulting in corrosion. Carbon fiber grid (G-Grid) reinforcement is proposed as a replacement for the WWF to address this problem.

This thesis presents an experimental program designed to investigate the longitudinal shear behavior of C-Grid reinforced concrete. Twenty-two single-shear test specimens were designed to simulate the joint of adjacent DTs with topping. The objective was to obtain the fundamental shear-slip behavior and compare it to that of WWF reinforced specimens. Parameters included the reinforcement ratio and grid orientation. In addition, this thesis also looks at, through direct tension tests, C-Grid's potential to interfere with the bond between the DT and the topping. It was found that, at least in the small-scale tests, steps should be taken to prevent this premature cold joint debonding. Two methods – chairing the C-Grid, or significantly roughening the DT surface – were shown to be adequate to prevent this phenomenon.

The results of this investigation demonstrate the suitability of C-Grid as reinforcement in cast-in-place toppings. The longitudinal shear behavior observed in C-Grid and WWF reinforced concrete were similar to the point that shear-friction models, intended to be used with steel reinforcement, were able to predict and design the longitudinal shear capacity of C-Grid reinforced toppings with slight modifications. Shear-friction design models from the 6th Edition of the PCI Design Handbook, ACI 318-08, and other published models were used in this comparison.

The Longitudinal Shear Behavior of Carbon Fiber Grid Reinforced Concrete Toppings

by

Hartley Ray Grimes

A thesis submitted to the Graduate Faculty of
North Carolina State University
In partial fulfillment of the
Requirements for the Degree of
Master of Science

Civil Engineering

Raleigh, North Carolina

2009

APPROVED BY:

_____	_____
Dr. Sami Rizkalla	Dr. Emmett Sumner

_____

Dr. Rudolf Seracino
Chair of Advisory Committee

DEDICATION

To my parents, Dr. Barbara Hartley Grimes and Dr. Larry Ray Grimes.

BIOGRAPHY

The author, Hartley R. Grimes, began his collegiate career at North Carolina State University in Raleigh, NC, pursuing a B.S. degree in Civil Engineering, concentrating on structures, in August 2003. While an undergraduate, Hartley gained meaningful real world experience as a summer intern for the Nuclear Steam Supply System engineering division of AREVA NP, Inc., a multinational nuclear energy company with North American headquarters in Lynchburg, VA. He then graduated summa-cum-laude and completed the University Scholars Program in May of 2007. After graduation, Hartley then enrolled in graduate school at North Carolina State University to pursue a M.S. degree in Civil Engineering. Hartley is a registered Engineering Intern. Also, he is a member of the of the Chi Epsilon Civil Engineering Honor Society, having served as Vice-President and President of the NCSU Chapter as well as a member of the Tau Beta Pi Engineering Honor Society, having served as Secretary and Treasure of the NC-Alpha Chapter. Upon graduation, the author will be employed by the Steel Structures Division of the Thomas & Betts Corporation in Memphis, TN.

ACKNOWLEDGEMENTS

Firstly, the author wishes to express his thanks to Dr. Rudolf Seracino, his advisor, committee chair, and mentor for the last two and half years as well as the primary investigator for this research. Dr. Seracino's supervision, guidance, and wisdom made this research a fulfilling and rewarding experience for the author. In addition, the author would like to extend his gratitude to the rest of his committee, Dr. Sami Rizkalla and Dr. Emmett Sumner, for their assistance in guiding this research to its completion. The author feels very fortunate to have worked with such a knowledgeable and affable committee.

The author would like to thank the Research and Development Committee of the Precast Concrete Institute for generously providing funding for this research through the Daniel P. Jenny Fellowship. For supplying essential financial, material, and technical support the author is particularly thankful to John Carson and Andrew Broadway of Chomarat and Harry Gleich of Metromont. In addition, the author would like to extend his appreciation to Greg Blaszak of BG International for his input and direction.

The author would also like to recognize the efforts of the Constructed Facilities Lab staff, including Jerry Atkinson, William Dunleavy, and Greg Lucier who were instrumental in instructing and assisting the author with the use, setup, and procedures for the various lab equipment, machinery, and electronics used to conduct the research. In addition, the author extends his gratitude to Diana Lotito, Renee Howard, and Amy Yonai for their help with administrative matters and procedures.

Special thanks are due to graduate students Barney Frankl, Vivek Hariharan, Dillon Lunn, Adolfo Obregon-Salinas, Maggie Williams, and John Wylie for their advice and support over the course of his graduate studies.

Finally, the author would like to thank his family for their past, present, and continued support and encouragement in all matters throughout his life.

TABLE OF CONTENTS

LIST OF TABLES

LIST OF FIGURES

CHAPTER 1 INTRODUCTION

1.1 GENERAL INFORMATION

In a typical Precast/Prestressed Double Tee (Precast DT) deck system a cast-in-place concrete topping, typically 50 to 75 mm (2 to 3 in) in thickness, is often cast on site. Amongst other things, this topping makes the entire system more rigid, especially at the longitudinal joints between two Precast DT elements. This cast-in-place topping is typically reinforced with some quantity of Welded Wire Fabric (WWF), which is simply a matrix of regularly spaced longitudinal and transverse steel wire welded together. This reinforcement is responsible for crack control of the cast-in-place topping as well as aiding in the shear transfer between the precast elements.

Because many Precast DT deck systems, such as parking decks, are exposed to elements such as moisture, salt, and other corrosive chemicals the cost to prevent and repair damage from corroded steel reinforcement is significant. At the joints of the precast deck, this is even more of a concern since this is a weak point of the system with higher stress concentrations due to geometry and high strain demand. This is where the concrete topping is most likely to crack and expose its internal WWF to corrosive elements, resulting in further cracking of the topping and potentially compromising its longitudinal shear capacity. For purposes of this research, longitudinal shear refers to the horizontal shear along the joints of Precast DT elements resulting from lateral loads from such sources as wind and seismic. This is illustrated in Figure 1-1.

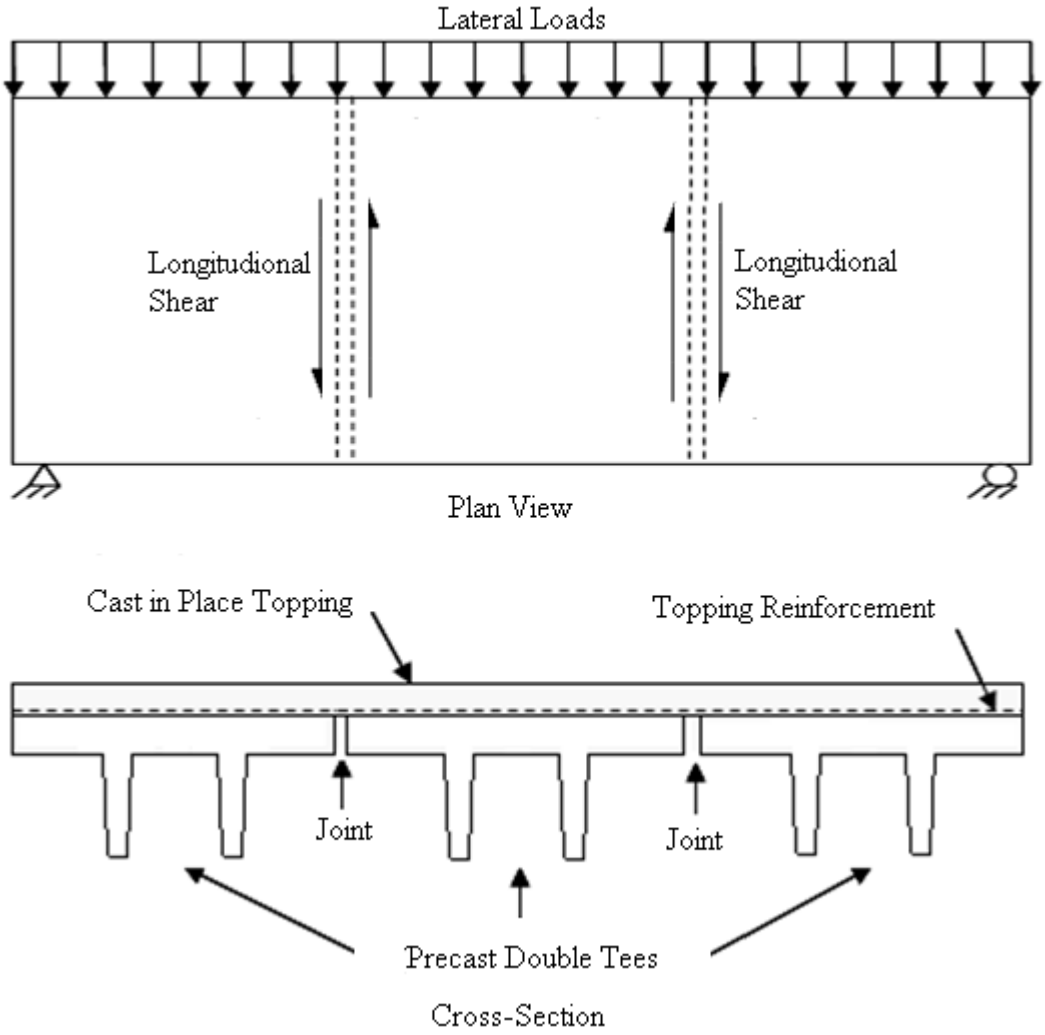

Figure 1-1 Precast DT system and longitudinal shear

As a result, in order to reduce the long-term maintenance cost of structures with Precast DT decking, a more durable reinforcing material that is not vulnerable to exposure to the elements yet behaves in a similar manner as WWF is desired. Carbon Fiber Grid is a material that potentially fulfills this desire.

1.2 OBJECTIVE

The main objective of this research was to determine if Carbon Fiber Grid is a suitable replacement of WWF as reinforcement of cast-in-place toppings of Precast DT systems. Currently, Carbon Fiber Grid is a proprietary material with the commercial name "C-Grid" which is produced by Chomarat North America headquartered in Anderson, SC and it is manufactured in France as well. C-Grid is a material composed of regularly spaced longitudinal and transverse strands of Carbon Fibers held together by an epoxy resin. See Figure 1-2 for a visual comparison of C-Grid to WWF.

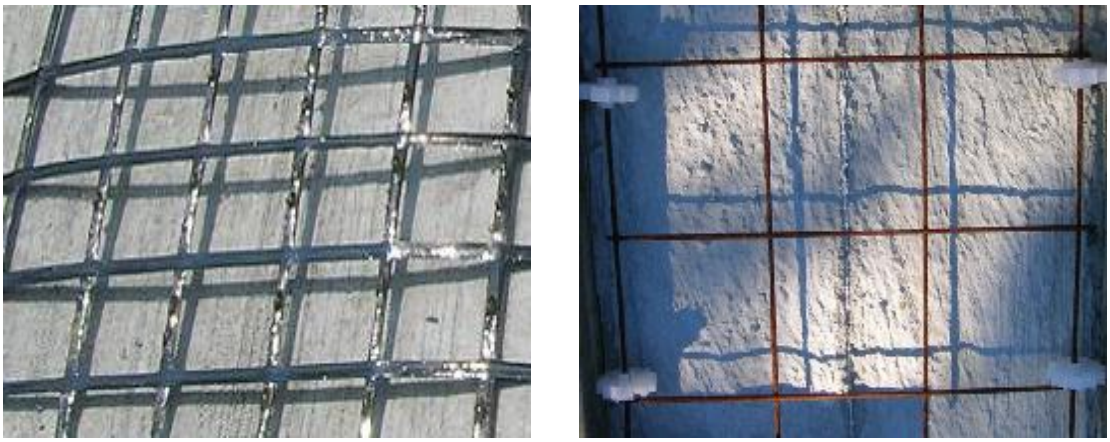

(a) C-Grid (b) WWF

Figure 1-2 Typical C-Grid and WWF

Since Carbon Fibers are not vulnerable to corrosion like WWF, C-Grid's suitability as a substitution for WWF as reinforcement in cast-in-place toppings will be determined by its performance related to four factors: the first two being issues unique to C-Grid, and the last two being comparisons of C-Grid to WWF.

The first factor is related to construction and placement issues unique to C-Grids. Since the material is lighter than WWF, it might be possible for the C-Grid, during the casting of the topping, to shift excessively (float) from its intended placement. The second factor is whether the C-Grid reinforcement, which does not bond to concrete, will interfere

with the cold joint bond formed between the top of the flange of the Precast DT and the cast-in-place topping (premature debonding). If premature debonding is an issue then solutions can be devised in order to avoid it. The third factor is if the shear-slip behavior of a C-Grid reinforced concrete topping is similar to that of a WWF reinforced concrete topping. The fourth and final factor is if the longitudinal shear capacity of the C-Grid reinforced toppings can be predicted using shear-friction models originally intended for use with steel reinforcement.

1.3 SCOPE

The next Chapter consists of a review of the relevant literature with respect to the scope of this research. The experimental program consisted of two types of tests. The first were tension tests of cored specimens from two layered slabs designed to simulate a cast-in-place topping, which were designed to test the cold joint bond between the two layers of concrete as well as to look for excessive movement of the C-Grid reinforcement during the casting process. This test and its results are presented in Chapter 3. The second type of tests were two series of single-shear specimens that were designed to further determine the effect C-Grid has on the cold joint bond and to determine and compare the shear-slip response of C-Grid to WWF reinforced toppings. These tests are presented in Chapters 4 and 5. Chapter 6 attempts to utilize various shear-friction models found in the literature to predict the shear capacity of the C-Grid and WWF reinforced single-shear specimens from the experimental program. Lastly, conclusions from this research are presented in Chapter 7.

CHAPTER 2 LITERATURE REVIEW

2.1 INTRODUCTION

This Chapter presents a review of the literature relevant to the experimental program and analytical work of this research. First, a review of Carbon Fiber Grid's (C-Grid) ability to mitigate shrinkage cracking is presented, as this is one of the reasons for adding reinforcement to cast-in-place toppings.

In addition, factors that affect the bond strength of two concrete layers are discussed. It is important to maintain the bond integrity between the cast-in-place topping and the precast deck/flange; otherwise, the structural performance will be compromised. Issues affecting bond strength include surface roughness of the existing concrete layer, which is the Precast/Prestressed Double Tee (Precast DT) within the scope of this research, and the moisture condition of said layer. Also discussed are the various methods available to test the bond strength and deciding which is best suited for the objectives and scope of this research.

Lastly, a survey of the literature is conducted reviewing various methods used to test the longitudinal shear of steel reinforced concrete as well as the development of shear-friction (or shear-transfer) models. These methods and models will be adapted to use with C-Grid reinforcement in order to compare its performance with that of Welded Wire Fabric (WWF).

2.2 SHRINKAGE CRACKING

To date, only Shao & Mirimiran (2007) studied the ability of C-Grid to control concrete shrinkage cracking. The experimental program found the C-Grids exceeded the minimum required amount of shrinkage reduction (40%) and it was found that the C-Grid slightly outperformed the WWF specimens tested for comparison. The results also show that C-Grids with a higher percentage of openness were generally more efficient at crack reduction. Openness is defined as the amount of open area in the C-Grid sheet over its total area.

Crack control is one of the main reasons why reinforcement is added to cast-in-place concrete toppings of precast systems. Shrinkage can be detrimental to a concrete topping as the precast element it is cast on is not shrinking, resulting in differential contraction producing internal stresses. The stresses can be enough to cause cracking in thin toppings or cause large deflections and stresses in the reinforcement (Stuart 2006). Based on this research, C-Grid has been shown to be a suitable material to control shrinkage cracking and therefore C-Grid's ability to resist longitudinal shear needs to be determined.

2.3 BOND STRENGTH OF TWO CONCRETE LAYERS

The scope of this research involves simulating a precast Double Tee flange deck with a cast-in-place topping. This process involves casting a fresh layer of concrete (the topping) on top of another layer of concrete that has already hardened and cured (the Precast DT flange), resulting in a cold joint bond at the interface of the two layers of concrete. The strength of this bond is critical; premature debonding of the two results in the whole system being compromised, and is to be avoided.

Therefore, it is important to examine the literature that studies the bond strength and the various properties that might affect it. Since this experimental program involves testing the bond strength of two layers of concrete (with C-Grid reinforcement), it is important to select an appropriate method of the many that exist.

2.3.1 Surface Roughness

The literature indicates that the bond strength of concrete is dependent in large part on the surface roughness of concrete. Studies done by Santos et al (2007), Júlio et al (2004), Cleland & Long (1997), and Austin et al (1995) clearly show that a rougher concrete surface results in a stronger bond between the two concrete surfaces, all other things being equal.

Since surface roughness plays such a vital role in the integrity of the bond, many methods have been devised in order to quantify the property. Work by Santos et al (2007) considers the use of a quantitative method to measure surface roughness based on a sample

of the actual concrete profile. Mathematical models are presented, such as the “average roughness”, “mean peak-to-valley height”, and “maximum peak-to-valley height”. However, as Santos points out, a method to obtain an appropriate profile of the concrete surface is required. Of the various methods used to obtain this surface profile some are destructive, such as that presented by Abu-Tair et al (2000) which involved the extracting of a core and using a line of needles placed against the concrete surface to obtain its profile. The literature appears to prefer the use of non-destructive optical type methods such as that used by Maerz et al (2001) which use laser profilimetry to produce a map of the concrete surface.

Qualitative methods include the International Concrete Repair Institute’s (ICRI, 1997) standard set of Concrete Surface Profiles (CSP). These profiles are identified by molded plastic tablets that represent a given surface roughness and range from CSP-1 to CSP-9, see Figure 2-1. The CSP values one through nine are indented to represent certain methods of surface preparations (for concrete already cured), ideally in order of increasing surface roughness, as described in Table 2-1.

Figure 2-1 CSP tablets

Table 2-1 CSP preparation methods

Concrete Surface Profile	Representative Surface Preparation Method
1	Acid Etching
2	Grinding
3	Light Shotblasting
4	Light Scarification
5	Medium Shotblast
6	Medium Scarification
7	Heavy Abrasive Blast
8	Scabbing
9	Heavy Scarification

These CSP tablets are not without faults, however. Matana et al (2005) studied the roughness of the CSP tablets using the methodology and analysis procedures of Maerz et al (2001). They found that, for CSP-1 through CSP-7, the increase in surface roughness was nearly linear, whereas CSP-8 represented more of an exponential increase. In addition, it

was found that CSP-9 represented a reduction of surface roughness (in between CSP-7 and CSP-8). Otherwise, Matana found the CSP tablets to be a reasonable measure of surface roughness, though it recommends avoiding the use of CSP-9.

Due to the time consuming nature of the quantitative methods, it was decided to use the ICRI standard Concrete Surface Profile system to measure the roughness of concrete surfaces used in the experimental program of this research. When in the field or at a precast concrete plant, it is much more convenient to use the ICRI profiles to quickly inspect and determine the concrete surface roughness versus a time consuming analytical model which requires a detailed mapping of the concrete surface. Concrete surfaces in the experimental program are finished to a surface roughness corresponding to CSP-4. If a rougher surface is required, a surface roughness corresponding to CSP-8 will be used (as opposed to CSP-9, for reasons discussed previously).

In the field there are many methods commonly used to increase the surface roughness of a pre-existing concrete surface. Júlio et al (2004) studied three methods, including sand-blasting, wire-brushing, and chipping with jackhammers with the study finding higher average bond strengths using the sand blasting method, where the chipping method was the worst performer. The literature in general recommends that chipping, especially with a jackhammer, be avoided as it damages the concrete.

Another method of surface preparation that showed good results is hydrojetting (also referred to as hydroblasting or hydrodemolition) as studied by Silfwerbrand (1990). In their pull-off tests, the specimens that had a hydrojetting surface preparation were considerably stronger than the specimens that were prepared by hammer chipping. They also found the surface roughness profile was considerably rougher using the hydrojetting method. Research by Hindo (1990) found similar results. Both of these studies believe the primary source of weakness in the hammer chipping method is the microcracking at and below the finished surface, resulting in a “bruised” layer of weakened concrete.

It would be best however if the concrete surface could be finished to the desired roughness when it is cast. Indeed, since the concrete surface roughness of concern in this research is that of the Precast DT flange, it can be easily specified and produced at the plant rather than roughened in the field after the concrete has set. In the event that the surface has to be roughened after the precast element has been produced, hydrojetting is the recommend method, followed by sandblasting; chipping should be avoided.

2.3.2 Moisture Level of the Existing Concrete Surface

Another variable that can affect the bond strength between two concrete layers is the moisture level of the (old) concrete surface before the second (new) layer is cast. Emmons (1993) states that an excessively dry surface could reduce the bond strength since it may absorb water from the new layer, resulting in shrinkage. Conversely, too much water might clog the pores of the old layer of concrete. Emmons believes the best condition is "saturated surface dry". Chorinsky (1986) had similar feelings on the subject, stating also that a dry surface might hinder the chemical reaction of the cement mortar at its most critical point, the interface between the two layers of concrete, and also that a overly wet surface could increase the water/cement ratio at said critical point.

Neither of these had any experimental data to back up these theories, therefore Austin et al (1995), experimented with four types of surface wetness ranging from air surface dry (ASD) to saturated surface wet (SSW). They found that the bond strengths of both ASD and SSW extremes were not as strong, but within the variation measured by the authors. Cleland & Long (1997) conducted similar tests with surface wetness conditions ranging from oven dry to saturated surface wet extremes. Their results were more conclusive with the extremes performing considerably worse than the moderate laboratory dry and saturated surface dry conditions, which performed equally better.

These results, combined with the fact that, according to Talbot et al (1994), pre-wetting the surface is common practice it was decided to pre-wet the surface of all concrete surfaces in this experimental program before casting. The amount of water used should be

limited to ensure no standing water was present before casting of the simulated cast-in-place topping layer.

2.3.3 Methods of Testing Bond Strength

Since part of this research program involves the testing of bond strength between two layers of concrete, it is important to select a method of testing that is both relatively straightforward and accurate. In the literature, there are many methods for testing the bond strength between two layers of concrete, which can vary depending on whether the specimens are procured from the field or produced in laboratory conditions and whether the specimens are tested on site (in-situ) or in the laboratory.

According to Hindo (1990), three common methods for testing the concrete bonding strength are the slant shear, direct tension, and direct shear tests. Specimens from all three of these types of tests require testing in a laboratory but are all procured on site (typically by coring) except for the slant shear tests. Due to the angled bonding interface, they cannot be practically obtained from the field and are typically prepared in the laboratory. A concise illustration of these methods is presented in Figure 2-2.

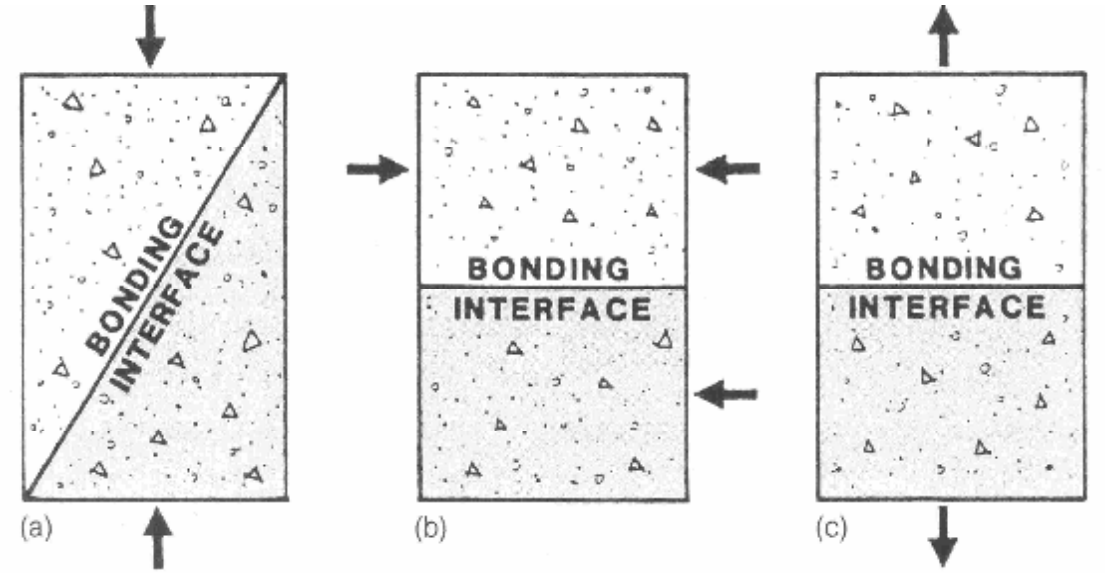

(a) Slant Shear (b) Direct Shear (c) Direct Tension

Figure 2-2 Methods for testing bond strength (Hindo 1990)

Other testing methods exist such as those discussed by Wall et al (1986) where it was found that the slant shear test is the most accurate and least variable method of testing bond strength between two concrete layers, however it should be noted that the authors were only considering methods that involve both laboratory preparation and testing. The other tests conducted were an indirect tension test and flexural type test. For similar reasons as the slant shear tests, the other tests use specimens that could not be obtained from the field.

Another means of testing the bond strength used in the literature is the pull-off test. The pull-off test is a form of the Direct Tension but modified. Instead of completely coring a specimen and testing it in the laboratory, the specimen is only partially cored; specifically it is cored completely through the topping layer and partially into the original layer. Therefore, both production and testing of the specimen are conducted in the field.

Hindo (1990) uses a proprietary testing apparatus to conduct pull-off tests and recommends its use for quality control purposes. Other papers that use the pull-off test

method are Talbot et al (1994), Austin et al (1995), Cleland & Long (1997), and Júlio et al (2004). It appears to be the most common test method in use.

With regard to the other test methods, the next most common is the slant shear test. According to Emmons (1993), this method is prone to overestimating the actual bond strength, particularly since it is a laboratory only test. Júlio (2004), which used both the slant shear and pull-off tests, found that a direct correlation between the two tests exists. The factor was determined to be 0.1855, indicating the slant shear tests resulted in bond strengths over five times that of the pull-off tests.

In this experimental program, it was decided to use the direct tension test method to determine the concrete-to-concrete bond strength, where the top layer of concrete simulates the cast-in-place topping reinforced with C-Grid and bottom layer simulates the Precast DT. One of the goals of this research, namely to determine whether C-Grid deflects from its placed position during casting of the topping, requires the entire profile of the core to be visible and undamaged. The pull-off method would destroy the core before it could be examined. Another reason for using the direct tension method is that it is easier to ensure each test is conducted in similar (laboratory) conditions.

2.4 TESTING LONGITUDIONAL SHEAR STRENGTH

Several methods can be used to test the longitudinal shear strength of – steel or otherwise – reinforced concrete. For instance, there are several types of single-shear specimens, such as those used in Hofbeck et al (1969) as well as Mattock and Hawkins (1972). As seen in Figure 2-3 they are the push-off, pull-off and modified push-off type test methods. For each of these methods, there is one plane of shear, hence the name single-shear. However, it is possible to have more than one shear plane (much like a bolt or rivet can have multiple shear planes depending on the number of plates it is fastened to). There is the possibility of using double-shear type tests as is often done in push-off tests for mechanical shear connectors, such as in Oehlers & Bradford (1995).

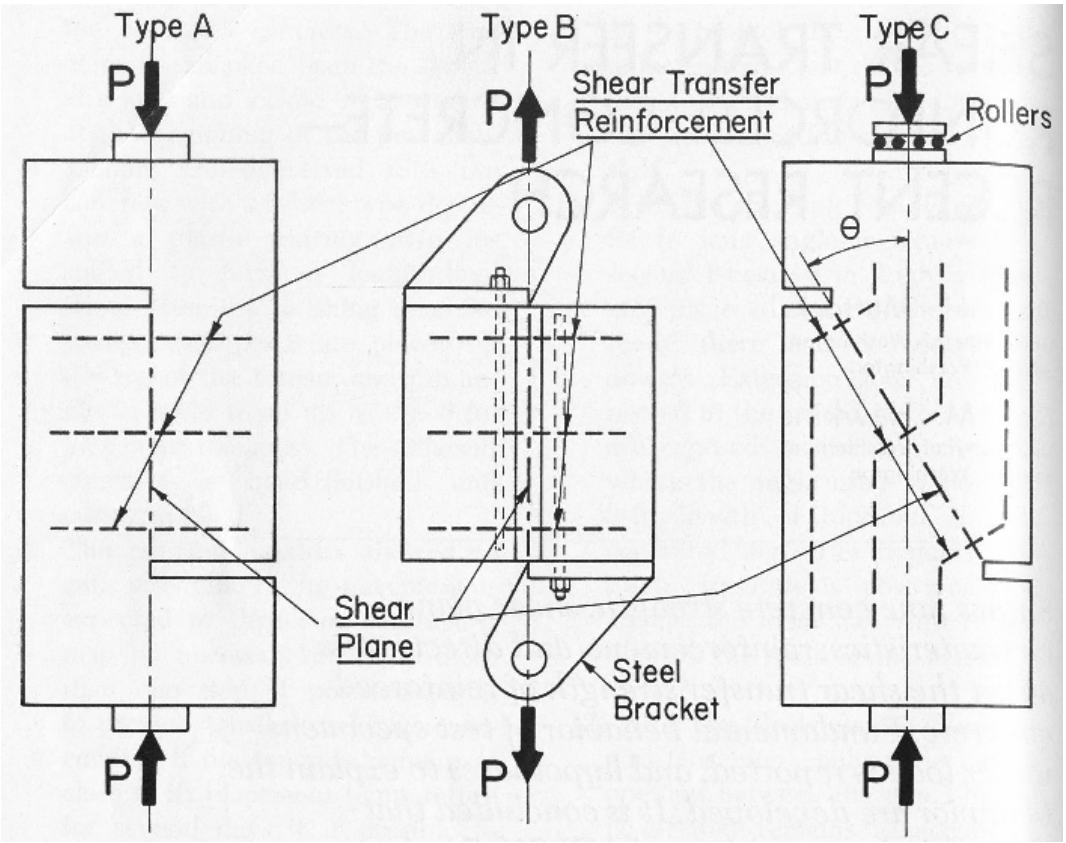

(a) push-off (b) pull-off (c) modified push-off

Figure 2-3 Single-shear test specimens diagram (Mattock & Hawkins 1972)

It is necessary, for purposes of determining the longitudinal shear behavior of C-Grid reinforced concrete, to select one of these types of test to use for the experimental program of this research. The push-off single-shear type test from Figure 2-3a was the one selected for use in this research, primarily due to its ease of construction as well as the fact that a double-shear specimen directly introduces a moment (as the applied and reaction forces form force couples). The pull-off test (Figure 2-3b) would require significantly more setup and the manufacture of specialized steel brackets as seen in the figure. The modified push-off test (Figure 2-3c) is impractical for C-Grid since it is highly unlikely that the C-Grid reinforcement could be manufactured or modified to the shape required for this type of test.

2.5 SHEAR-FRICTION MODELS

This section of the literature review will focus on models for the shear capacity of a steel reinforced concrete section. They are often referred to as shear-friction (or shear-transfer) models.

The models presented here will be later modified for the purposes of this research in Chapter 6. The motivation for reviewing these shear-friction models is to use them to predict the shear strength of C-Grid reinforced concrete, despite the fact that these were originally developed for steel reinforced concrete.

A typical shear-friction model considers a cracked concrete element (along the line of shear) in which the two concrete faces slip against one another due to the applied shear force. The amount of resistance due to friction depends on the roughness of the cracked concrete faces as well as the magnitude of the normal force acting on the concrete element. In this case, compressive normal forces will contribute to the shear-friction resistance, while tensile normal forces will reduce it. One component of this normal force is the axial strength of the transverse reinforcement. As the cracked concrete faces begin to slip, they also begin to dilate. This will induce tension in the reinforcement as it resists the crack dilation. As a result, in order to maintain equilibrium, there is a resultant compressive force normal to the cracked concrete faces. This can be thought of as a passive or internal normal force. Active or externally applied forces normal to the cracked concrete faces are another potential component of overall normal force. Although these components come from different sources (internal or external), they both affect the shear resistance through shear-friction. It should also be noted that dowel action, in which the reinforcement resists the applied shear force as it deforms along the shear plane, may also be included in the shear-friction model.

2.5.1 ACI 318-08

A shear-friction design method is presented in ACI 318 (2008) §11.7.4. The model gives the absolute shear transfer load (as opposed to a shear stress or a shear flow) that a given reinforced concrete section can resist as:

$$V_n = A_{vf}\, f_y \mu \qquad [2\text{-}1]$$

were V_n is the nominal shear strength of the section, A_{vf} is the area of shear reinforcement, f_y is the yield strength of the shear reinforcement, with a limit specified by the code of 413.7 MPa (60,000 psi), and μ is the coefficient of friction as described in Eq. [2-2] below. Although it is not directly stated in the design equation, a strength reduction factor φ of 0.65 is applied for design. The coefficient of friction is determined by the manner in which the concrete plane in shear was constructed:

$$\mu = \begin{cases} 1.4\lambda & \text{Concrete placed monolithically} \\ 1.0\lambda & \text{Concrete placed against hardened concrete with surface intentionally roughened.} \\ 0.6\lambda & \text{Concrete placed against hardened concrete not intentionally roughened.} \\ 0.7\lambda & \text{Concrete anchored to structural steel by headed studs or reinforcing bars} \end{cases} \qquad [2\text{-}2]$$

where λ is a correction factor related to the unit weight of concrete, which is taken as 1.0 for normalweight concrete.

In addition, the ACI 318 code specifies two upper limits to the shear strength, which are:

$$V_n \le 0.2\, f_c' A_c$$
$$V_n \le 800 A_c \qquad [2\text{-}3]$$

where A_c is the area of the concrete section resisting shear transfer. The code commentary states the reason for this limit is that Eq. [2-1] becomes un-conservative at higher values.

It is interesting to note that, with the exception of one of the upper limits in Eq. [2-3], this method does not account for the strength of the concrete in calculating the shear capacity. Since this is presented as a design equation for a code of practice it is reasonable to assume the model considers a cracked concrete plane and is likely to be quite conservative given the brittle nature of shear failures.

Although the primary design equation is dimensionally correct, the limit states are not, so it is important to either only use the prescribed units of inches and pounds or otherwise alter the equations for SI metric units.

2.5.2 6th Edition of the PCI Design Handbook

Another shear-friction model is presented in the sixth edition of the Precast/Prestress Design Handbook PCI (2004) §4.3.6. Like the previous model in Section 2.5.1 this model does not account for the strength of the concrete in its determination of shear force being transferred. In addition, the model is not dimensionally correct and requires modification in order to use units other than inches and pounds. Lastly the model equation is setup to give a minimum area of shear reinforcement for a given ultimate shear force with appropriate safety factors, as opposed to solving for a resistance with a known or assumed amount of reinforcement. The equation is:

$$A_{vf} = \frac{V_u}{\phi f_y \mu_e}$$
$$\mu_e = \frac{1000 \lambda A_{cr} \mu}{V_u} \qquad [2\text{-}4]$$

where φ is the strength reduction factor, A_{vf} is the area of reinforcement, f_y is the yield strength of the reinforcement with a limit of 413.7 MPa (60,000 psi), V_u is the applied factored shear force, μ and μ_e are shear-friction coefficients, and A_{cr} is the area of the crack interface.

The PCI model further defines the shear-friction coefficients based on the method of concrete placement at the point of shear transfer. The coefficient μ is defined as:

$$\mu = \begin{Bmatrix} 1.4\lambda & \text{Monolithically cast concrete} \\ 1.0\lambda & \text{Concrete to hardened concrete with roughened surface} \\ 0.6\lambda & \text{Concrete to concrete} \\ 0.7\lambda & \text{Concrete to steel} \end{Bmatrix} \qquad [2\text{-}5]$$

where λ is a factor for use with lightweight concrete (i.e. $\lambda = 1.0$ for normalweight concrete). The coefficient μ_e is given an upper bound limit based on the crack interface condition:

$$\mu_e = \begin{Bmatrix} \leq 3.4 & \text{Monolithically cast concrete} \\ \leq 2.9 & \text{Concrete to hardened concrete with roughened surface} \\ \leq 2.2 & \text{Concrete to concrete} \\ \leq 2.4 & \text{Concrete to steel} \end{Bmatrix} \quad [2\text{-}6]$$

In the PCI model, no upper bound limit for the shear force is given.

2.5.3 Mattock et al

Another model which has been introduced and developed in the literature is a model first seen in Mattock & Hawkins (1972), which was based off of research done by Hofbeck et al (1969); and further studied by Mattock et al (1975).

Hofbeck et al (1969) used push off specimens (see Figure 2-3 for an illustration) to test the shear transfer along a plane of concrete. Though no design model was presented, the authors observed three things. First, they felt that concrete strength did not play a significant role in the overall shear transfer strength. Secondly, they found that an increase in the amount of reinforcement resulted in a proportional increase in shear strength except (and this is their third finding) up to a certain point. Therefore, they proposed an upper bound limit that is governed by the concrete strength.

These conclusions were reached again in Mattock & Hawkins (1972) which sought to model the shear transfer of concrete using a variety of single-shear type push off and pull-off specimens, as illustrated in Figure 2-3 from the paper. Many of the specimens and graphs published in this article originated from Hofbeck et al (1969).

Based off these results, an equation was developed to model the shear transfer across a crack in monolithic concrete:

$$v_u = 200\,psi + 0.8(pf_y + \sigma_{Nx}) \quad [2\text{-}7]$$

where v_u is the ultimate shear transfer strength, pf_y is the reinforcement parameter (p is the reinforcement ratio and f_y is the reinforcement yield strength), and σ_{Nx} is the externally

applied direct stress perpendicular to the shear plane. The value of 200 psi is the contribution to shear resistance that the (cracked) concrete plane along the shear plane will provide (presumably through friction and aggregate interlock).

Along with this there is an upper bound imposed on this model that is:

$$v_u \leq 0.3 f_c^{'} \qquad [2\text{-}8]$$

where f_c' is the compressive strength of the concrete.

Also, a restriction on the sum of the reinforcement strength parameter pf_y and externally applied force parameter σ_{Nx} is imposed:

$$pf_y + \sigma_{Nx} \geq 200\,psi \qquad [2\text{-}9]$$

This is justified by the understanding that an insufficient amount of force being applied normal to the plane of shear transfer will result in a lower than expected contribution to the shear resistance by the friction of the concrete, which itself is set as a fixed 200 psi in Eq. [2-7].

The authors compare the developed equation to the ACI code equation (such as it was at the time their work was published) as well as to other experimental work. They showed their model to be more accurate and allowed for higher, yet still conservative shear strength values then the ACI code model. The graph in Figure 2-4 is a comparison of the calculated versus experimental shear transfer strengths. As can be seen, the model appears to be accurate, yet conservative for all data points.

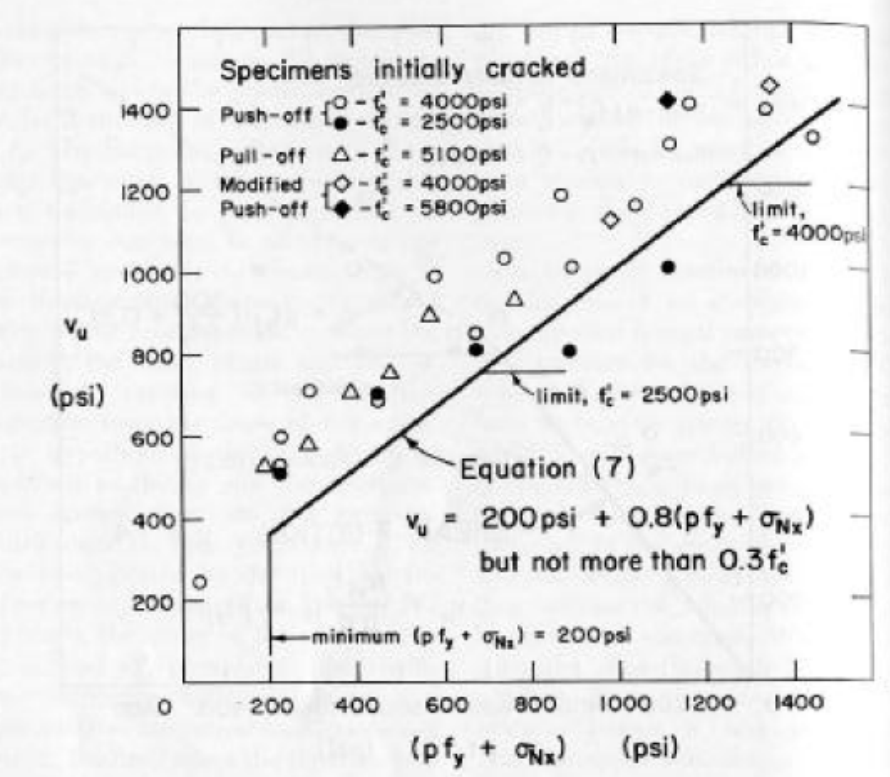

Figure 2-4 Comparison of shear-transfer strength (Mattock & Hawkins 1972)

Like other models within this Section, this one does not directly consider the effect of the concrete strength. Recall that Hofbeck et al (1969) made this conclusion as well. The reasoning provided is that the authors did not believe a significant difference existed between two identical specimens except for differing concrete strengths up to a certain point. The paper presents a plot to illustrate this; it is reproduced in Figure 2-5.

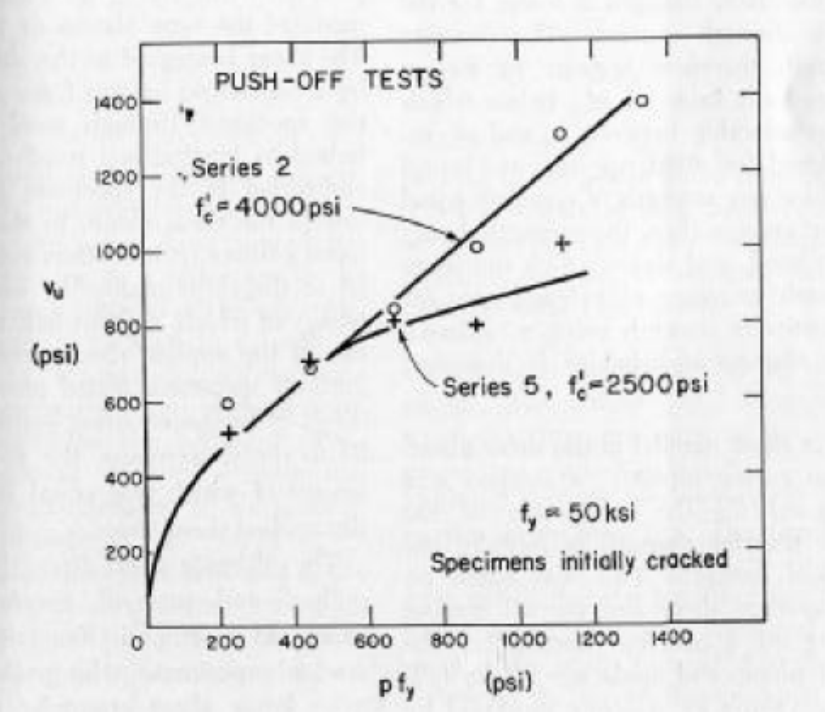

Figure 2-5 Effect of concrete strength on shear-transfer (Mattock & Hawkins 1972)

The authors explain that, beyond v_u of 700-800 psi, the strength of the concrete (or lack thereof) causes the relationship between v_u and pf_y to break down. This is why the authors proposed an upper limit to v_u of $0.3f_c'$ (see Eq. [2-8]), which in the case of the fifth series (in Figure 2-5), is 750 psi, about where the two series begin to deviate. Below this upper bound cut-off, the behavior between the two series of specimens is the same, despite different concrete strengths. So in effect, the authors are saying that the shear transfer strength becomes dependent on the concrete strength after a certain point.

Also, consider that a design equation should always consider a cracked concrete interface – as the authors noted – since any number of things not related to the applied load can cause the section to crack, such as shrinkage or handling.

Combining these two points is why the authors do not use concrete strength in their shear transfer strength model. Future work however edits their model to include concrete strength.

This model is used again by Mattock et al (1975) to predict the behavior of initially cracked concrete both with and without the direct shear stress term σ_{Nx}. In this paper, the experimental specimens were corbels (as seen in Figure 2-6) and push off specimens as seen in Figure 2-3a.

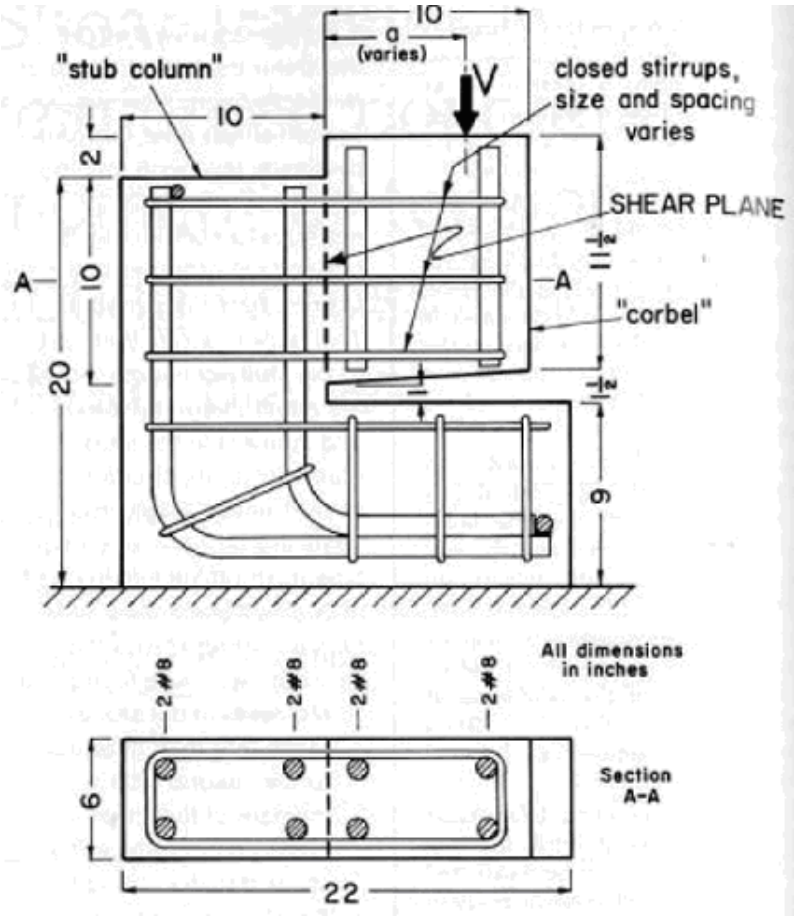

Figure 2-6 Corbel type push off specimen (Mattock et al 1975)

However, the paper used a different equation; the reason for this seems to be modifying the model to calculate the mean strength, as opposed to producing a conservative (characteristic) design equation. The modified equation is:

$$v_u = 400\,psi + 0.8(pf_y + \sigma_{Nx}) \qquad [2\text{-}10]$$

This can be seen by the graph of this altered model versus the experimental data in Figure 2-7. One can see the plotted curve of the altered model goes roughly down the center of the experimental scatter, as opposed to a design model which would be expected to be a lower bound of the scatter in order to be conservative. This demonstrates that the equation can be modified relatively easily to suit different purposes; which is done in future work by Oehlers & Bradford (1995, 1999).

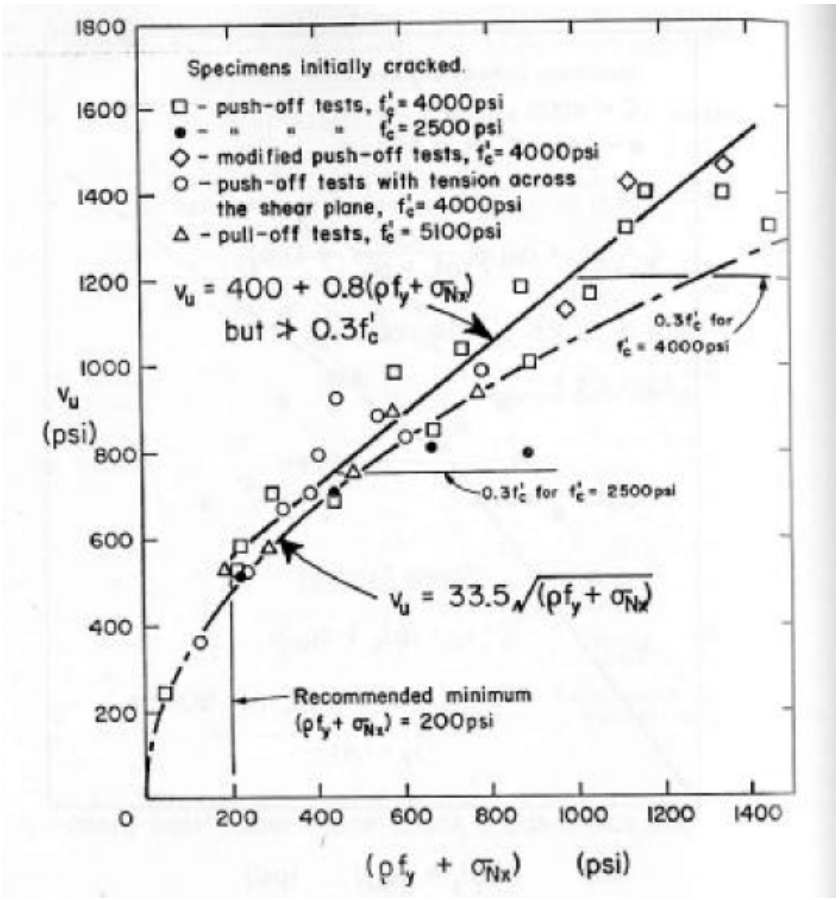

Figure 2-7 Altered model (Mattock et al 1975)

2.5.4 Oehlers & Bradford

This shear-transfer model across concrete is further studied and modified in two separate books by Oehlers & Bradford (1995 and 1999) which refers to the work from Section 2.5.3 as the Mattock Model. The first book (1995) introduces different nomenclature to the Mattock model from Mattock & Hawkins (1972) and adapts it to SI metric units of N and mm. The adapted equation takes the form:

$$\begin{aligned} (v_u)_{ch} &= v_{lock} + v_{dow} + v_{fric} \\ v_{lock} &= 1.4 \text{ MPa} \\ v_{dow} &= 0.8 pf_{yr} \\ v_{fric} &= 0.8\sigma_{nf} \end{aligned} \qquad [2\text{-}11]$$

where v_{lock} is the strength attributed to interface interlock, v_{dow} is the dowel resistance, v_{fric} is the active frictional resistance, and $(v_u)_{ch}$ is the characteristic (design) shear strength of a cracked shear plane, σ_{nf} is the stress normal to the shear plane, and pf_{yr} is the yield stress of the reinforcing material per unit area of the shear plane.

The book proceeds to make several modifications and additions to the Mattock model. The first is the modification of the v_{lock} term to – instead of being a constant value of 1.4 MPa (200 psi) –a function of the tensile strength f_{ct}.

This is reasonable considering how much the understanding of aggregate interlock has progressed from the time of the original publishing of the Mattock model (1972) to the writing of Oehlers & Bradford (1995). Recall that Hofbeck et al (1969) and Mattock & Hawkins (1972) observed that concrete strength became a factor at a certain shear strength value; therefore, it would be reasonable to allow the concrete strength to be a factor for any shear strength value. The book considers the tensile strength of the concrete to be the primary contributor to aggregate interlock forces. Therefore, the term for v_{lock} becomes:

$$v_{lock} = 0.66 f_{ct} \qquad [2\text{-}12]$$

where the factor of 0.66 is a normalization of the concrete strengths used to develop the Mattock model in the original paper. Considering the Mattock model originally used 200 psi

(1.4 MPa) for v_{lock} and a concrete strength of predominately 4000 psi (27.6MPa). Substituting 27.6 MPa for f_c' in Eq [2-12] results in a v_{lock} of 1.4MPa. This factor of 0.66, which was not given a name by Oehlers & Bradford, is defined for convenience as the concrete/statistical coefficient Γ for the purposes of this literature review and research.

Oehlers & Bradford (1995) further developed the original Mattock model by deriving different values of Γ for different scenarios and statistical considerations. For instance, in Mattock et al (1975) as discussed in the previous Section, the Mattock model can be easily changed to predict the mean (average) values as opposed to calculating lower bound characteristic (design) values. Oehlers & Bradford (1995) adequately changed the Mattock model from a characteristic (design) to a mean model by using a value of 1.1 for Γ.

In addition to that, the strength of an uncracked concrete shear plane (note all previous values were under the assumption of a cracked concrete shear plane) can be arrived at by using a Γ of 1.6. Therefore, the model can be used in many applications for both predicting actual (mean) strength or as a conservative design model (characteristic) for cracked and uncracked situations as given in Table 2-2. Note that there is no Γ value for the characteristic uncracked condition. This is because it would be imprudent to design with the assumption that the shear resisting concrete section will remain uncracked for its service life, an inherently un-conservative assumption.

Table 2-2 Adaptation of the Mattock model to different circumstances

Concrete Condition	Mean	Characteristic
Initially Cracked	Γ = 1.1	Γ= 0.66
Initially Uncracked	Γ = 1.6	N/A

Recall that the original Mattock model specified a lower bound limit to the sum of the reinforcement strength parameter (now called v_{dow}) and externally applied force parameter (now called v_{fric}) from Eq. [2-9]. Oehlers & Bradford not only rewrote this lower bound limit

as given by the following expression but indirectly describe what happens when the lower bound, which is given in Eq. [2-13], is not met.

$$pf_{yr} + \sigma_{nf} \geq 0.66 f_{ct} \qquad [2\text{-}13]$$

Below this lower bound, Oehlers & Bradford show the shear strength decreasing in a parabolic manner to zero when pf_{yr} is zero. The graph is reproduced in Figure 2-8 and the region in question is the dashed-line parabola 0B. Note a similar parabolic curve from Mattock et al (1975) in Figure 2-7. The point of the lower bound limit is point B where the parabola and the linear portion BC intersect. Note that as the parabola 0B approaches point B, the slope approaches that of the slope of the line BC.

Again, the reasoning for this limit is that a certain minimum dowel force plus external applied forces is required in order to completely develop the concrete interlock force (v_{lock}). When this limit is not met, v_{lock} cannot be completely developed; therefore, it decreases in a parabolic manner to the point where v_{lock} is zero if v_{dow} plus v_{fric} is zero. This would make sense from a theoretical standpoint, as it would be impossible for a cracked concrete section to resist any shear via shear-friction without any sort of clamping action from internal reinforcement or applied external normal forces. Although equations for the parabolic portion of the curve are not defined in any of this literature, it is possible to derive the equations since sufficient boundary conditions are known (see Section 6.2.3).

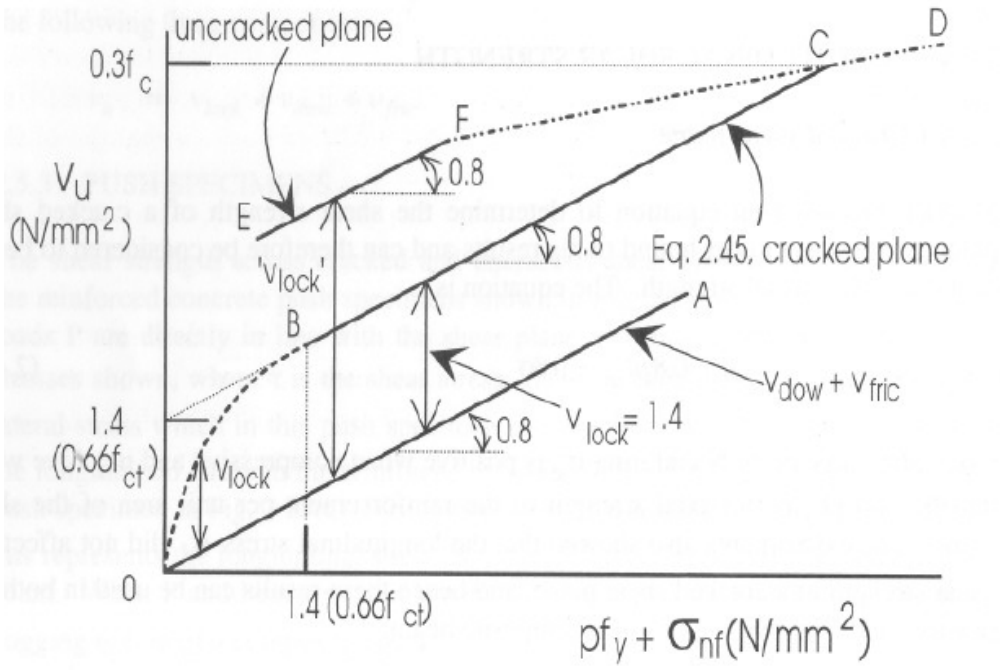

Figure 2-8 Modified Mattock model (Oehlers & Bradford 1995)

Oehlers & Bradford (1999) is a continuation of their previous work that presents one more modification to the Mattock Model. That is simply transforming the equation to a per unit length basis. The model is now written in terms of shear flow given by:

$$Q_{ch} = 0.66 f_{ct} L_p + 0.8 A_{tr} f_{yr} + 0.8 F_{nf} \qquad [2\text{-}14]$$

where Q_{ch} is the shear flow strength, f_{ct} is the tensile strength of the concrete, L_p is the depth of the shear plane, A_{tr} is the area of transverse reinforcement per unit length, f_{yr} is the yield strength of the transverse reinforcement, and F_{nf} is the normal force per unit length. A specific definition for f_{ct}, using units of N and mm, is given as:

$$f_{ct} = 0.4\sqrt{f_c'} \qquad [2\text{-}15]$$

The upper limit is rewritten as:

$$Q_{ch} \le 0.3 f_c' L_p \qquad [2\text{-}16]$$

and the lower bound limit is rewritten as:

$$0.8(A_{tr} f_{yr} + F_{nf}) \geq 0.53 f_{ct} L_p \qquad [2\text{-}17]$$

Equation [2-17] can be simplified and written as:

$$A_{tr} f_{yr} + F_{nf} \geq 0.66 f_{ct} L_p \qquad [2\text{-}18]$$

Finally, Eq. [2-14] can be rewritten to include the modifications of Oehlers & Bradford (1995), mainly the introduction of the concrete/statistical coefficient Γ as introduced in Table 2-2:

$$Q_{ch} = \Gamma f_{ct} L_p + 0.8 A_{tr} f_{yr} + 0.8 F_{nf}$$

where:

$$\Gamma = \left\{ \begin{array}{ll} 0.66 & \text{characteristic strength of cracked concrete} \\ 1.1 & \text{mean strength of cracked concrete,} \\ 1.6 & \text{mean strength of uncracked concrete} \end{array} \right\} \qquad [2\text{-}19]$$

Equations [2-16] through [2-19] are the ultimate result of all the works from this Section and the previous. Unlike the other models studied in Section 2.5, this model does consider the strength of the concrete and has provisions for considering more than just the design (characteristic) condition.

CHAPTER 3 EFFECT OF C-GRID ON THE COLD JOINT BOND

3.1 INTRODUCTION

In this Chapter, two objectives are addressed regarding the feasibility of the use of Carbon Fiber Grid (C-Grid) instead of Welded Wire Fabric (WWF) as reinforcement in cast-in-place topping slabs of Precast/Prestressed Double Tee (Precast DT) systems. The first is to determine the amount, if any, that C-Grid may deflect vertically during casting of the topping on top of the Precast DT. This effect will be referred to as "floating". This is of concern because C-Grid is a very light material, approximately 10% the density of steel. It is also flexible and not likely to be restrained against upward or downward deflection. If the C-Grid floats too much from its expected position, then calculations (such as flexural analysis) which assume the C-Grid is at its original placed location will obviously be inaccurate.

The second objective is to determine the amount, if any, that the location of the C-Grid during casting of the topping compromises the cold joint bond (interface) between the two layers of concrete cast at different times. This is of concern since the quality of the bond affects the integrity of the structural floor system and the ability of it to provide adequate diaphragm action. In that case, there might be a concrete cover requirement for sufficient concrete to concrete (cold joint) bond.

These objectives are achieved primarily by cored direct tension tests, which are utilized to test the bond strength of the cold joint bond for reasons discussed in Section 2.3.3. The use of cored cylinders from a C-Grid reinforced slab allows its profile to be observed visually to inspect for floating of the C-Grid reinforcement.

3.2 MATERIALS AND METHODS

3.2.1 Casting of Slabs

Two 1.22 m by 2.44 m (4 ft by 8 ft) concrete slabs (named "Slab 1" and "Slab 2") were cast in two separate layers. The bottom layer simulates the flange of Precast DTs, with

a typical specified concrete strength of f_c' = 34.5 MPa (5000 psi) and thickness t = 90 mm (2.75 in). The bottom layer was given a surface roughness finish of CSP-4 (as discussed in Section 2.3.1. The top layer simulates the cast-in-place topping, with a typical specified concrete strength of f_c'= 20.7 MPa (3000 psi) and thickness t = 70 mm (2.75 in). The top layer was cast four weeks after the first. Before the top layer was cast, the surface of the bottom layer was wetted to a degree such that there was no standing water on the surface before casting. Given the hot temperatures in which the top layer was cast – approximately 32-35 ºC (90-95 ºF) – this pre-wetting was deemed important, as discussed in Section 2.3.2.

Before casting of the top layer, several sizes of C-Grid (see Table 3-1 and Figure 3-1) were placed on top of the bottom layer using various chairing or restraining methods as shown in Figure 3-2 and Figure 3-3. The C-Grids were placed in intervals along the slab to allow for thirteen different variations including two controls of plain concrete topping (no C-Grid reinforcement). A schematic of the two slabs, Slab 1 and Slab 2, is shown in Figure 3-4 and Figure 3-5 shows the actual slabs with the bottom layer of concrete cast and the C-Grid reinforcement in place, awaiting the top layer of concrete.

The four sizes of C-Grid, in order of increasing strand spacing and hence lower reinforcement ratios, are C50 1.6x1.8, C50 2.2x2.2, C50 2.9x2.9, and C50 3.5x4.0 (as the strength properties of the C-Grid are not critical here, they are given in Chapter 4). These C-Grids are representative of those used in current applications. For comparative purposes, C-Grids with relatively lower or higher strand spacing (and hence higher or lower reinforcement ratios) are referred to as being more or less dense, respectively.

The five methods of restraining C-Grid used in this experiment and are representative of various ways that the C-Grid could be economically placed in the field. The first method is simply laying the C-Grids flat on the surface of the bottom layer of concrete without any restraint ("no restraint" or NR). The second is to hot glue the C-Grid to the concrete surface at regular intervals ("hot glue" or HG). The third and fourth methods involve attaching (by hot glue) pieces of a rubber material, which would (assuming no floating) lift the C-Grid by

10 mm (0.4 in). Two different shapes were used, Figure 3-3 illustrates the different shapes, which for convenience are referred to as flat cylindrical rubber chairs ("flat chair" or "FC") and roller shaped rubber chairs (roller chair or "RC"). The fifth method simply used a ferris-wheel shaped plastic chair ("wheel chair or "WC") normally used to chair steel WWF by 25 mm (1 in).

Laying the C-Grids flat with no restraint would be the quickest and cheapest way of placing the C-Grid; however, this is also likely to be more susceptible to floating. Chairing options are being considered because the C-Grid will be offset from the interface of the two concrete layers, likely reducing the affect on the bonded interface. However, the chaired C-Grid may "float" both up or down from its initial position during casting.

Table 3-1 C-Grid dimensional properties

C-Grid Designation	Longitudinal Spacing† mm (in)	Transverse Spacing† mm (in)
C50 - 40x44 (C50 - 1.6x1.8)	40.64 (1.6)	45.72 (1.8)
C50 - 56x56 (C50 - 2.2x2.2)	55.88 (2.2)	55.88 (2.2)
C50 - 72x72 (C50 - 2.9x2.9)	73.66 (2.9)	73.66 (2.9)
C50 - 89x102 (C50 - 3.5x4.0)	88.90 (3.5)	101.6 (4.0)

†center-to-center

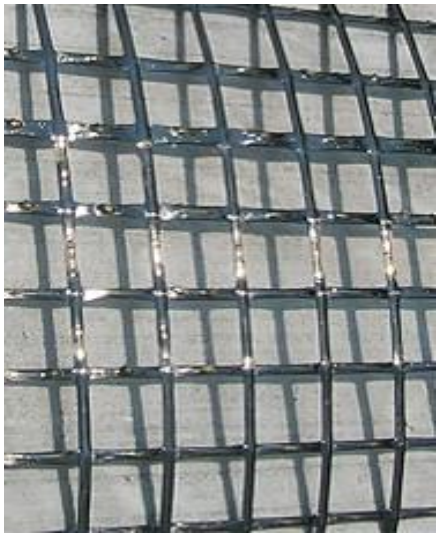

(a) C50 1.6 x 1.8

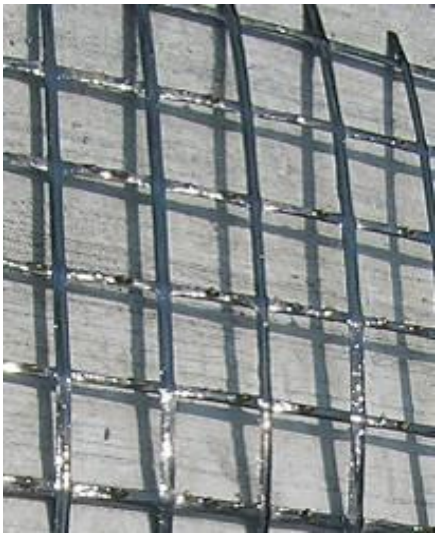

(b) C50 2.2 x 2.2

(c) C50 2.9 x 2.9

(d) C50 3.5 x 4.0

Figure 3-1 C-Grid sizes

(a) “NR” No Restraint, C-Grid laid flat

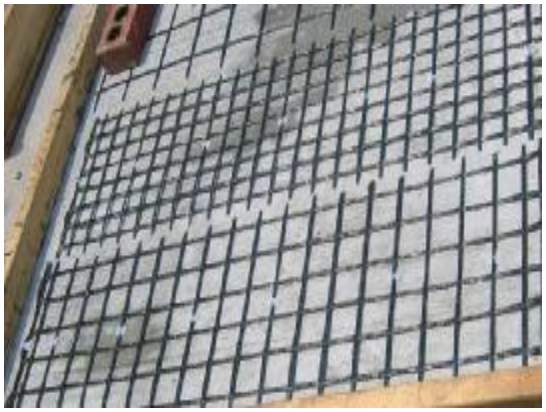

(b) “HG” C-Grid secured by Hot Glue

(c) “FC” Flat cylindrical rubber Chairs

(d) “RC” Roller shaped rubber Chairs

(e) “WC” – plastic Wheel Chairs (WWF)

Figure 3-2 Restraining methods

(a) “FC” type

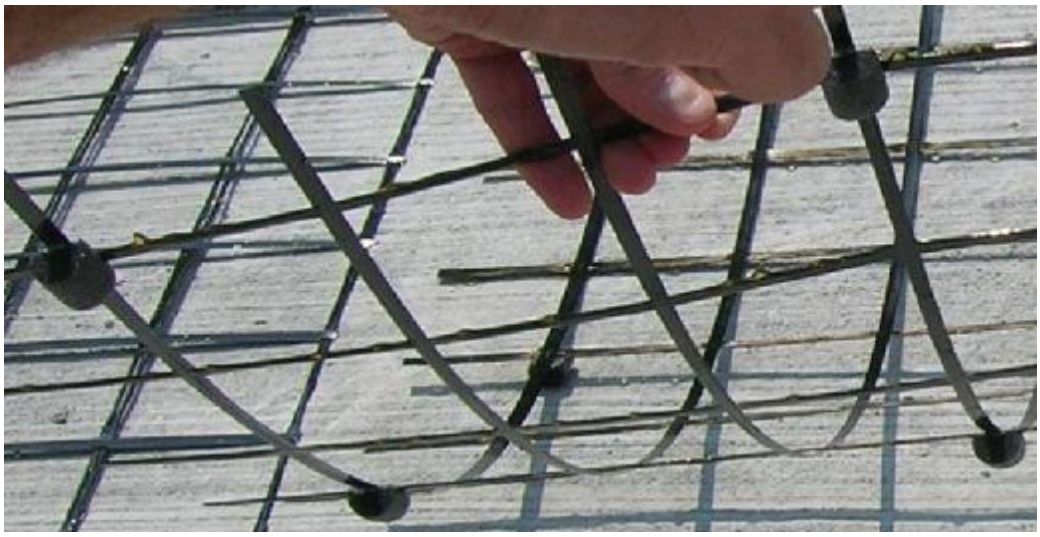

(b) “RC” type

Figure 3-3 Close-up of FC and RC chairs

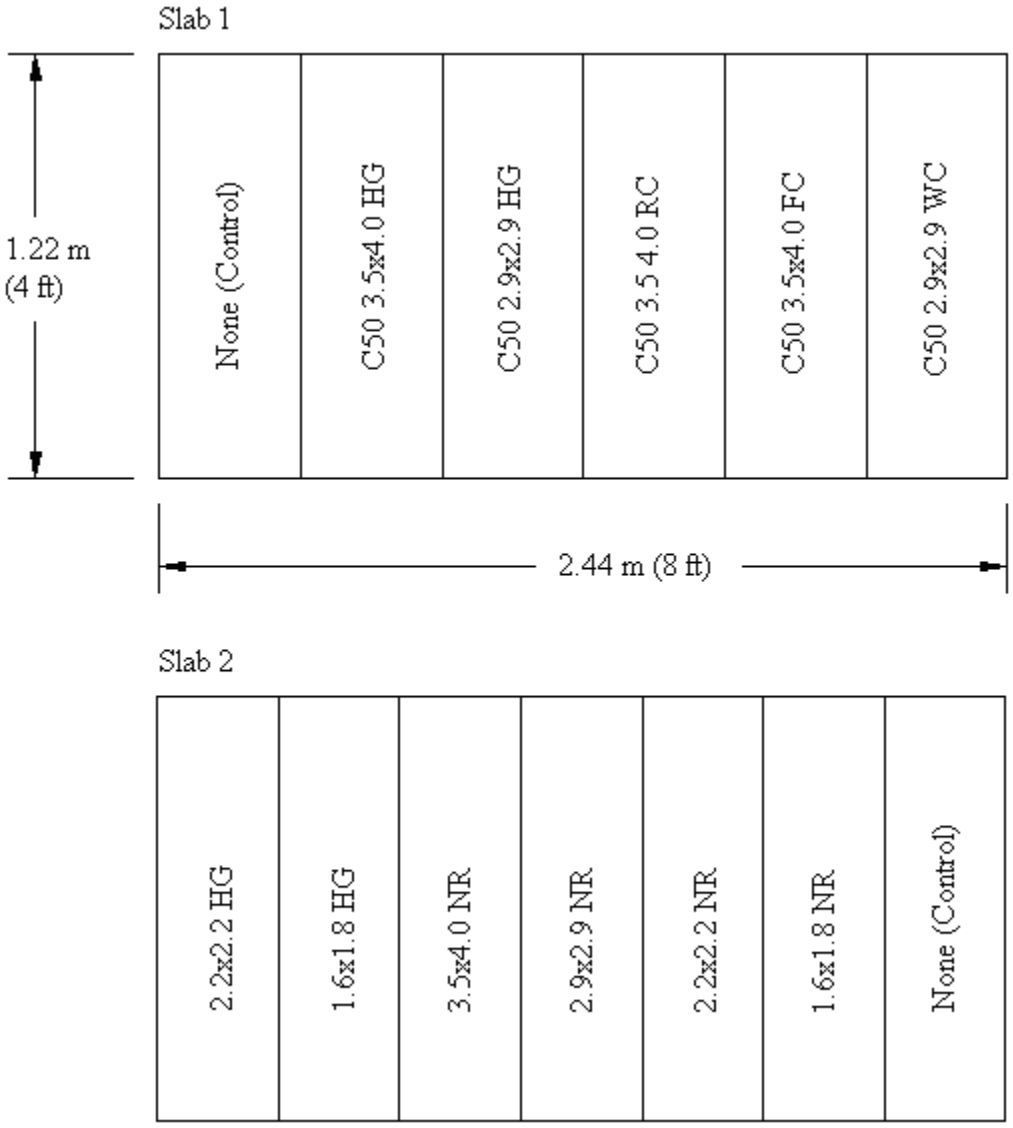

Figure 3-4 Schematic of slabs

(a) Slab 1

(b) Slab 2

Figure 3-5 Slabs prior to casting of top layer

3.2.2 Coring of Specimens

After casting the top layer of concrete, the slabs were cured for approximately a month. Three 152.4 mm (6 in) diameter cores from each of the thirteen sections were cut. The cores were cut in locations such that the entire core contained only one type of C-Grid. This resulted in thirty-nine specimens in total (A1-A39). Figure 3-6 demonstrates the coring process. This process first required the cores to be individually marked. In order to obtain a good sample, a core was cut at approximately mid-length of the slab and the other two cores cut from each end. The most important reason to mark the core was to ensure the entire core contained the correct C-Grid type. The cores were then cut with a coring machine all on the same day. The cored specimen schedule is shown in Table 3-2.

(a) Core locations marked and numbered

(b) Specimens being cored

Figure 3-6 Marking and coring of slabs

Table 3-2 Schedule of cores

Specimen No.	C-Grid	Restraint
A1	C50 2.9x2.9	WC
A2	C50 2.9x2.9	WC
A3	C50 2.9x2.9	WC
A4	C50 3.5x4.0	FC
A5	C50 3.5x4.0	FC
A6	C50 3.5x4.0	FC
A7	C50 3.5x4.0	RC
A8	C50 3.5x4.0	RC
A9	C50 3.5x4.0	RC
A10	C50 2.9x2.9	HG
A11	C50 2.9x2.9	HG
A12	C50 2.9x2.9	HG
A13	C50 3.5x4.0	HG
A14	C50 3.5x4.0	HG
A15	C50 3.5x4.0	HG
A16†	None	N/A
A17†	None	N/A
A18†	None	N/A
A19†	None	N/A
A20†	None	N/A
A21†	None	N/A

Specimen No.	C-Grid	Restraint
A22	C50 1.6x1.8	NR
A23	C50 1.6x1.8	NR
A24	C50 1.6x1.8	NR
A25	C50 2.2x2.2	NR
A26	C50 2.2x2.2	NR
A27	C50 2.2x2.2	NR
A28	C50 2.9x2.9	NR
A29	C50 2.9x2.9	NR
A30	C50 2.9x2.9	NR
A31	C50 3.5x4.0	NR
A32	C50 3.5x4.0	NR
A33	C50 3.5x4.0	NR
A34	C50 1.6x1.8	HG
A35	C50 1.6x1.8	HG
A36	C50 1.6x1.8	HG
A37	C50 2.2x2.2	HG
A38	C50 2.2x2.2	HG
A39	C50 2.2x2.2	HG

†Control Specimens with no C-Grid reinforcement.

3.2.3 Experimental Procedure

Around the circumference of the cored cylinder it is possible to identify and measure the level of both the cold joint (interface) plane between the two concrete layers (which appears as a line between two different textures of concrete) and the plane of the C-Grid strands (which appear in cross-section) in the top layer. Therefore, the edge-to-edge distance between the C-Grid and the cold joint was measured at four equally spaced points along the circumference of each cylinder (see Figure 3-7). For each cylinder, the four values are averaged and this value is termed the "final location". The float (vertical displacement as a result of the casting process) is quantified by comparing the final location with the "initial location", which depends on the restraining method used.

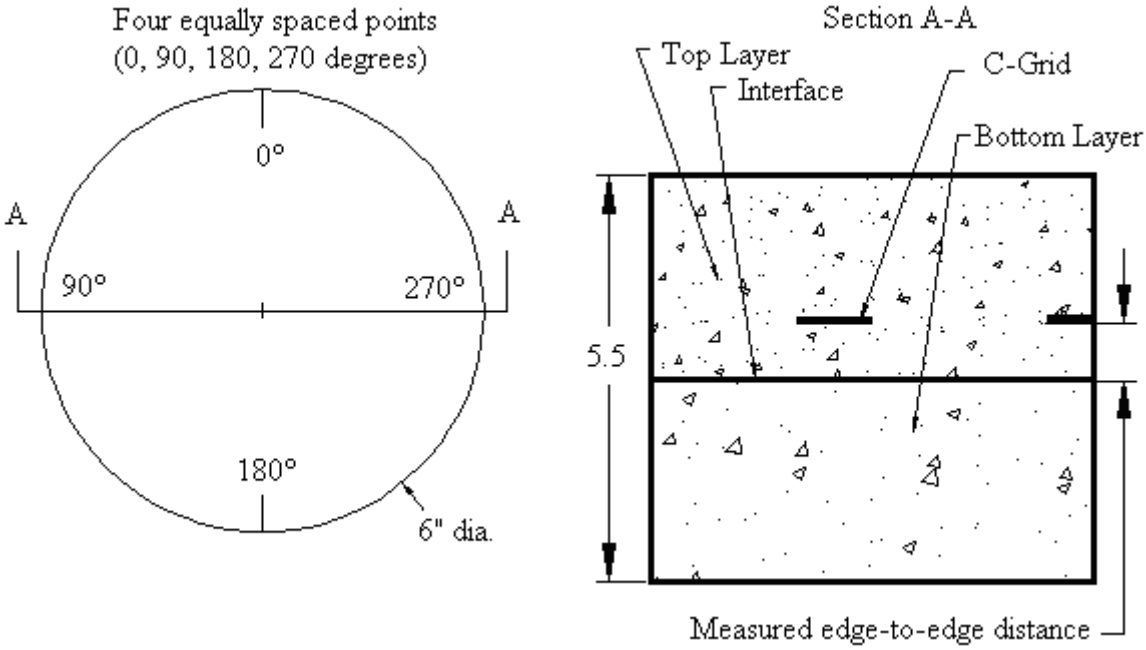

Figure 3-7 Measuring C-Grid float in cores

After geometric measurements were completed, each cylinder was tested in direct tension at a constant rate of 22,241 N/min (5,000 lb/min) until failure. Steel attachments,

which consist of a flat 152.4 mm (6 in) diameter base welded to a 25.4 mm (1 in) diameter rod with stiffeners (Figure 3-8), were epoxy glued to the top and bottom face of the specimen. So that the epoxy may cure properly and to ensure vertical alignment of the steel attachments, (to produce pure axial load) a steel frame jig (Figure 3-9) was used to secure the specimen while the epoxy cures. The epoxy was allowed to cure for a minimum of 72 hours prior to testing as seen in Figure 3-10. A schematic of the finished specimen is illustrated in Figure 3-11. Each specimen was then tested in an MTS testing machine to apply a direct tension force to the core (Figure 3-12).

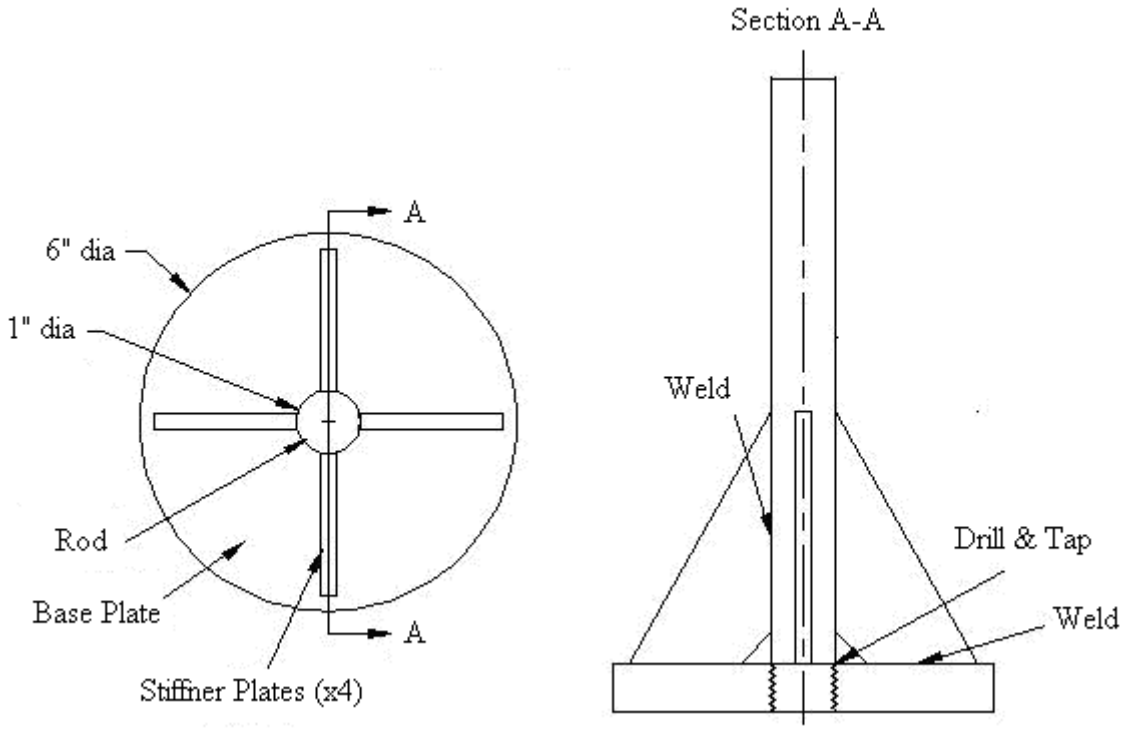

Figure 3-8 Steel attachments

Figure 3-9 Jig for curing of epoxy

Figure 3-10 Epoxy curing of specimens

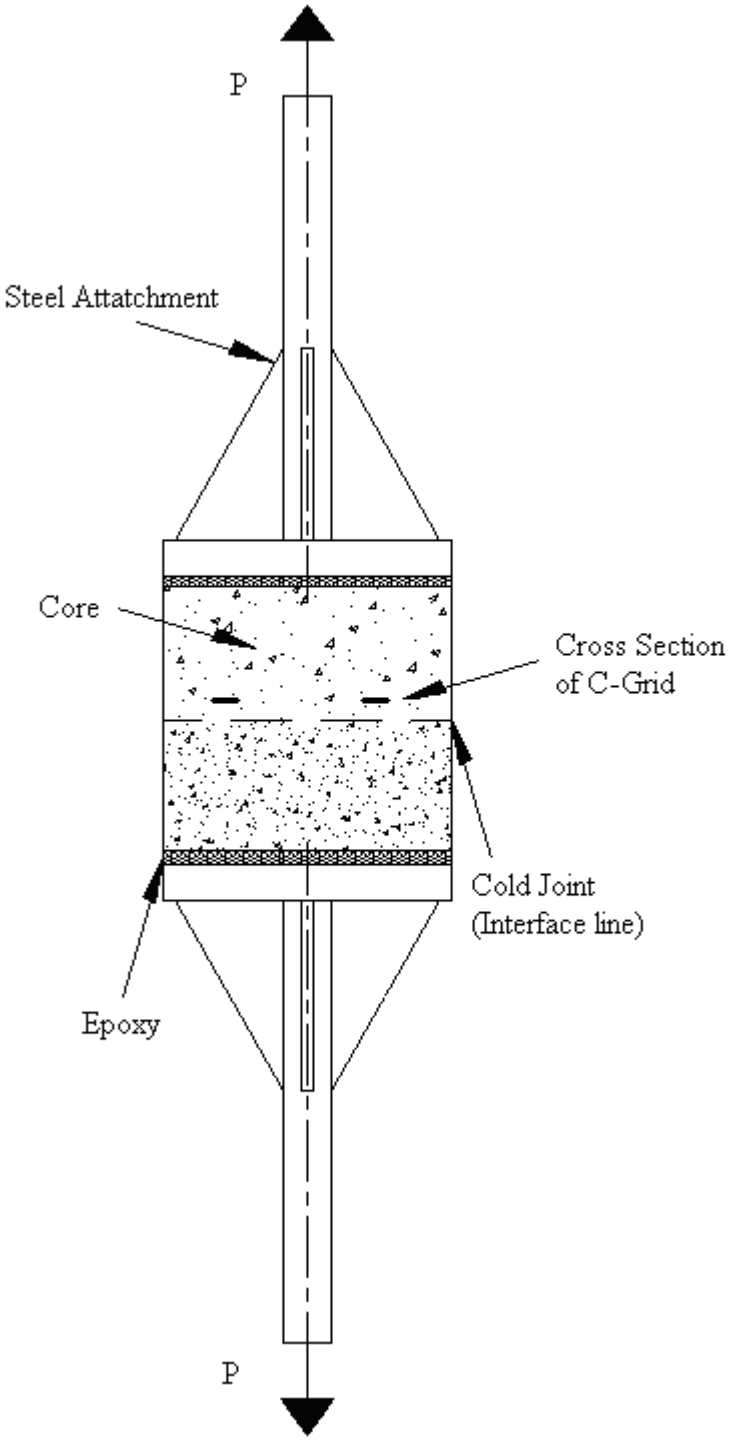

Figure 3-11 Schematic of specimen

(a) Specimen loaded in MTS (b) Specimen failure in MTS

Figure 3-12 Specimen in MTS machine

3.3 RESULTS

3.3.1 C-Grid Floating

The initial location of the C-Grid is 0 mm for HG and NR restraints (since they are laid flat on the concrete surface), 25.4 mm (1 in) for WC, and 9.5 mm (0.375 in) for FC and RC relative to the interface.

Table 3-3 contains the results of each set of three cores averaged including standard deviation and float as a percentage of the height of the 70 mm (2.75 in) topping layer as well

as the extreme values (maximum, minimum, and the difference between the two). Appendix A contains the raw data for the C-Grid final locations and float calculations.

Note that, because specimen A4 (one of the three C50 3.5x4.0 flat chair specimens) is so different from the rest of the specimens of that sample (and indeed, of all the cores), the calculations for 3.5x4.0 FC are repeated twice in the table. The entry with an asterisk (*) is calculated without specimen A4 included as it can be considered an outlier. It is apparent by visual inspection of this specimen that the plane of the C-Grid strands is considerably eccentric as opposed to parallel with the plane of interface as was the case with all other specimens.

Figure 3-13 is a graphical representation of the initial and final location of the C-Grid scaled relative to the actual size of the cores, that is, the vertical axis spans 140 mm (5.5 in) which is the overall height of the cored cylinders with 0 mm being the interface between the two concrete layers.

Table 3-3 Float results summary

Specimen Set	Average Float mm	Standard Deviation mm	Float as % of 70mm†	Max mm	Min mm	(Max - Min) mm	(Max - Min) as a % of 70mm
1.6x1.8 NR	3.08	1.23	4.4%	6	1.5	4.5	6.4%
2.2x2.2 NR	5.08	0.40	7.3%	7.5	4	3.5	5.0%
2.9x2.9 NR	4.54	1.04	6.5%	6.5	1.5	5	7.1%
3.5x4.0 NR	1.50	0.38	2.1%	2	0.5	1.5	2.1%
1.6x1.8 HG	2.92	0.26	4.2%	4	1.5	2.5	3.6%
2.2x2.2 HG	1.96	0.19	2.8%	3	1	2	2.9%
2.9x2.9 HG	4.21	0.88	6.0%	7	2	5	7.1%
3.5x4.0 HG	1.38	0.13	2.0%	2.5	0.5	2	2.9%
3.5x4.0 FC	-0.83	8.24	-1.2%	19	-8	27	38.6%
3.5x4.0 FC*	-5.83	1.33	-8.3%	-2.5	-8	5.5	7.9%
3.5x4.0 RC	-5.75	1.31	-8.2%	-1	-7	6	8.6%
2.9x2.9 WC	-12.75	3.15	-18.2%	-3	-17.5	14.5	20.7%

* Specimen A4 excluded

† Positive values indicate upward float

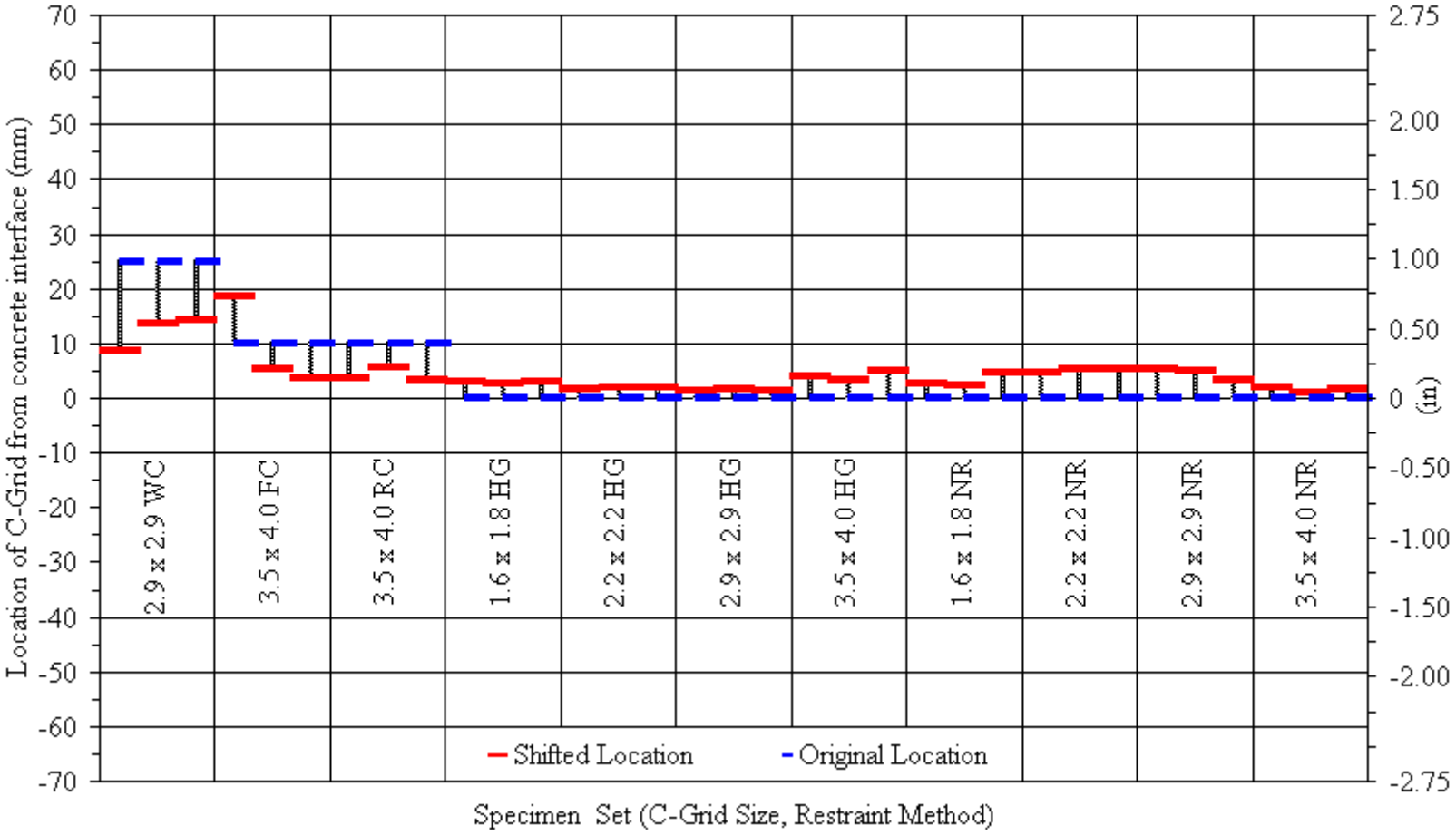

Figure 3-13 C-Grid location after casting

3.3.2 Direct Tension Tests

Appendix B contains the raw data for the breaking (maximum) load and stress of each individual core along with the average stress and average stress as a percentage of the control stress for each specimen set. Table 3-4 summarizes the tension test data and includes: average stress, standard deviation of stress, the percentage variation (standard deviation divided by average stress), the stress as a percentage of the average control stress (no C-Grid), and the stress as a percentage of the tensile strength of concrete used in the topping.

The tensile strength can be found by using the following equation from ACI 318-08:

$$f_t' = 6\sqrt{f_c'} \; . \qquad [3\text{-}1]$$

Note Eq. [3-1] is not dimensionally correct and requires the use of psi units. From Appendix C, the compressive strength of concrete was determined to be f_c' = 28.01 MPa (4062 psi) for the top layer and f_c' = 50.41 MPa (7312 psi) for the bottom layer. Since the upper layer is the weaker of the two, it controls; this results in a tensile strength f_t' = 2.65 MPa (382 psi) according to Eq. [3-1].

Figure 3-14 contains a graph of tensile stress on the ordinate and the specimens arranged on the abscissa according to the C-Grid spacing in the given specimen. Also shown as lines is the average tensile stress of the control stress and the ACI 318-08 tensile strength. Figure 3-15 combines both the average stress from this section and average final positions from Table 3-3. Other graphs were produced in order to determine if the tensile (bond) strength is influenced by the following characteristics: C-Grid size (Figure 3-14), C-Grid restraint (Figure 3-14), or the final location (Figure 3-15).

Table 3-5 contains information on the failure planes of the cores. The failure planes observed were either the plane of the cold joint of the two layers of concrete, along the plane of the C-Grid, or a combination of the two. See Figure 3-16 for typical pictures of these failure planes.

Table 3-4 Tension test summary

Specimen Set	Avg. Max Stress MPa (psi)	Std. Dev. Stress MPa (psi)	Variation, %	Stress as a % of control stress	Stress as a % of Eq. [3-1]
Control	1.714 (248.5)	0.349 (50.6)	20.4%	100.0%	65.0%
1.6x1.8 NR	0.556 (80.7)	0.263 (38.2)	47.3%	32.5%	21.1%
2.2x2.2 NR	0.821 (119.1)	0.394 (57.2)	48.0%	47.9%	31.2%
2.9x2.9 NR	0.872 (126.5)	0.166 (24.1)	19.1%	50.9%	33.1%
3.5x4.0 NR	0.717 (104.0)	0.051 (7.40)	7.1%	41.8%	27.2%
1.6x1.8 HG	1.185 (171.9)	0.051 (7.40)	4.3%	69.2%	45.0%
2.2x2.2 HG	0.904 (131.1)	0.035 (5.10)	3.9%	52.7%	34.3%
2.9x2.9 HG	1.156 (167.7)	0.503 (73.0)	43.5%	67.5%	43.9%
3.5x4.0 HG	0.735 (106.6)	0.476 (69.1)	64.8%	42.9%	27.9%
3.5x4.0 FC	1.171 (169.9)	0.273 (39.6)	23.3%	68.4%	44.4%
3.5x4.0 RC	1.584 (229.8)	0.524 (76.0)	33.1%	92.5%	60.1%
2.9x2.9 WC	1.252 (181.6)	0.169 (24.5)	13.5%	73.1%	47.5%

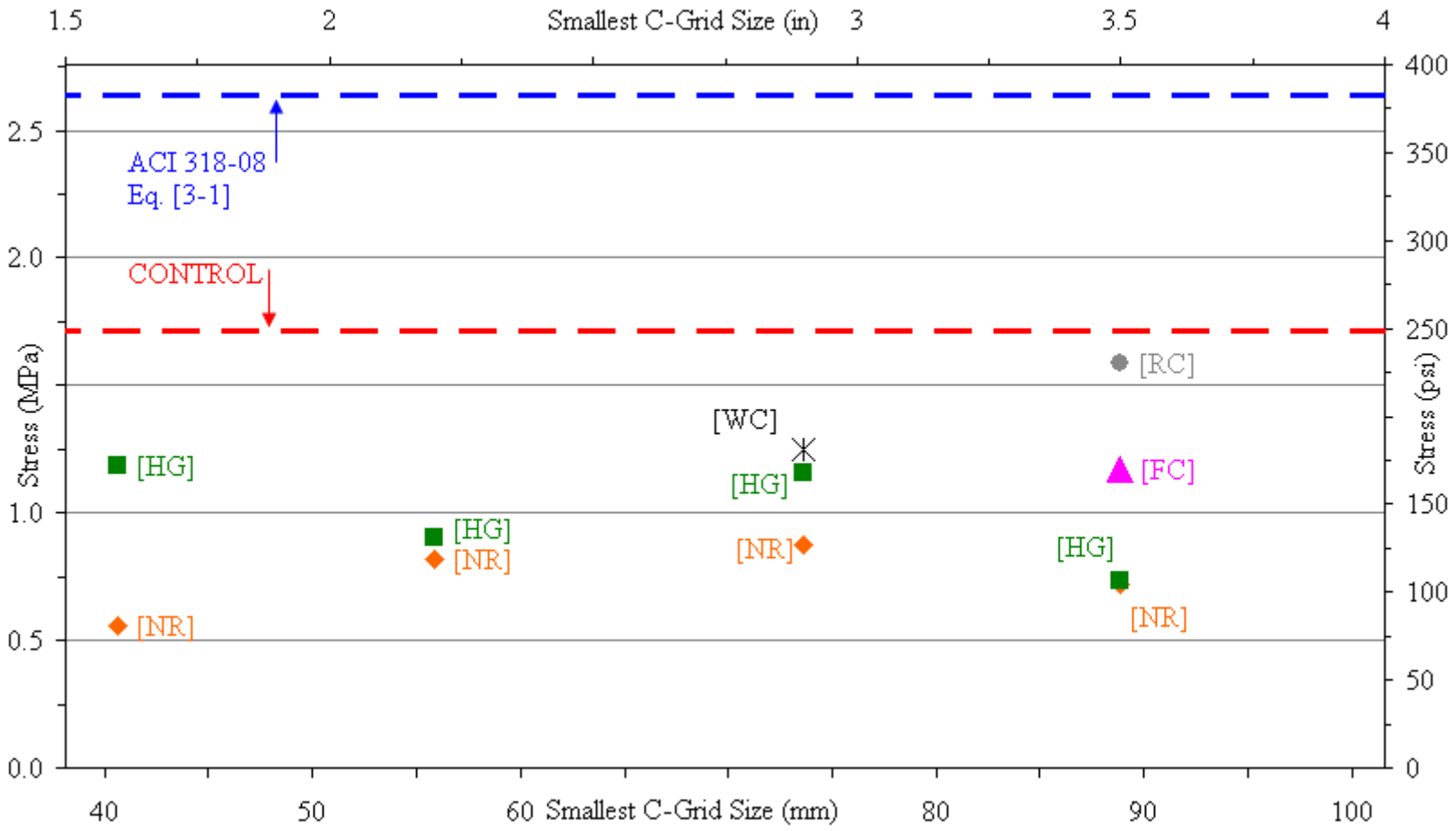

Figure 3-14 Average tensile stress as a function of C-Grid size and restraint

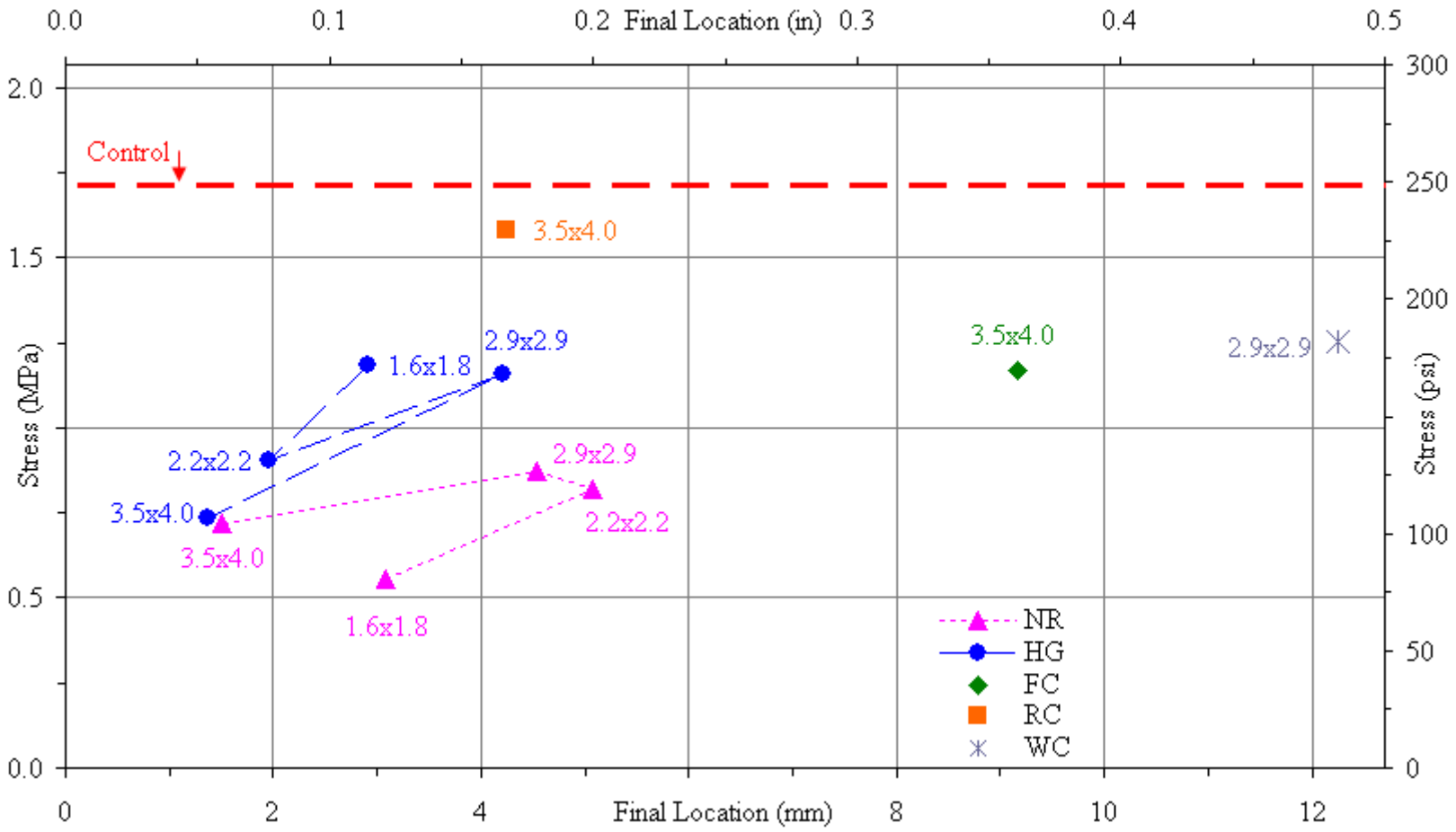

Figure 3-15 Average tensile stress as a function of the final C-Grid location

(a) Interface plane

(b) C-Grid plane

(c) Combined plane

Figure 3-16 Typical core failure planes

Table 3-5 Failure plane profiles

Specimen Set	Specimen No.	Failure Profile†
2.9x2.9 WC	1	Interface
2.9x2.9 WC	2	Interface
2.9x2.9 WC	3	Combined
3.5x4.0 FC	4	Interface
3.5x4.0 FC	5	Interface
3.5x4.0 FC	6	Combined
3.5x4.0 RC	7	C-Grid
3.5x4.0 RC	8	C-Grid
3.5x4.0 RC	9	Interface
3.5x4.0 HG	10	Combined
3.5x4.0 HG	11	Combined
3.5x4.0 HG	12	Combined
2.9x2.9 HG	13	Interface
2.9x2.9 HG	14	Combined
2.9x2.9 HG	15	Combined
Control	16	Interface
Control	17	Interface
Control	18	Interface
Control	19	Interface
Control	20	Interface
Control	21	Interface

Specimen Set	Specimen No.	Failure Profile†
1.6x1.8 NR	22	Combined
1.6x1.8 NR	23	Combined
1.6x1.8 NR	24	Interface
2.2x2.2 NR	25	Interface
2.2x2.2 NR	26	Interface
2.2x2.2 NR	27	Interface
2.9x2.9 NR	28	Interface
2.9x2.9 NR	29	Interface
2.9x2.9 NR	30	Interface
3.5x4.0 NR	31	Combined
3.5x4.0 NR	32	Combined
3.5x4.0 NR	33	Combined
1.6x1.8 HG	34	Interface
1.6x1.8 HG	35	Combined
1.6x1.8 HG	36	Combined
2.2x2.2 HG	37	Interface
2.2x2.2 HG	38	Combined
2.2x2.2 HG	39	Interface

† See Figure 3-16

3.4 DISCUSSION

3.4.1 C-Grid Float

Overall, the biggest individual specimen float was +8.63 mm (+0.340 in) and -16.38 mm (-0.645 in), while the average float was +5.08 mm (+0.200 in) and -12.75 mm (-0.502 in), according to Appendix A.

Core four, which is an outlier, is believed to be caused by disturbance during construction. The concrete vibrator or a concrete shovel could have easily shifted the C-Grid in the area around the core out of place. Caution must be observed when casting C-Grid reinforced concrete, including ensuring that all concrete tools do not impact the C-Grid. Excluding the outlier, the largest individual specimen float was +5.38 mm (0.211 in).

Both the No Restraint and the Hot Glue specimens maintained their position very well. Interestingly enough, there is not a lot of difference in float between the various C-Grid sizes as well as the two restraint methods themselves. C-Grid sizes 1.6x1.8 and 3.5x4.0 performed the best while 2.2x2.2 and 2.9x2.9 floated a few millimeters more. Considering though that the largest float was 5.4 mm (0.21 in) individually and 5.1 mm (0.20 in) on average, it can be said that float is not a concern with these methods of restraint and with all of these C-Grids since 5.4 mm and 5.1 mm are 7.7% and 7.3% of the height of the top layer of concrete, respectively. If one desires to place the C-Grid flat against the surface of the Precast DT, there really is not a need to Hot Glue (or otherwise secure) the C-Grid.

The chairing methods of restraint all suffered, to varying degree, from downward movement from their initial location. This is most likely caused by the weight of the concrete bearing down on the C-Grid. In the case of the RC and FC chairs, the weight of the concrete also has the potential to compress the rubber chairs. Overall, this downward movement should not pose much of a problem as long as the chairs are closely spaced. It is possible that the experiment exaggerated this effect since only 0.30 by 1.22 m (1 by 4 ft) strips of C-Grid were used in the Slabs, as opposed to a continuous roll of C-Grid. All of them deflected to approximately just over halfway between the intended location and the interface line. The FC chaired C-Grids floated, on average, -5.83 mm from an initial height of 10 mm (58.3%), the RC chaired C-Grids floated -5.75 mm from 10 mm (57.5%), and the WC chaired C-Grid floated -12.75 mm from 25 mm (51.0%).

The difference between the flat chair and roller chairs was negligible, but the Wheel Chairs did not perform well at all and their use is not recommended. In order to make the

test fair, no one was allowed to step on the slabs during casting, however in a practical application construction workers would have to walk on the top of the Precast DT and would end up stepping on the C-Grid. This is another reason to recommend against the use of wheel chairs. As the RC and FC chairs are constructed of flexible rubber and are only 10 mm in height, they are far less susceptible to damage from construction and being stepped on.

3.4.2 Direct Tension Tests

As a result of having two layers of concrete with a cold joint, the strength drops 35% from the ACI 318-08 tensile strength (if the core was one uniform layer instead of two). In addition, having any form of C-Grid drops the strength further, ranging from 21% to 60% of f_t'.

When the specimens were broken, the two faces where failure had occurred were observed and pictured (samples of which are shown in Figure 3-16). In many of these, it was clear where the C-Grid had interfered with the concrete paste from the top layer being able to flow under the C-Grid and bond to the existing layer of concrete. The evidence is the discoloration/indentation of the bottom surface matching the shape of the C-Grid and the voids that appear in this region (unlike the rest of the failure plane, which was compacted well). This does not occur in Figure 3-16(a) since that was a specimen with no C-Grid. This could certainly be responsible for the reduction of the bond strength of the cold joint.

Based on Figure 3-14, the strength varies on the type of restraint used rather than the type of C-Grid used. For instance, all the Hot Glue specimens are (by varying amounts) stronger than the No Restraint specimens. In addition, all the chaired specimens are stronger than any non-chaired C-Grids. The best performer was the Roller Chairs at 93% the control strength. Conversely, when looking at just C-Grid size, no apparent trend was observed.

In addition, there does not appear to be much of a correlation between the height (final location) of the C-Grid and the strength. It is possible that the strength is dependent, to

varying amounts, on all of these factors combined (C-Grid size, height, and restraint method).

Lastly, one should notice the considerable range of values of the peak load for specimens of the same C-Grid size and restraint. Variations range from 4% to 65%, with the average being 27%. This suggests that bond strength can contain localized weak spots and that quality control is very important, specifically ensuring compaction near the interface of both layers of concrete.

Clearly, there is a detrimental effect on the integrity of the bond between the two layers of concrete. Based on the results of this Chapter, which represents a worse case scenario in using the direct tension pull tests, it is recommended that C-Grid be chaired at least 10 mm (0.4 in) above the surface of the Precast DT in order to allow for a sufficiently strong cold joint between the two layers of concrete. The effect of C-Grid on the cold joint bond strength will be observed further in the single-shear tests of the next Chapter.

CHAPTER 4 LONGITUDINAL SHEAR-SLIP BEHAVIOR OF C-GRID REINFORCED CONCRETE

4.1 INTRODUCTION

The objective of this Chapter is to quantify the effect of Carbon Fiber Grid (C-Grid) on the longitudinal shear strength and shear-slip relationship of a cast-in-place concrete topping of a Precast/Prestressed Double Tee (Precast DT) system using small-scale single-shear tests to determine the fundamental longitudinal shear-slip response. Since the longitudinal joint between two Precast DT sections is the weakest plane, this experiment focuses on the longitudinal shear strength at this location. Various C-Grid sizes and orientations of C-Grid (the angle of the C-Grid fibers relative to the line of shear) were tested.

4.2 MATERIALS AND METHODS

4.2.1 Specimens

Ten "double-L" push-off single-shear specimens (for reasons discussed in Section 2.4) with dimensions as seen in Figure 4-1 were cast in two separate layers. The 76.2 mm (3 in) gap between the L's was designed to allow sufficient slip in order to observe the full shear-slip response. In a similar fashion as the slabs produced in Chapter 3 the bottom layer simulates the flange of a Precast DT with a specified concrete strength of f_c' = 34.5 MPa (5000 psi) and thickness t = 70 mm (2.75 in). Note that the actual concrete strengths at the time the specimens were tested were 50.95 MPa (7389 psi) and 26.53 MPa (3848 psi) for the bottom and top layers, respectively (see Appendix C). In addition, the top surface of this layer of concrete was finished to a surface roughness condition of CSP-4 (as discussed in Section 2.3.1 and used in the Slabs for the tension tests of Chapter 3). As the primary focus of this research is at the joint between two Precast DT flanges, the bottom layer of concrete

was cast with a discontinuity (gap) along the line of shear. This gap, which was about 3 mm (1/8 in) in width, represents the joint between the two Precast DTs. The top layer simulates the cast-in-place topping, with a specified concrete strength of f_c' = 20.7 MPa (3000 psi) and thickness t = 70 mm (2.75 in). The top layer was cast four weeks after the first layer was cast. As was described in Chapter 3, the surface of the bottom layer of concrete was pre-wetted, but no standing water was present when the top layer of concrete was cast (recall the discussion from Section 2.3.2). Note that the specimens of this Chapter were constructed at the same time as the Slabs of Chapter 3 and with the same batches of concrete for the top and bottom layers. However the measured concrete strengths were slightly different given that specimens A1-A39 from Chapter 3 were tested at a different time then specimens B1-B10 of this Chapter, see Appendix A.

The result is a specimen in which only the top layer of concrete (the topping) and C-Grid reinforcement resist the shear force. This set up assumes the Precast DT shapes are not connected together in any way (effectively the tests represent a worst-case scenario).

Before casting of the top layer, several sizes (the same sizes from Chapter 3) and orientations of C-Grid were placed flat on top of the bottom layer of concrete (restraint method "NR", from Figure 3-2). Combining this and the surface layer roughness applied to the top of the bottom layer the Reinforcement Placement Method can be termed (for future reference) as NR-CSP-4 for these single-shear tests. Details of the dimensional and material properties of C-Grid are found in Table 3-1 and Appendix D, respectively (note that the C-Grid used in this series of tests was from the same batch used throughout this research).

There were two control specimens; one with no C-Grid (only the top layer of concrete resisting shear) and the other with a discontinuity (gap) in both layers of concrete (only the C-Grid resists shear). Table 4-1 shows a complete schedule of specimens, including the controls. In addition, the Strands Crossing the Shear Line column is a count of the total number of strands crossing the 257.4 mm (18 in) line of shear.

Figure 4-2 illustrates the various C-Grid orientations used in rectangular and square C-Grids, respectively. Rectangular C-Grids (C50 - 1.6x1.8, C50 - 3.5x4.0) are those with unequal strand spacing in the transverse and longitudinal direction, hence a "strong" and "weak" orientation. Square C-Grids (C50 – 2.2x2.2, C50 – 2.9x2.9) are those with equal strand spacing in both directions, and can be placed so that the strands are oriented at a 0º/90º angle or a ±45º angle, hence "perpendicular" and "diagonal" orientations, respectively. Note that, with regard to the number of strands crossing the shear line and diagonally oriented C-Grids, all strands crossing were counted, regardless if the strand was +45 º or -45º, the reason for this is explained in Appendix D. Also note that specimens with identical C-Grid size and orientation have the same number of strands crossing the shear line (for example, B2 and B5 both have C50 2.2x2.2 oriented perpendicularly and have eight strands crossing the line of shear).

Table 4-1 Shear specimen schedule

Specimen	C-Grid	Top Layer of Concrete	Orientation of C-Grid	Strands Crossing Shear Line
B1 (ctrl)	None	Continuous	None	N/A
B2 (ctrl)	C50 2.2x2.2	Discontinuous	Perpendicular	8
B3	C50 1.6x1.8	Continuous	Strong	11
B4	C50 1.6x1.8	Continuous	Weak	9
B5	C50 2.2x2.2	Continuous	Perpendicular	8
B6	C50 2.9x2.9	Continuous	Perpendicular	6
B7	C50 3.5x4.0	Continuous	Strong	5
B8	C50 3.5x4.0	Continuous	Weak	4
B9	C50 2.2x2.2	Continuous	Diagonal	12
B10	C50 2.9x2.9	Continuous	Diagonal	9

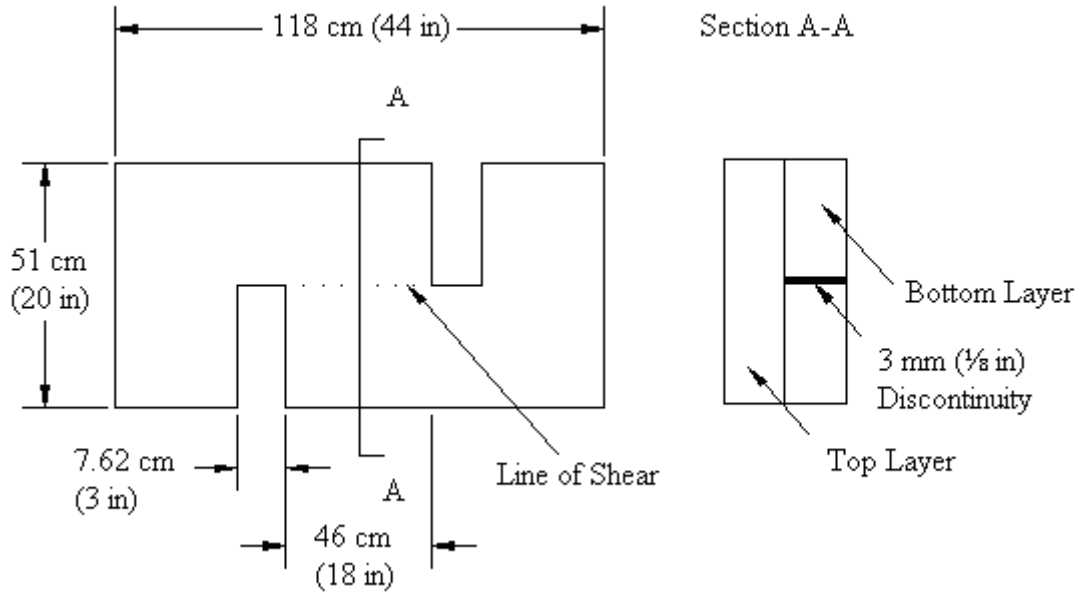

Figure 4-1 Shear specimen diagram

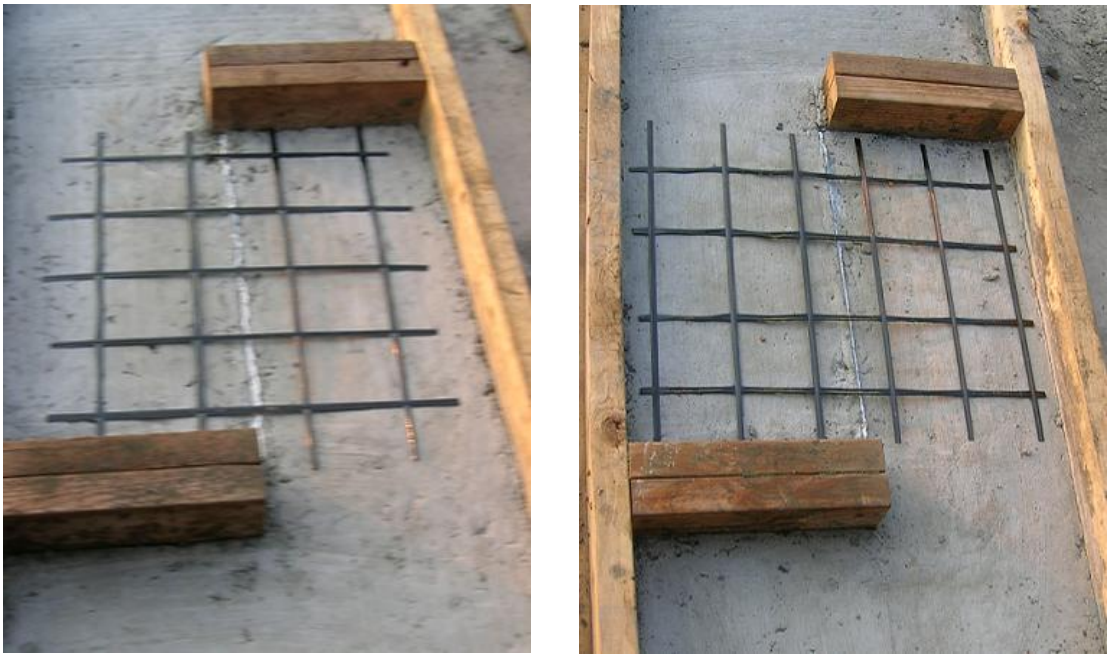

(a) Strong Orientation (more strands) (b) Weak Orientation (fewer strands)

Figure 4-2 Rectangular C-Grid orientations

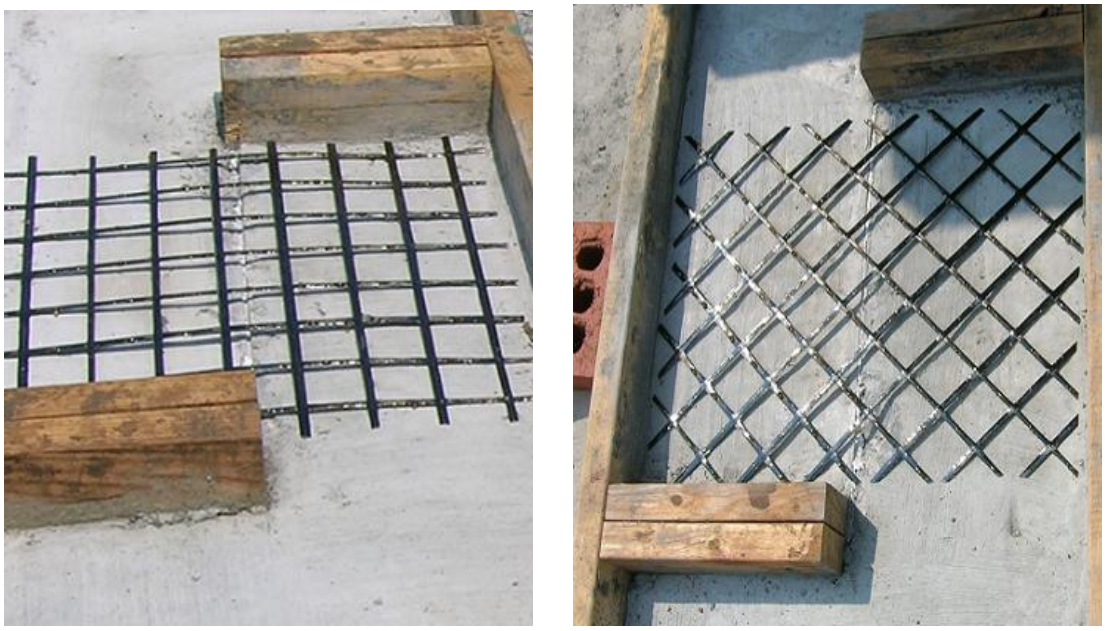

(a) Perpendicular Orientation (0º/90º) (b) Diagonal Orientation (+45º/-45º)

Figure 4-3 Square C-Grid orientations

4.2.2 Experimental Procedure

After curing, the single-shear specimens were placed into a testing rig, as seen in Figure 4-4, and loaded in direct compression. In that figure, on the right is a yellow loading jack and a load cell on the left side with the specimen in between which rests on a steel bed made of HSS sections laid together which are in turn elevated by short, large W-shapes shimmed to make the bed level. The load cell is placed on the opposite end of the load jack so that any applied force resisted by friction is not measured. The specimens were loaded by hand pump; shock loading was avoided and the pump was operated as smoothly as possible. The load rate was determined to be 670 to 1110 N/s (150 to 250 lb/s).

After being placed in the test rig, four string pots were located across the gaps to measure the longitudinal slip to generate the experimental shear-slip response. In addition, two spring-loaded pots were placed perpendicular to and across the line of shear where shear cracks were expected to form in order to measure crack width and separation of the shear crack. Figure 4-5 shows the specimen with all instrumentation prior to testing. Also seen in Figure 4-5 is external steel reinforcement to prevent splitting at the intersection of each leg of each L (ensuring the individual L shapes behave as rigid bodies). Note that the double-L shape as a whole is not eccentrically loaded, but the individual shapes are, thus the possibility of said split.

Each specimen was loaded until the residual shear resistance reduced to 10% or less of the peak resistance recorded. The four string pot values were averaged to determine the longitudinal slip (relative displacement between the L's along the line of shear) of the specimen. The maximum average shear per unit length (q) was calculated by dividing the peak load (i.e. the total shear force) by the 457.2 mm (18 in) length of the line of shear.

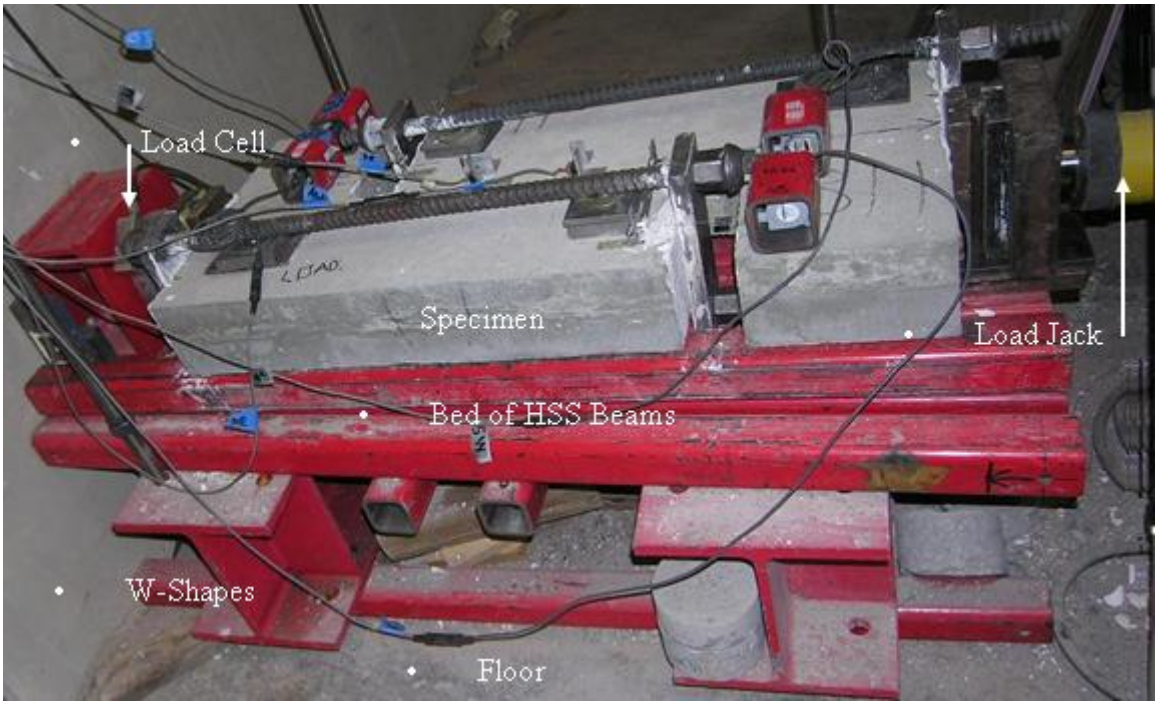

Figure 4-4 Shear specimen rig

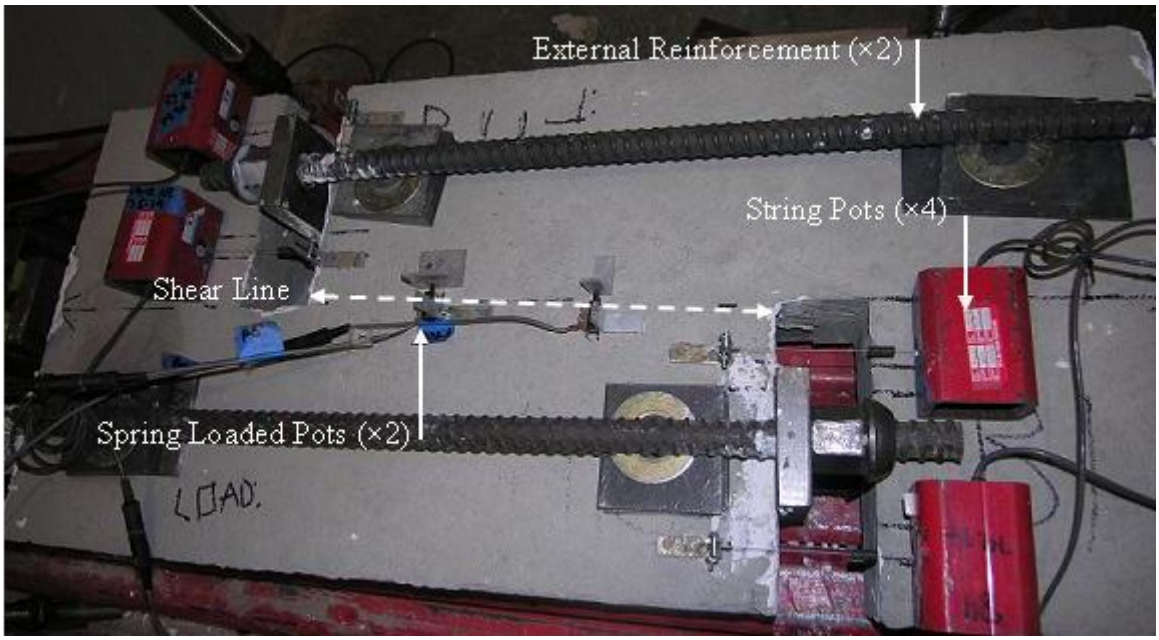

Figure 4-5 Shear specimen instrumentation and final test setup

4.3 RESULTS

All of the single-shear specimens resisted load predominantly in an elastic fashion with some softening as the peak load was approached (with the exception of the control specimen with C-Grid only). Three failure modes were observed and are referred to as Shear/Flexure Cracking, Cold Joint Debonding, or C-Grid Only Rupture. These failure modes are illustrated in Figure 4-6.

In the Shear/Flexure Cracking mode the concrete and C-Grid (if any) failed in a combination of shear and flexure along and around the line of shear. When peak load was reached in this failure mechanism, the concrete would suddenly and completely crack, but often the C-Grid reinforcement would remain intact. This results in a post-peak plateau where the C-Grid reinforcement would continue to resist a fraction of the peak load until the C-Grid ruptures and the specimen would split along the line of shear; all resistance lost.

The Cold Joint Debonding mode of failure occurred when the specimen would suddenly split in two along the plane of the cold joint (interface plane) of the two layers of concrete, much like the core tension tests in Chapter 3. In this failure mechanism, the line of shear remained intact with no visible cracking.

The last failure mode, C-Grid Only Rupture, was only observed with the control specimen with a full discontinuity in the concrete at the line of shear. The C-Grid takes load until sudden rupture, similar to the post peak plateau of the Shear/Flexure Cracking mode.

The specimens did not exhibit large deflections or deformation until after the peak load and there was no visible warning that any of the specimens were nearing their peak load. All failures were of a brittle nature, no visible concrete cracking was observed in any of the failure mechanisms until after the peak load was reached.

The peak load, displacement, shear force per unit length q, and the failure mechanism observed are recorded in Table 4-2.

Note that specimen B4 was tested in a prototype test rig that was inadequate and led to the development of the test rig as shown in Figure 4-4. Specimen B5 appears to have been

damaged during casting or moving as it had partially split in two along the interface of the concrete layers prior to testing. Therefore, the results from these specimens are not included in Table 4-2.

(a) Shear/Flexure Cracking (b) Interface Debonding (c) C-Grid-Only Rupture

Figure 4-6 Shear specimen failure modes

Table 4-2 Single shear test results

Specimen	Peak Load kN (kip)	Slip at Peak Load mm (in)	Peak Shear per unit length q kN/m (kip/ft)	Failure Mode†
B1 (ctrl)	67.8 (15.2)	0.544 (0.021)	145.0 (10.2)	Shear/Flexure Crack
B2 (ctrl)	8.6 (1.90)	3.711 (0.146)	18.4 (1.30)	C-Grid-Only Rupture
B3	79.0 (17.8)	0.599 (0.024)	169.0 (11.8)	Cold Joint Debonding
B6	98.6 (22.2)	0.330 (0.013)	210.9 (14.8)	Shear/Flexure Crack
B7	116.0 (26.1)	0.325 (0.013)	248.2 (17.4)	Shear/Flexure Crack
B8	97.1 (21.8)	0.602 (0.024)	207.7 (14.6)	Shear/Flexure Crack
B9	115.7 (26.0)	0.866 (0.034)	247.4 (17.3)	Cold Joint Debonding
B10	108.4 (24.4)	0.615 (0.024)	231.9 (16.3)	Shear/Flexure Crack

†See Figure 4-6 for illustration

For comparative purposes, several shear-slip response plots – with the load expressed as the shear per unit length, q (in kN/m and kip/ft) – were generated for various groups of specimens. The graphs plot q on the ordinate and the slip on the abscissa. In Figure 4-7 the specimens are the same C-Grid size, but different orientations. Figure 4-8 compares the same C-Grid in strong and weak orientation. The various C-Grid sizes oriented diagonally are shown in Figure 4-9. The various C-Grid sizes oriented perpendicularly are shown in Figure 4-10. Lastly, Figure 4-11 is a comparison of the supposed strength of the control specimens if their strengths were added together via compatibility versus the weakest of all the C-Grid reinforced specimens that failed in Shear/Flexure Cracking. Each graph in Figure 4-7 through Figure 4-11 contains the control specimen's response for comparison. Note that a discussion of each figure is given in the next Section.

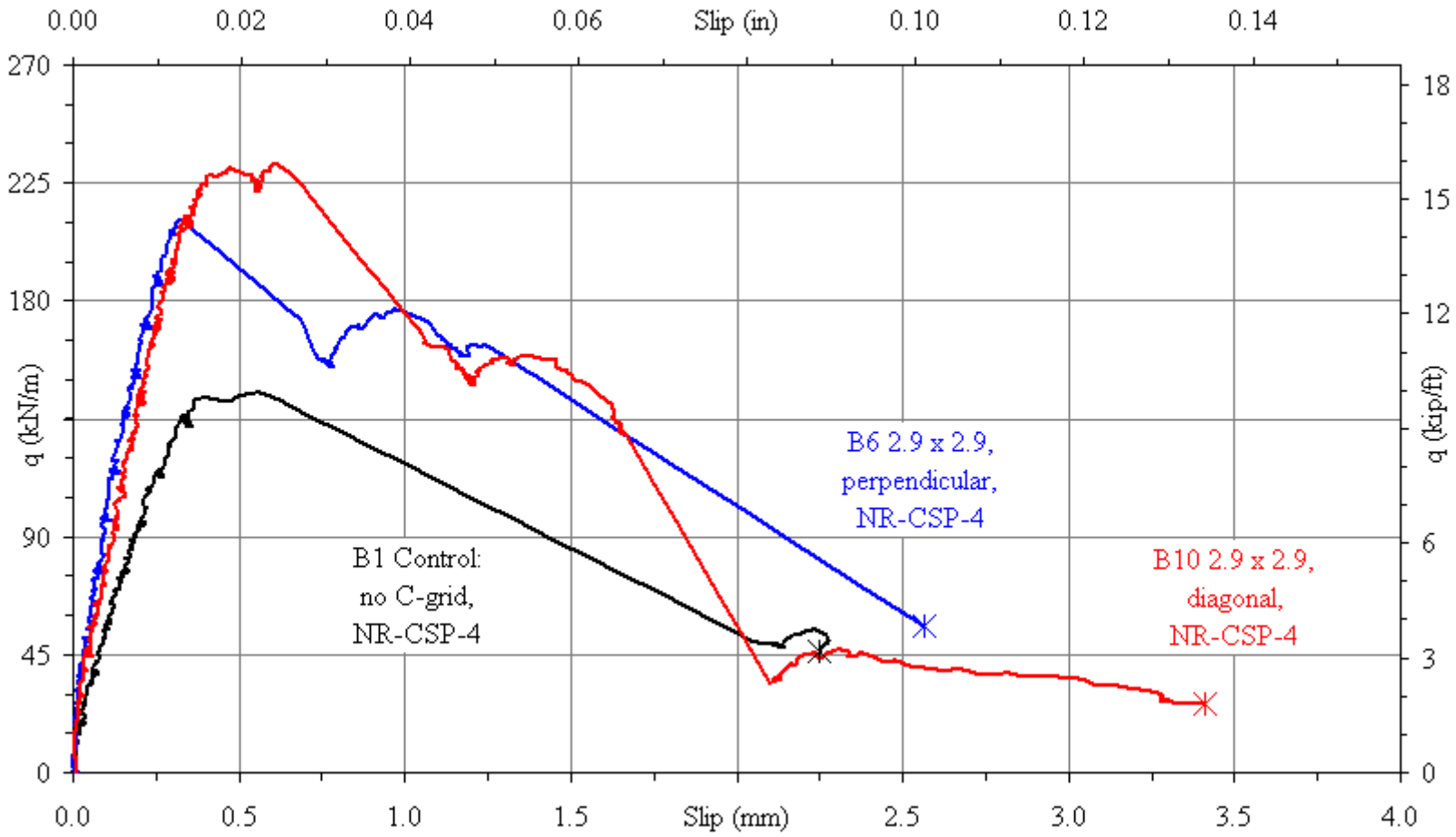

Figure 4-7 2.9x2.9 C-Grids with varying orientation

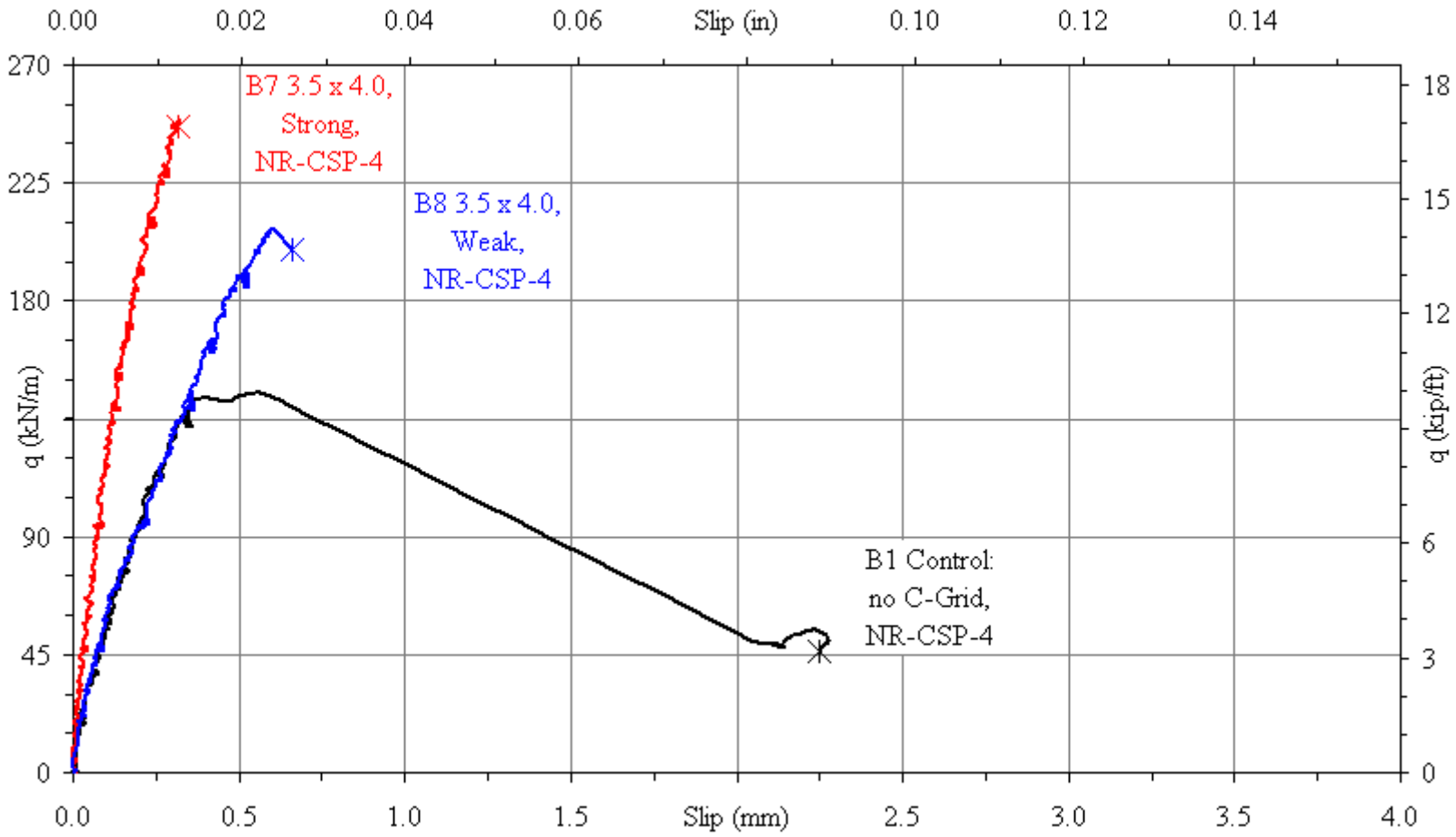

Figure 4-8 3.5x4.0 C-Grids with varying orientation

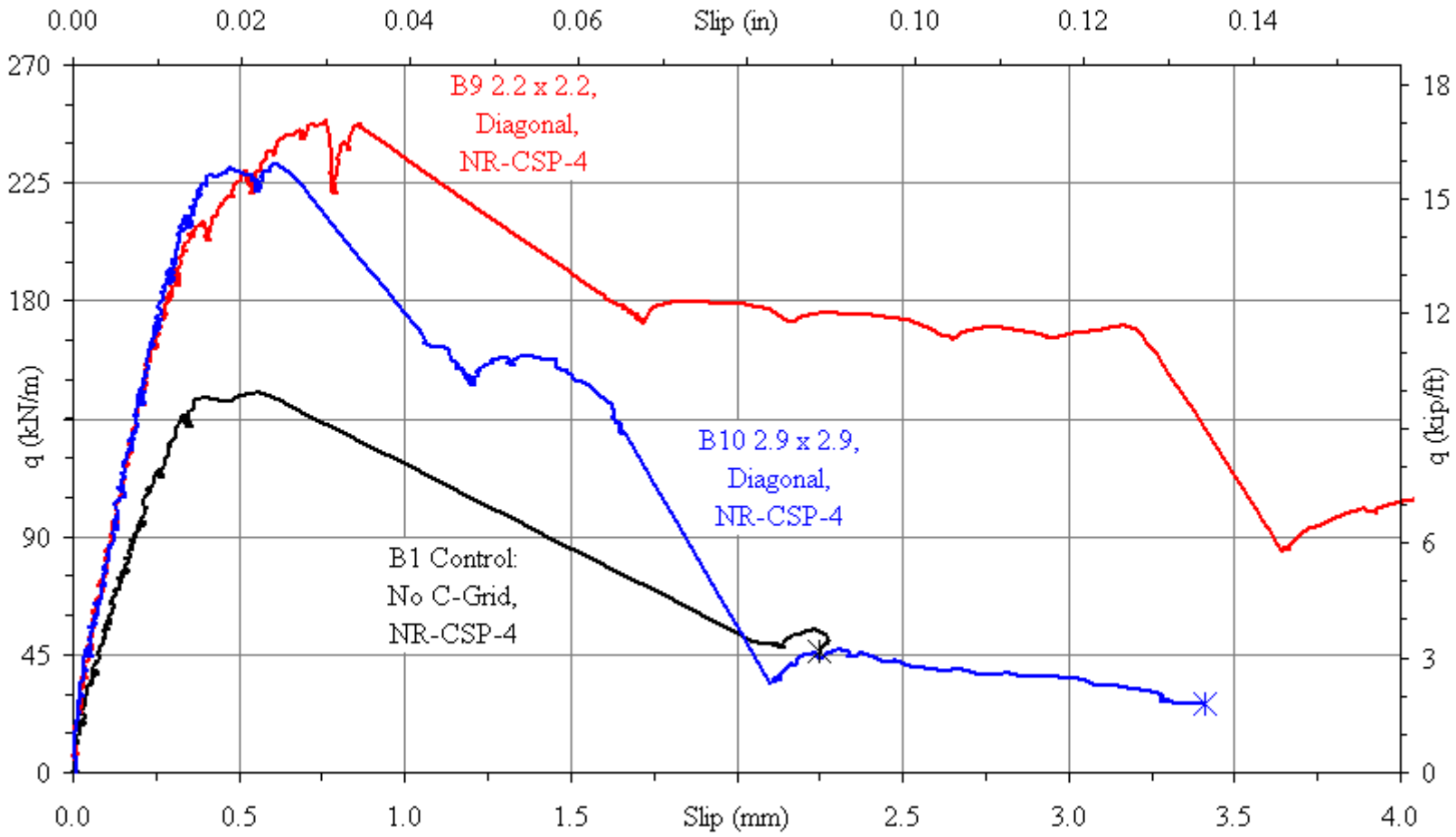

Figure 4-9 Diagonally oriented C-Grids with varying size

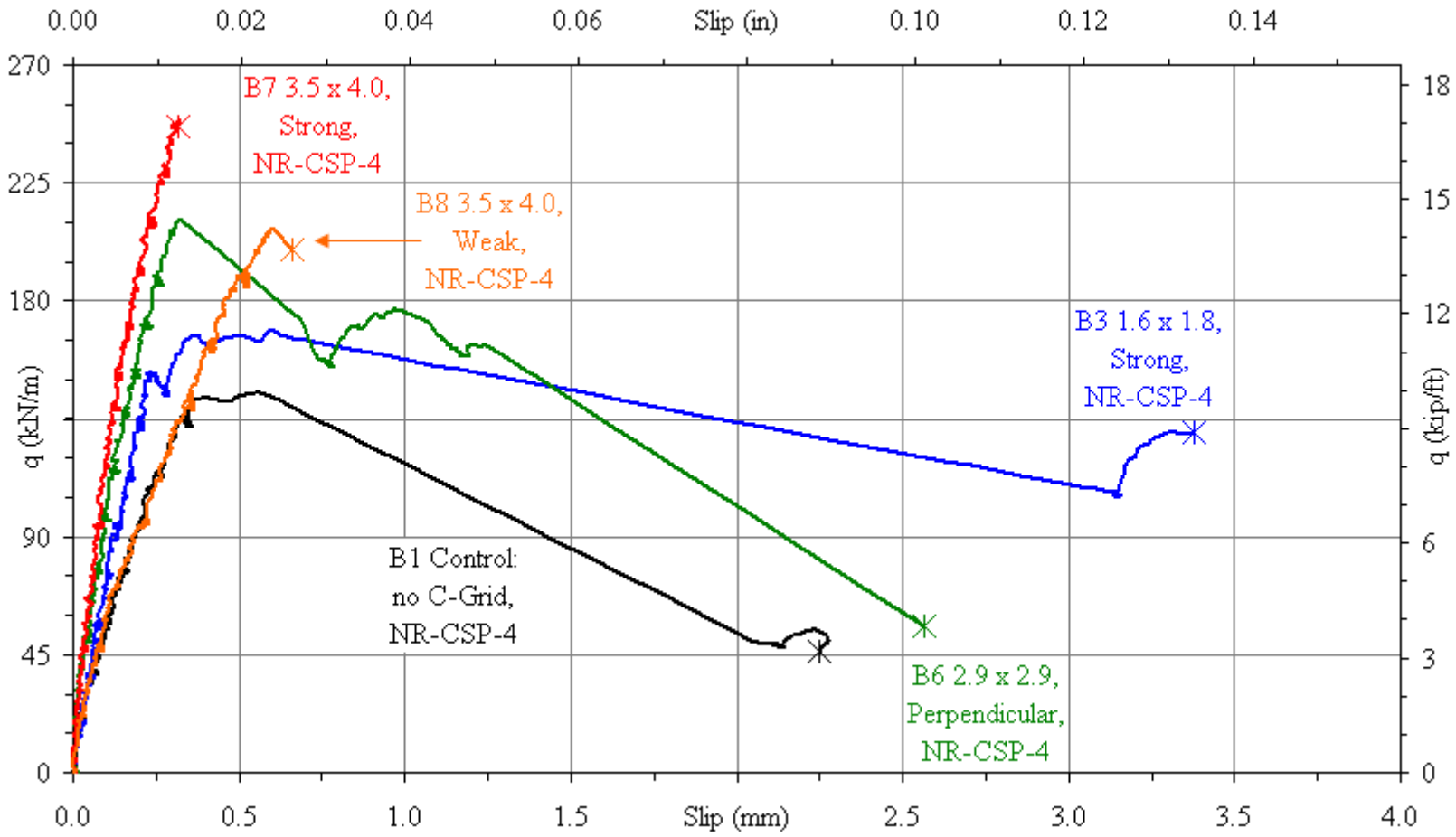

Figure 4-10 Perpendicularly oriented C-Grids with varying size

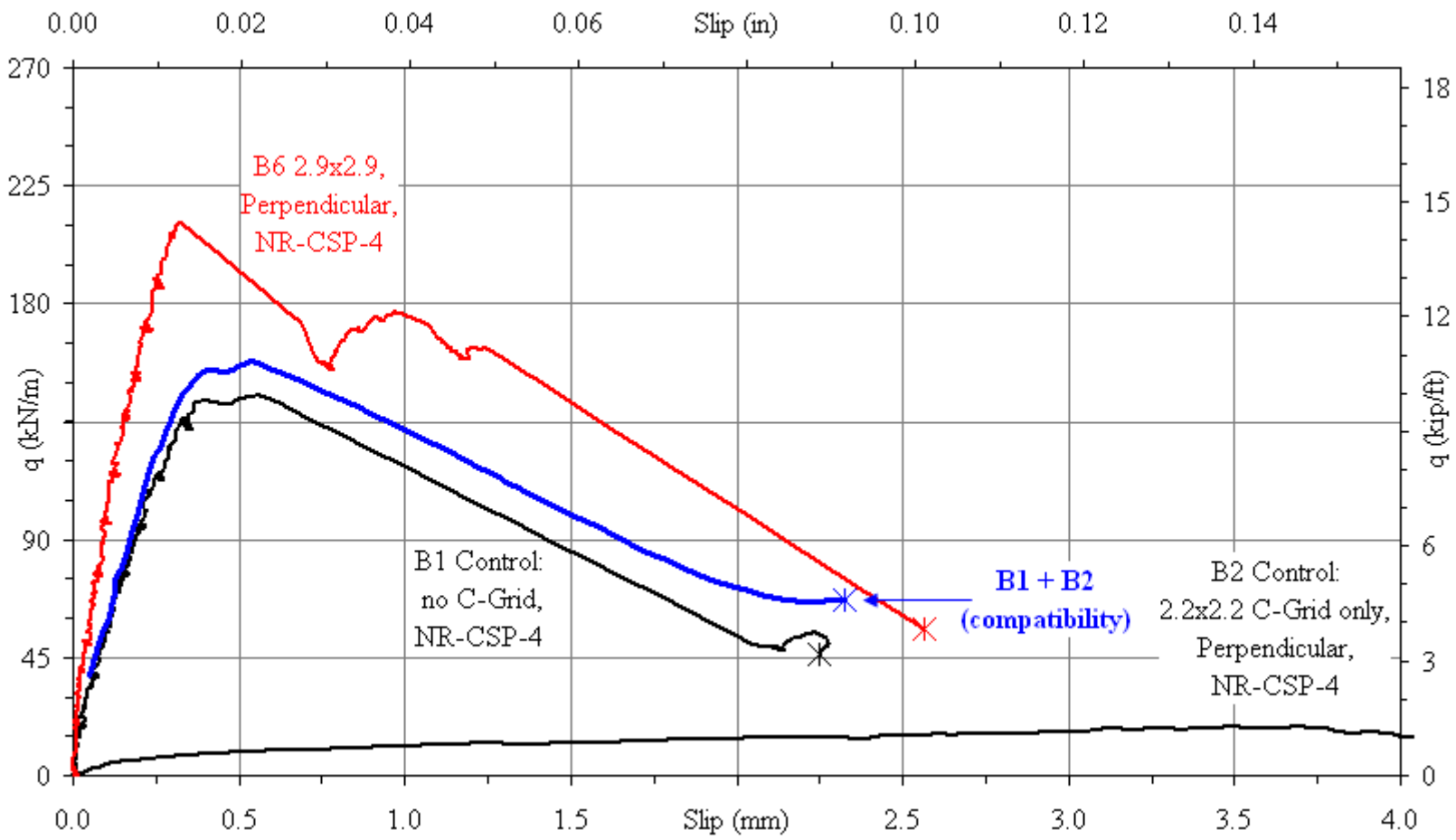

Figure 4-11 Control specimens with compatibility comparison

4.4 DISCUSSION

4.4.1 General Observations

As expected, all of the specimens with C-Grid had more shear capacity than the plain concrete control specimen had. With regard to stiffness, there was a slight increase in stiffness of specimens reinforced with C-Grid versus the plain concrete control specimen.

With respect to slip and deformability of the specimens, the second control specimen with C-Grid only was the only one considerably more deformable than the rest. Excluding that, all the specimens deformed very little before reaching peak load and failure. It appears that C-Grid did very little to increase the deformability of the specimen in shear, as they all failed before one millimeter (0.04 in) of slip. In fact, the deformability of the C-Grids was not much different from the control specimen with just plain concrete for which a slip of approximately one-half millimeter (0.02 in) was recorded.

4.4.2 C-Grid Orientation

The results obtained from this test series suggest that the orientation of the C-Grid has a noticeable effect on its performance as a reinforcing material.

With respect to C-Grid being oriented diagonally or perpendicularly, the following was observed. Placing the 2.9x2.9 C-Grid diagonally, while not increasing the deformability, increased the shear capacity by 10% versus the perpendicular orientation (see Figure 4-7). It was hoped that this diagonal orientation would have resulted in a higher percentage increase in strength. Reasons why the diagonally oriented C-Grids performed slightly, but not significantly, better could be due to a combination of factors. First, given that C-Grid strands are stronger in tension than in shear, having a 45 degree orientation does not put the strands in pure shear as they resist the longitudinal slipping, unlike a 90 degree orientation. Also, with respect to crack dilation, there are more strands crossing the line of shear in the diagonal orientation, which results in more strands able to resist the opening of longitudinal shear

cracks (clamping action). However, again because C-Grid strands are stronger in tension than in shear, the perpendicular orientation, though having fewer strands to resist crack opening, those strands would be loaded in pure tension, whereas the clamping action puts the diagonally oriented C-Grids in both tension and shear. Consider Table 4-3 below. This is also discussed later in Section 4.4.4 and Chapter 6.

Table 4-3 C-Grid strand loading conditions vs. resistance mode

C-Grid Orientation	Longitudinal Shear (Slip resistance)	Clamping Action (Crack dilation resistance)
Diagonal (±45º)	Combined Shear/Tension	Combined Shear/Tension
Perpendicular (0º/90º)	Pure Shear	Pure Tension

With respect to C-Grid being oriented in its strong or weak direction, it was observed that specimen with 3.5x4.0 C-Grid oriented in the strong direction resulted in a shear capacity increase of 23% versus the same C-Grid in the weak direction (see Figure 4-8). This is reasonable, as there are more strands (25% more in this case) crossing the line of shear in the strong direction orientation. This can be seen in Figure 4-2 with the weak direction having four stands and the strong direction having five strands.

Without looking at the material closely, it may not be readily apparent which direction is the strong or weak one, yet mistakenly placing the C-Grid in its weak direction would be considerably detrimental to the longitudinal shear strength performance. Considerable care should be applied to ensure proper orientation of this material should it be deemed suitable to use within the scope of this research.

4.4.3 Premature Debonding of the Cold Joint (Interface)

One unusual observation comes from Figure 4-10 and that is the specimen with the most dense C-Grid spacing (1.6x1.8) oriented in the strong direction resulted in a lower shear capacity than the specimen with 2.9x2.9 C-Grid, which were in turn both weaker than the one with 3.5x4.0 reinforcement oriented in the strong direction. This suggests another

mechanism was taking place and it is believed that the cold joint bond integrity of the concrete is at fault. Recall that the 1.6x1.8 strong specimen failed prematurely due to interface debonding and it was clear from observing the split specimen – as seen in Figure 4-12 – that the C-Grid interfered with the cold joint bond. This is similar to the direct tension tests in Chapter 3 where the unrestrained 1.6x1.8 specimens were the weakest in direct tension, suggesting the most interference with the cold joint bond (see Table 3-4).

Figure 4-12 Specimen B3 interface (premature debonding failure)

Interestingly, the 2.2x2.2 diagonally oriented specimen, as would be expected, was stronger than the 2.9x2.9 diagonally oriented specimen even though the former also failed due to debonding. Even though it was the strongest specimen in terms of shear capacity, it can be assumed the former could have been slightly stronger had premature debonding been

avoided (recall Figure 4-9). Therefore, the results from this Chapter reflect the results from Chapter 3, which had suggested that C-Grid could interfere with the bond integrity of the concrete especially if it was placed by the "no restraint" method.

The debonding at the cold joint interface should be considered an unfavorable mode of failure, and it should be avoided. Therefore, it is deemed imperative to find a solution to this problem in order for C-Grid to be considered a suitable reinforcing material within the scope of this research. In fact, as part of this research program, another series of single-shear tests was constructed in part to solve this issue (see Chapter 5).

4.4.4 Shear-Friction

In addition to the shear strength of the concrete and/or C-Grid materials themselves, the clamping force applied to the specimen by the reinforcement influences the overall shear capacity of these specimens. Recall from Section 2.5, when shear force is applied to the line of shear of the specimens, in addition to the relative slip along the line of shear, dilation (separation) in the directional normal to the line of shear must also occur. Therefore, the C-Grid reinforcement not only resists the longitudinal slipping of the specimen (increases longitudinal capacity) but it also resists crack dilation and separation in the normal direction. Crack dilation puts the reinforcing material in tension, similar to tension reinforcement in a reinforced concrete beam as it acts to restrain crack widening. For equilibrium, there is a resultant compression force developed normal to the crack at the concrete face. Ultimately, there is a net increase in the longitudinal shear strength because of the shear-friction mechanism developed.

This effect is why, as observed in Figure 4-11, a specimen with C-Grid reinforcement has a larger shear resistance than the sum of the individual C-Grid and concrete shear resistance components. Consider the shear flow resistance q from the control specimen with just plain concrete (B1), and the specimen with just C-Grid reinforcement (B2), which are added together without violating compatibility as in Eq. [4-1]:

$$q\left(\mathrm{B1}_{\text{at slip } x}\right) + q\left(\mathrm{B2}_{\text{at slip } x}\right) = q\left(\mathrm{B1{+}B2}_{\text{at slip } x}\right) \quad [4\text{-}1]$$

This value can be compared to a non-control specimen with C-Grid reinforcement. As Figure 4-11 illustrates, the sum of the two control specimens (B1+B2) is less than that of the 2.9x2.9 C-Grid reinforced specimen (B6), which is used for comparison because it was the weakest (non-control) specimen that failed in Shear/Flexure Cracking in this series of tests. In fact, even specimen B3 was stronger than B1+B2 despite having prematurely debonded.

Based on this assessment, it is reasonable to assume that the C-Grid reinforcement provides the same clamping action (and resultant shear-friction) as is well known in shear failure planes of steel reinforced concrete.

This may also explain why the diagonally oriented C-Grids are not much stronger than the perpendicularly oriented ones as discussed in Section 4.4.2. When the C-Grids are oriented perpendicularly; they are in the optimum direction to resist the concrete's tendency to want to separate, as this puts the strands in direct tension, which is C-Grid's strongest direction. Therefore, when the C-Grids are oriented diagonally, the clamping action resistance is in the form of a combination of tension and shear in the C-Grid (recall from Table 4-3). If it assumed that, with respect to clamping action, C-Grid offers no clamping action resistance in its shear direction, the diagonally oriented C-Grid is only 70.7% (sin 45º) as effective as the perpendicular C-Grid is at providing clamping force.

Since the number of strands between the two is nearly the same (eight versus nine, see Table 4-1), it is reasonable to assume the perpendicular C-Grid, despite being weaker as *direct* shear resistance, offers more potential clamping action and hence more *indirect* shear resistance then diagonal C-Grid. This might explain why the difference in shear capacity between the perpendicular and diagonal C-Grids is fairly small.

This will be discussed further in Chapter 6, but first, the previously mentioned issue of premature debonding as well as the desire for a direct comparison of C-Grid to WWF provided the motivation for developing a second series of single-shear tests, which is the topic of the following Chapter.

CHAPTER 5 FURTHER STUDY OF LONGITUDIONAL SHEAR-SLIP BEHAVIOR OF C-GRID REINFORCED CONCRETE

5.1 INTRODUCTION

With the completion of the first series of single-shear tests as described in the previous Chapter, a second series of shear tests was developed and tested. This second series was conducted in order to address two different areas of interest that will help to fulfill the overall goal of this research.

The first of these is to directly compare the performance and behavior of the Carbon Fiber Grid (C-Grid) reinforcement to traditional steel Welded Wire Fabric (WWF) reinforcement and observe the results. Therefore, some specimens within this series of tests are reinforced with typical WWF along side similar C-Grid sizes used in the previous test series.

The second area of interest is to resolve the issue of the undesirable premature debonding at the cold joint interface of the two layers of concrete as was observed in Section 4.4.3. This is imperative in order for C-Grid to be considered a suitable reinforcing material so a valid solution must be realized. Therefore, in order to meet this objective, two different methods were devised in order to solve this issue and eliminate premature debonding. Each method will be evaluated for its effectiveness with the desire that one, or both, would be a valid solution.

5.2 MATERIALS AND METHODS

5.2.1 Specimens

Twelve "double-L" push-off single-shear specimens with the same dimensions and construction procedure as those from the first series of specimens were cast (see Section 4.2.1). Although similar concrete was ordered for this series of tests, the resulting concrete strengths for the bottom and top layers at the time of testing were 16.06 MPa (2329 psi) and

20.55 MPa (2980 psi), respectively. This time there were three control specimens, one with no C-Grid (only the top layer of concrete resisting shear), and the other two have a discontinuity in both layers of concrete (such that only the C-Grid resists shear). Of these two, the same C-Grid was used but in different orientations, diagonal and perpendicular (recall Figure 4-2). The conditions during the casting of this series of tests were different from that of the previous tests. Temperatures during casting of the top layer were approximately 5-9 ºC (41-48º F). Although not as necessary as when the top layer of the first series was cast in much hotter weather, for consistency the bottom layer of each specimen was pre-wetted in a similar manner as was done in Chapter 4 with no visible water present before casting of the top layer.

In this set of single-shear specimens, two methods devised to avoid the premature debonding issue were implemented. The first method uses C-Grid laid flat against a surface finished using a rake, resulting in a surface roughness of at least CSP-8. A rougher surface should result in a better bond between the two layers. The specimens from the first series of tests (Chapter 4) had a finish applied by a light broom resulting in a surface roughness of approximately CSP-4 (NR-CSP-4). Henceforth this method will be referred to as "NR-CSP-8" with the term NR referring to an unrestrained specimen laid flat (recall from Figure 3-2).

The other method is to chair the C-Grid so that the C-Grid sits approximately 10-12 mm (0.4 to 0.5 in) above the interface between the two layers of concrete. The "FC" chairs from the tension tests in Chapter 3 (see Figure 3-3) were utilized. Recall that from the tension test results (see Figure 3-14) the "FC" chaired C-Grid specimens did not suffer as much of a loss in tensile (bond) strength than the un-chaired ones. The difference in tensile strength indicates a stronger cold joint bond thus the potential for premature debonding may be reduced or eliminated altogether. This method is hereafter referred to as "FC-CSP-4", as it will utilize the light broom finish of the previous tests.

Figure 5-1 shows the surface roughness CSP-4 and CSP-8 for comparison (note the control specimens with only C-Grid use the FC-CSP-4 placement) and Figure 5-2 shows the

differences between the two methods of C-Grid placement/surface treatment; including the one used in Chapter 4 with specimens placed flat on a CSP-4 surface, referred to as "NR-CSP-4".

In addition to the aforementioned C-Grid specimens, two specimens were cast with WWF reinforcement (see Figure 5-3) in order to obtain a direct comparison to C-Grid. The WWF used were 6x6 W1.7/W1.7 and 6x6 W4.0/W4.0, made from grade 60 steel. See Table 5-2 and Appendix E for WWF dimensional and material properties, respectively and note that the WWF were chaired using the WC chairs from Figure 3-2. In addition, a CSP-4 surface roughness was applied, resulting in a "WC-CSP-4" concrete surface and reinforcement placement condition.

Finally, in addition to the C50 series of C-Grids (from Figure 3-1), another type of C-Grid was used from the C150 series of C-Grids, namely the C150 2.4. This C-Grid has three times the number of carbon fibers per strand (150,000) as regular C50 C-Grid with center-on-center spacing of 61 mm (2.4 in). Also note that this material is intended to be stressed only in the longitudinal direction; the transverse strand's (which are not C150) primarily role is to hold the C-Grid matrix together, which is why the nomenclature only includes one spacing dimension, the transverse strands are also spaced 61mm (2.4 in) center-on-center. As can be seen in Figure 5-4, unlike the C50 C-Grids, it is easy to tell which direction is the strong orientation. The strength properties of the C-Grid, including the C150 C-Grid, can be found in Appendix D.

Table 5-1 Shear specimen schedule (second series)

Specimen	C-Grid or Welded Wire Fabric	Top Layer of Concrete	Reinforcement Placement Method	Orientation of C-Grid	Strands/ Wires Crossing Shear line
B11 (ctrl)	None	Continuous	N/A	None	N/A
B12 (ctrl)	C50 2.2x2.2	Discontinuous	FC-CSP-4	Perpendicular	8
B13 (ctrl)	C50 2.2x2.2	Discontinuous	FC-CSP-4	Diagonal	9
B14	C50 1.6x1.8	Continuous	FC-CSP-4	Strong	11
B15	C50 2.2x2.2	Continuous	FC-CSP-4	Perpendicular	8
B16	C50 2.2x2.2	Continuous	FC-CSP-4	Diagonal	12
B17	6x6 W1.7/W1.7	Continuous	WC-CSP-4	Perpendicular	3
B18	6x6 W4.0/W4.0	Continuous	WC-CSP-4	Perpendicular	3
B19	C50 1.6x1.8	Continuous	NR-CSP-8	Strong	11
B20	C50 2.2x2.2	Continuous	NR-CSP-8	Perpendicular	8
B21	C50 2.2x2.2	Continuous	NR-CSP-8	Diagonal	12
B22	C150 2.4	Continuous	NR-CSP-8	Strong	7

Table 5-2 WWF dimensional properties

Welded Wire Fabric Designation	Longitudinal & Transverse Spacing center-to-center	Longitudinal & Transverse Wire Cross-Section Area	Wire Gauge Size
6x6 W1.7/W1.7 (152x152 MW11.1/11.1)	152.4 mm (6.0 in)	11.1 mm^2 (0.017 in^2)	9 gauge
6x6 W4.0/W4.0 (152x152 MW25.8/25.8)	152.4 mm (6.0 in)	25.8 mm^2 (0.040 in^2)	4 gauge

(a) CSP-4 (b) CSP-8

Figure 5-1 Surface roughness (of bottom layer of concrete)

(a) FC-CSP-4 (second series)

(b) NR-CSP-8 (second series)

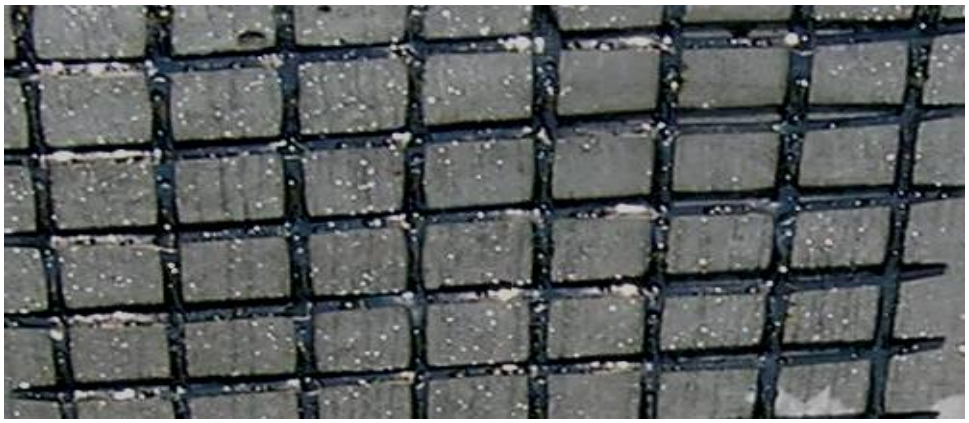

(c) NR-CSP-4 (first series)

Figure 5-2 C-Grid placement methods

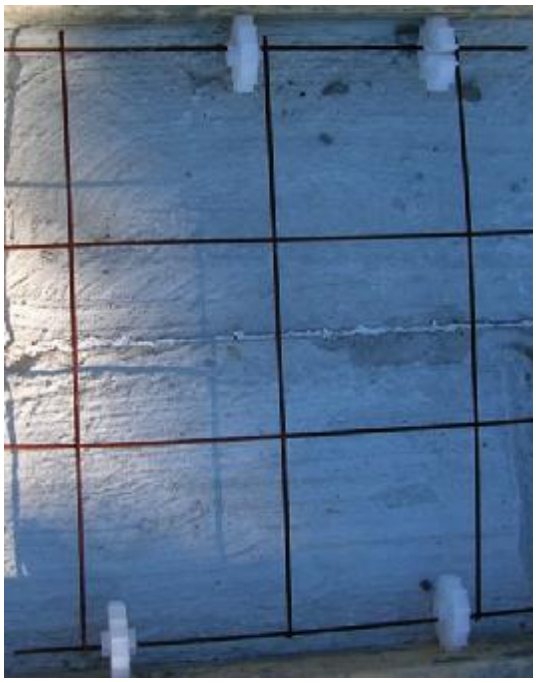

(a) 6x6 W1.7/W1.7

(b) 6x6 W4.0/W4.0

Figure 5-3 WWF sizes (WC-CSP-4)

Figure 5-4 C150 2.4 C-Grid

5.2.2 Experimental Procedure

After curing for a minimum of two weeks, the specimens were placed into the same testing rig as used and described in Section 4.2.2. The same instrumentation described in Section 4.2.2 and pictured in Figure 4-4 was used as well.

Each specimen was loaded until the residual shear resistance reached less than 10% of the peak resistance recorded (failure of both the C-Grid or WWF and concrete). The four string pot values were averaged to determine the longitudinal slip (relative displacement between the L's along the shear failure plane) of the specimen. The maximum average shear per unit length q was calculated by dividing the peak load (i.e. the total shear force) by the length of the line of shear, which is 457.2 mm (18 in).

5.3 RESULTS

Similar to the previous shear tests in Chapter 4, all of the specimens in this series behaved elastically with slight softening as the peak load was approached. The failure modes observed were Shear/Flexure Cracking, Cold Joint Debonding, and C-Grid-Only Rupture, as in Figure 4-6 and described in Section 4.3. Note that none of the reinforced specimens failed in the Interface Debonding mode, the specimen that debonded prematurely was the control with no reinforcement. The quality of the concrete mix is likely the cause of the debonding of the control specimen. Also, note that specimen B16 was discarded as it suffered from a severe lack of compaction.

Only one specimen (B18 with 6x6 W4.0/W4.0 WWF reinforcement) exhibited any visible signs of impending failure before the peak load was reached. The first visible signs of cracking occurred at about 90% of the peak load as seen in Figure 5-5. The specimen shown in Figure 5-6 illustrates the typical Shear/Flexure Cracking failure, with no visible cracking along the line of shear until the peak load (and failure) is reached.

The peak load, displacement, shear force per unit length q, and the failure mechanism observed are recorded in Table 5-3.

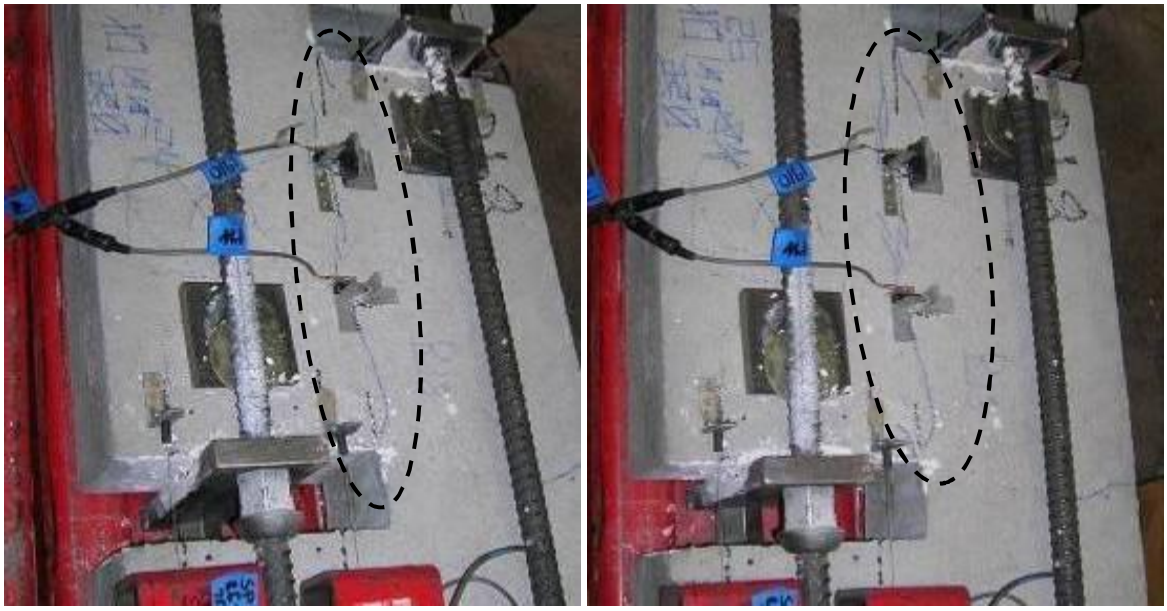

(a) 92% of peak load (cracks visible) (b) 99% peak load (near complete cracking)

Figure 5-5 Specimen B18 pre-peak load cracking

(a) 94% peak load (no cracks evident) (b) 100% peak load (immediate failure)

Figure 5-6 Typical failure with no visible cracking (B20)

Table 5-3 Shear test results (second series)

Specimen	Peak Load, kN (kip)	Slip at Peak Load, mm (in)	Peak Shear per unit length q, kN/m (kip/ft)	Failure Mode†
B11 (ctrl)	75.7 (17.0)	0.257 (0.010)	161.8 (11.3)	Cold Joint Debonding
B12 (ctrl)	19.8 (4.4)	2.540 (0.100)	42.3 (3.0)	C-Grid Rupture
B13	15.1 (3.4)	0.472 (0.019)	32.3 (2.3)	C-Grid Rupture
B14	105.9 (23.8)	0.401 (0.016)	226.5 (15.9)	Shear/Flexure Crack
B15	98.9 (22.2)	0.439 (0.017)	211.5 (14.8)	Shear/Flexure Crack
B17	72.1 (16.2)	0.208 (0.008)	154.1 (10.8)	Shear/Flexure Crack
B18	116.5 (26.2)	1.080 (0.043)	249.2 (17.5)	Shear/Flexure Crack
B19	97.7 (22.0)	1.199 (0.047)	209.0 (14.6)	Shear/Flexure Crack
B20	75.9 (17.1)	0.409 (0.016)	162.3 (11.4)	Shear/Flexure Crack
B21	81.7 (18.4)	0.470 (0.019)	174.7 (12.2)	Shear/Flexure Crack
B22	111.2 (25.0)	0.800 (0.032)	237.9 (16.7)	Shear/Flexure Crack

†See Figure 4-6 for illustration

As was done in Section 4.3, several shear-slip response plots were generated. The load is expressed as a shear per unit length q on the ordinate and the slip is plotted on the abscissa. First, the three control specimens are illustrated in Figure 5-7. Figure 5-8 shows the two WWF reinforced specimens compared to the control specimen with no C-Grid (plain concrete). The steel specimens are plotted again in Figure 5-9 along with all the C-Grid reinforced specimens from this series of tests. All of the specimens with chaired C-Grid and a "smooth" surface of the bottom layer of concrete (FC-CSP-4) – the first of two methods

devised to prevent premature debonding – are shown in Figure 5-10. The specimens using the second method – C-Grid placed flat against a roughly finished surface (NR-CSP-8) – are illustrated in Figure 5-11. Lastly, Figure 5-12 is a plot of the same type of C-Grid (1.6x1.8 oriented in the strong direction) across both test series with different surface finishes (CSP-4, CSP-8) and placement schemes (NR, FC). Note that a discussion of each figure is given in the next Section.

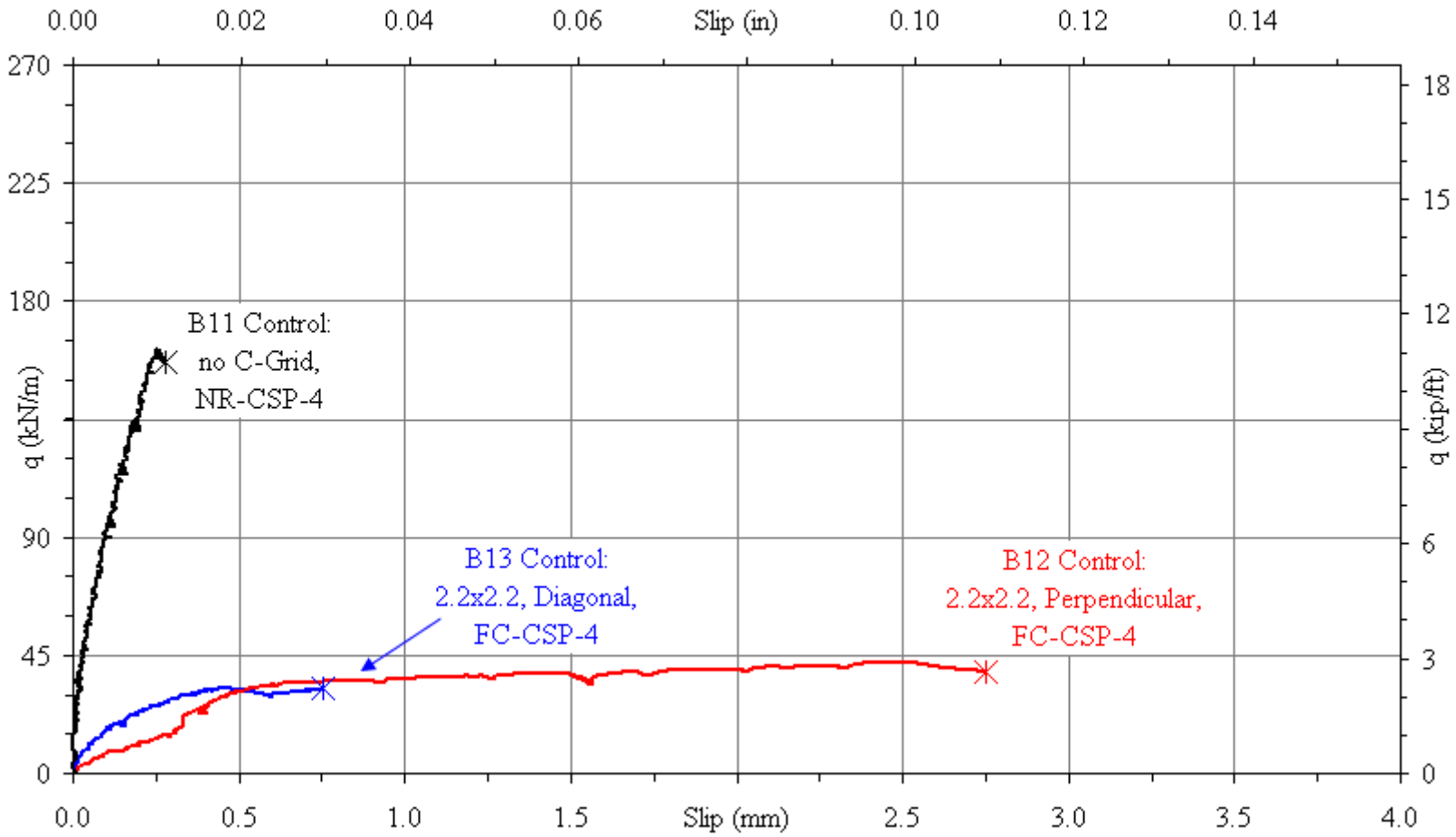

Figure 5-7 Control Specimens (Second Series)

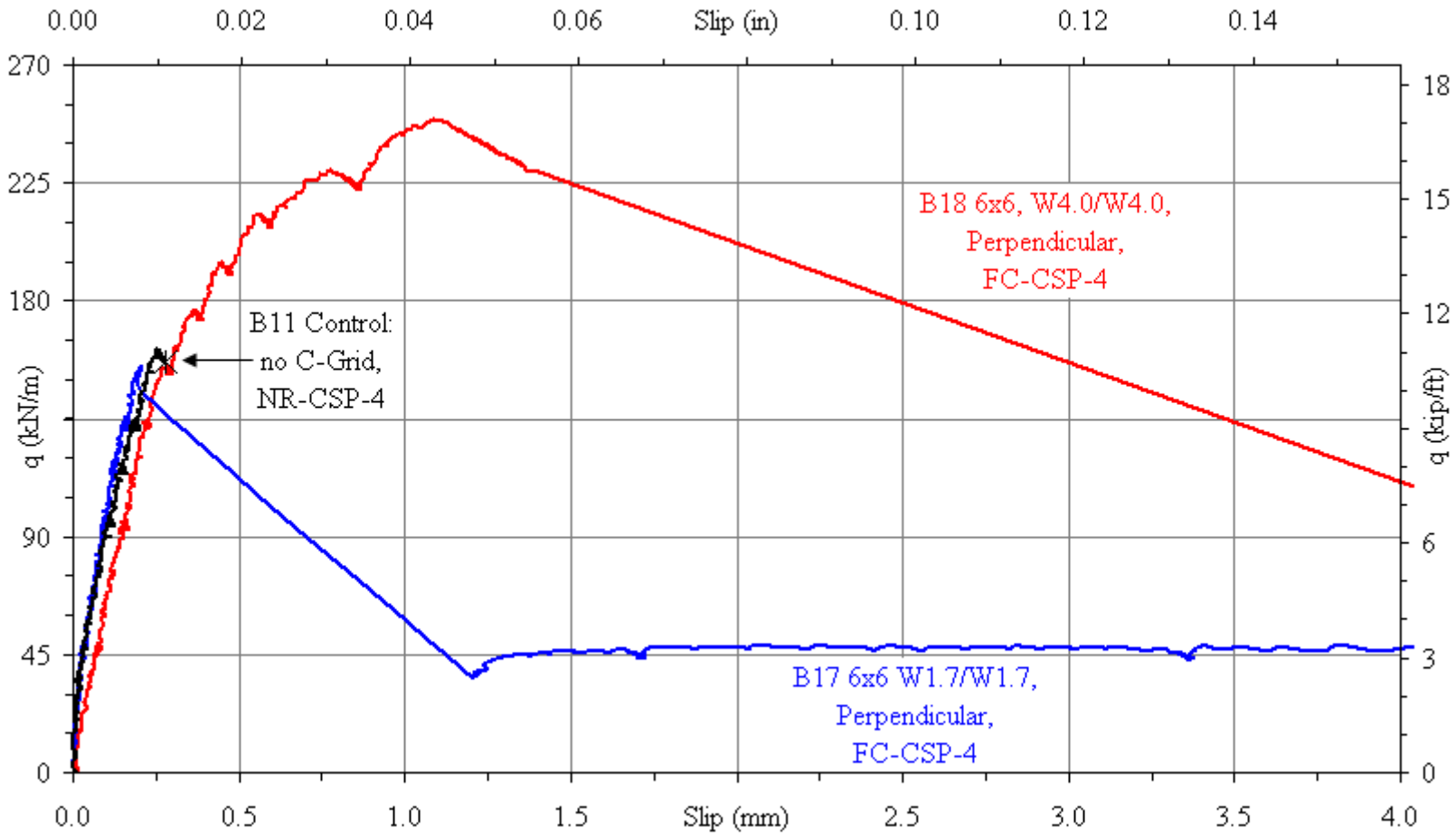

Figure 5-8 WWF reinforced specimens

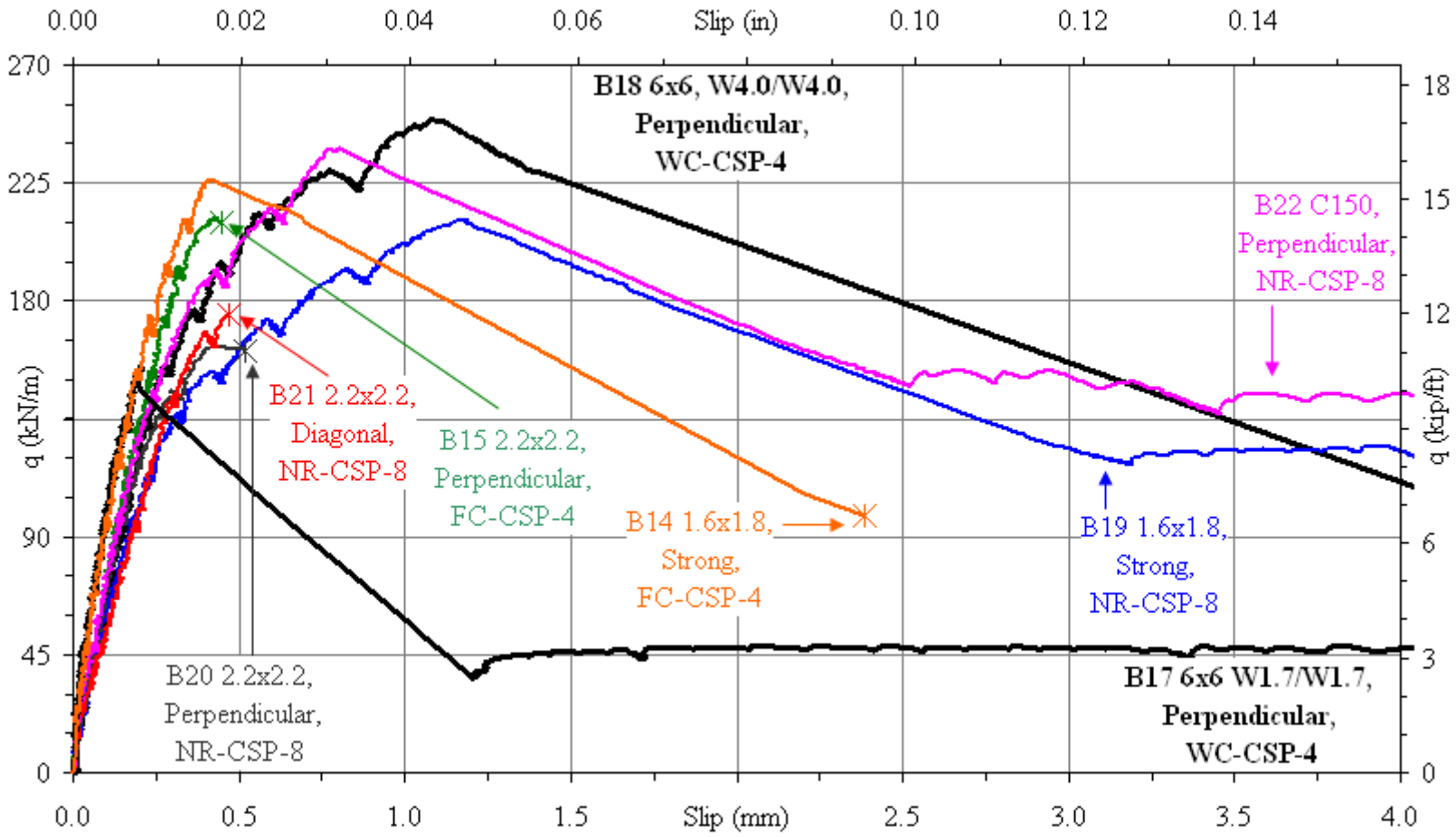

Figure 5-9 Comparison of WWF and C-Grid specimens (second series)

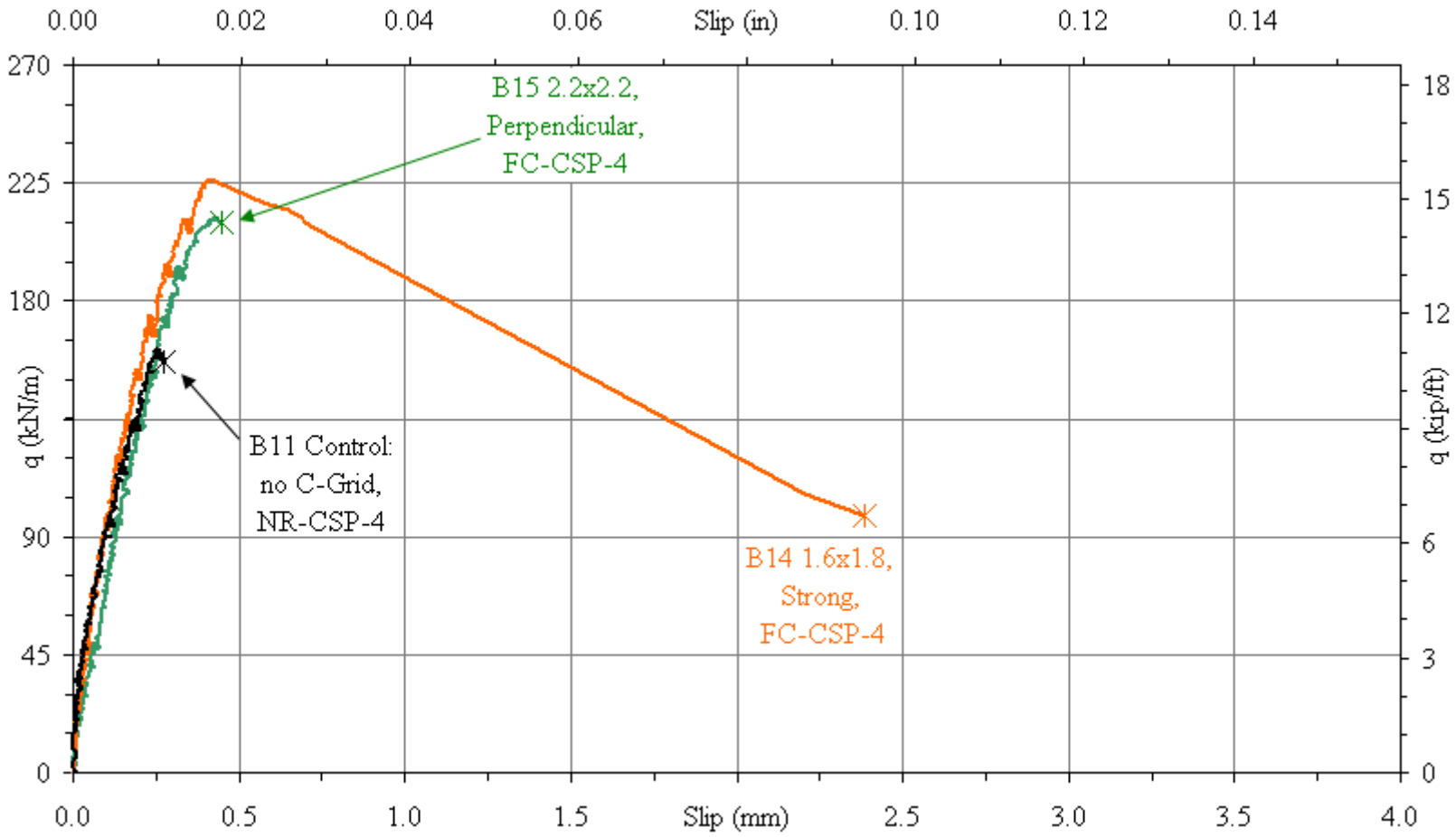

Figure 5-10 Chaired C-Grid on a smooth surface finish (FC-CSP-4)

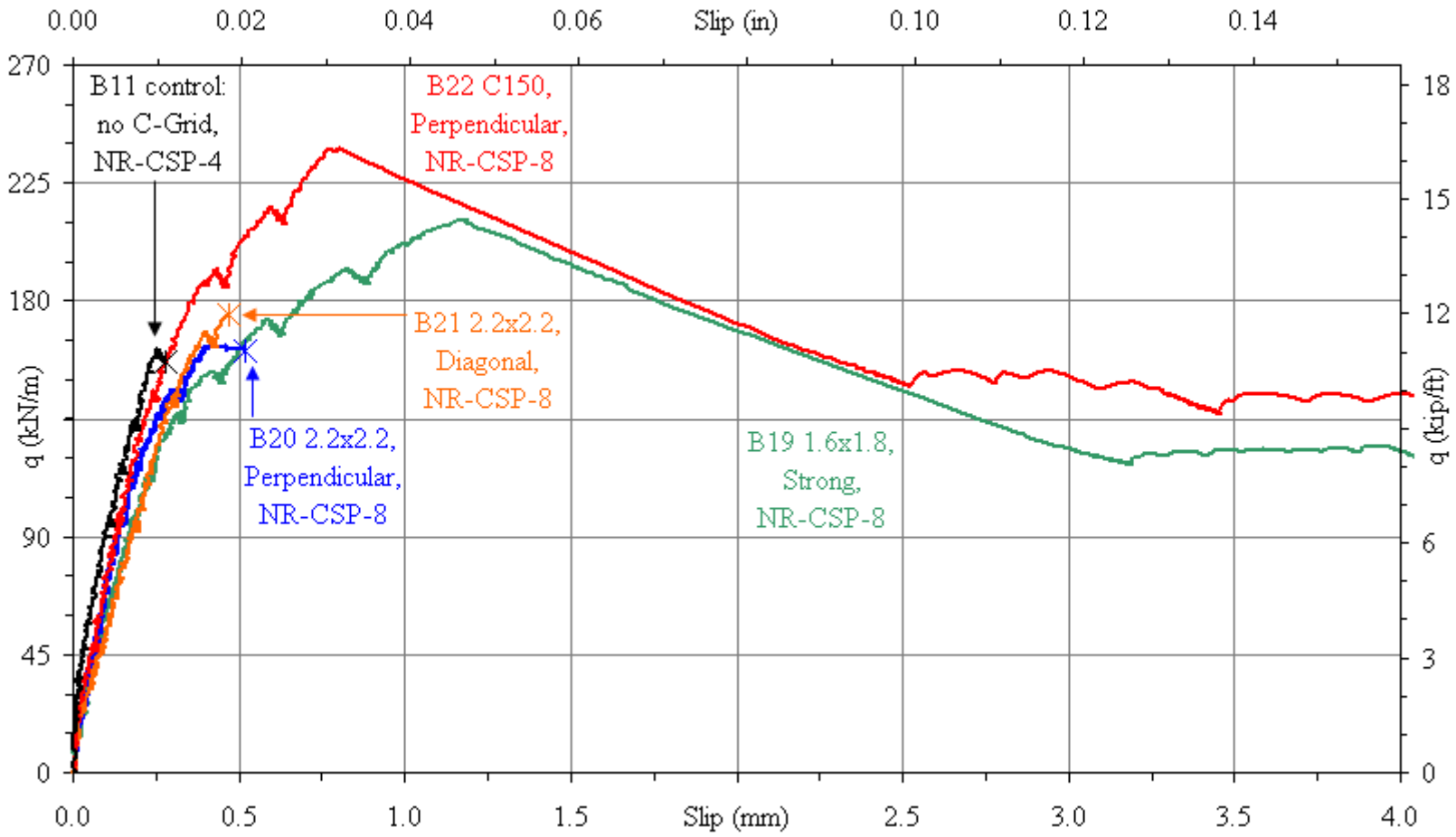

Figure 5-11 C-Grids laid flat on a rough surface finish (NR-CSP-8)

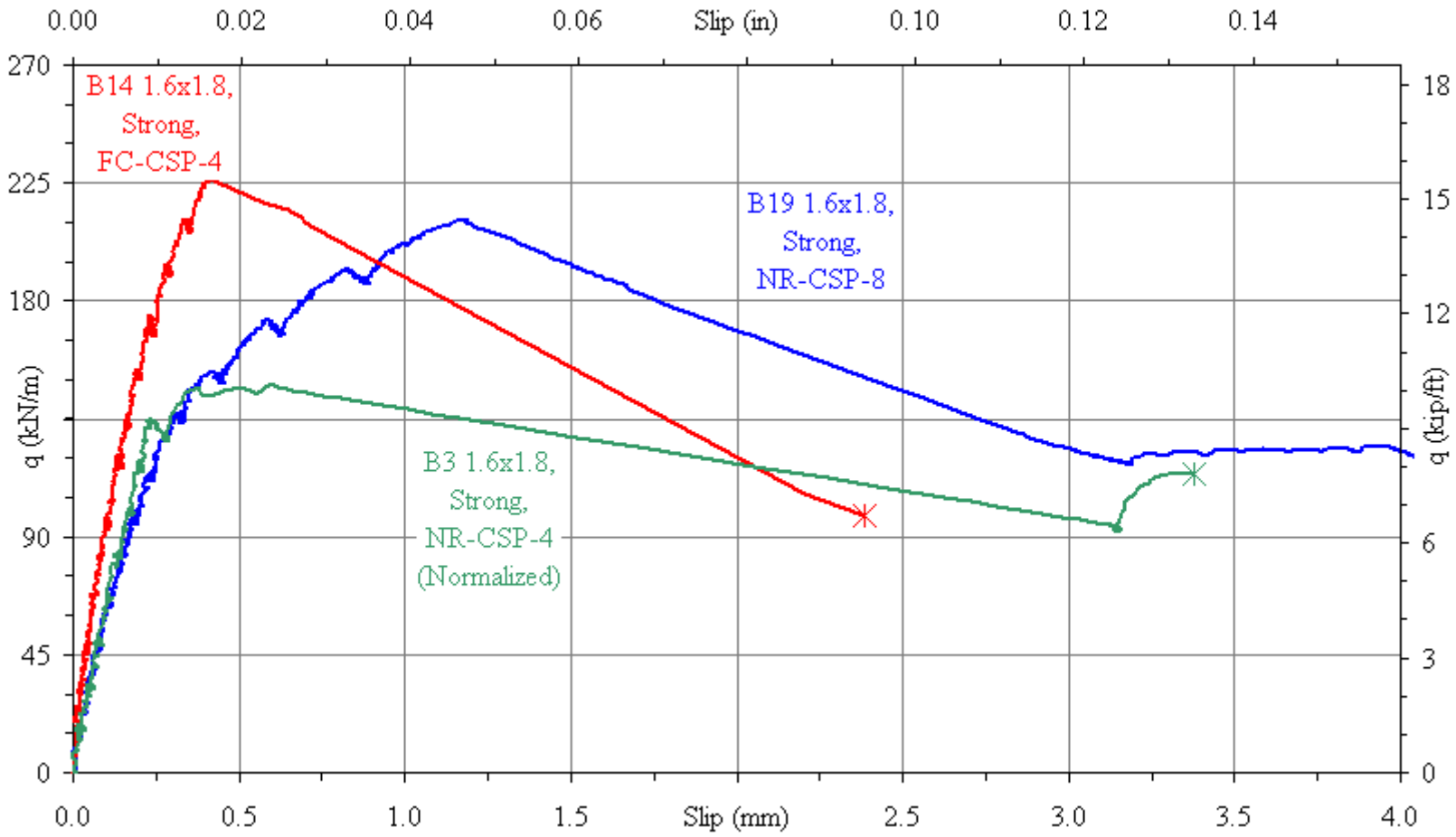

Figure 5-12 Comparison of 1.6x1.8 strong oriented C-Grid from both test series

5.4 DISCUSSION

5.4.1 Cold Joint Bond Integrity

Of the two main areas of interest for this series of tests, the first is whether premature debonding of the specimens (due to the C-Grid's interference with the bond between the two concrete layers) could be avoided by implementing one of two methods described in Section 5.2.1. It appears that both methods were successful, as none of the specimens suffered debonding issues like those from the previous tests. Note that the C-Grids used in this series of tests were ones that caused debonding failures in the previous series of tests from Chapter 4. No method appeared to be more effective than the other was; both methods achieved the desired results.

Chairing the specimen approximately 10-12 mm (0.4-0.5 in), as the results of the tension tests in Chapter 3 realized, reduced the negative impact of the C-Grid on the bond strength between the concrete layers. Despite the fact that the casting of the top layer of the concrete results in the C-Grid profile being, on average, forced downwards approximately half the height of the chair (see Figure 3-7) there appears to have been a sufficient amount of concrete flowing under the C-Grid such as to maintain sufficient bond strength. In this method, the top of the bottom layer of concrete (against which the C-Grid is placed) does not require an excessively roughened surface finish (such as CSP-8) and a lighter finish (CSP-4) can be used.

By creating a very rough surface finish on the bottom layer during its casting the overall surface area of the bottom layer is increased as well as allowing for the mechanical interlocking of the cold joint. Both of these add to the strength of the cold joint bond. In addition, the rough surface in a way acts as a built in chairing mechanism for the C-Grid. As illustrated in Figure 5-13, the "hills" of the surface act as a chair for the C-Grid raising it above the "valleys" of the surface. In this method, no chairing of the C-Grid is required and it can be laid flat on the surface placed with No Restraint.

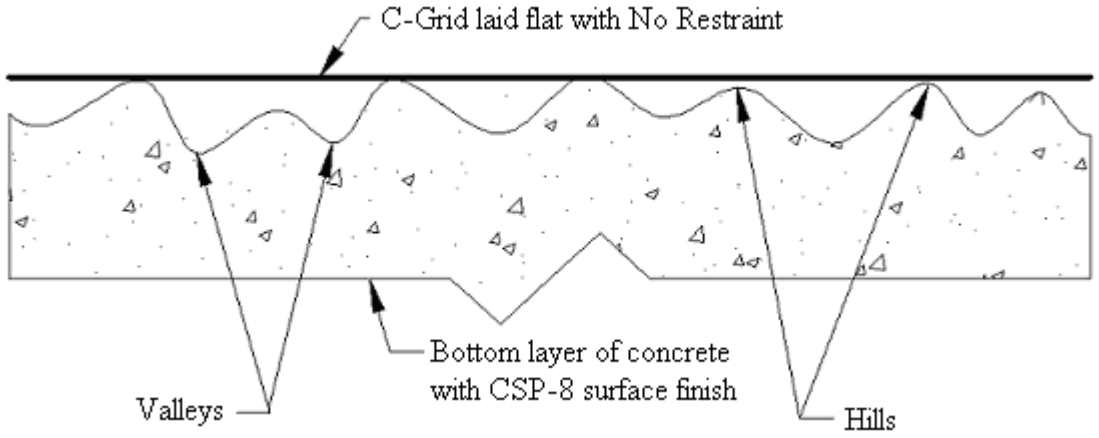

Figure 5-13 Rough surface finish profile view

As both methods appear to be successful, it is possible to select one or the other based on construction and cost considerations. In that regard, it must be decided which is the most cost and time effective route: chairing all of the C-Grid before placing the cast-in-place topping or applying a sufficiently rough surface finish to the Precast DT during the manufacturing process. This is beyond the scope of this research; however, it is clear that, especially with the use of a dense C-Grid reinforcement, one of these two methods should be implemented.

As a result, the paradoxical trend observed in Section 4.4.3 where denser C-Grids (and hence a larger reinforcement ratio) resulted in lower shear capacity values than the less dense C-Grids has been overturned. Recall that there were two C-Grid placement/surface finish treatment methods used (NR-CSP-4 and FC-CSP-8). Looking at the C-Grids of the former method in Figure 5-10 the 1.6x1.8 C-Grid, as would be expected, outperformed the 2.2x2.2 C-Grid. This same trend was observed in the latter method as seen in Figure 5-11. This reversal is indicative of the need to prevent premature debonding using one of the two methods described in this Chapter. If the debonding issue were not resolved, what may appear to be a stronger, denser, C-Grid reinforced concrete could turn out to be ***weaker*** in longitudinal shear than a less dense C-Grid size with a lower reinforcement ratio.

5.4.2 Comparison with WWF Reinforcement

The second area of interest with this second series of shear tests is comparing the C-Grid reinforced concrete behavior to that of traditional WWF reinforced concrete. Figure 5-8 shows a large difference in strength of the two WWF reinforced specimens, the one reinforced with the lighter gauge WWF (6x6 W1.7/W1.7) in fact performed no better than the control specimen. The heavier gauge WWF (6x6 W4.0/W4.0) performed very well and, as illustrated in Figure 5-5, was the only specimen to exhibit visible cracking along the line of shear before reaching the peak load capacity. This was expected since WWF is a more ductile material than C-Grid.

A comparison of the two materials (which are graphed in Figure 5-9) shows that the C-Grid reinforced specimens performed within a range bound by that of the WWF reinforced specimens, in terms of shear capacity. No C-Grid specimen reached the capacity achieved by the upper bound heavy gauge WWF reinforced specimen nor was any C-Grid specimen lower in capacity than the lower bound light gauge WWF.

With regard to deformability, the slip values obtained from the WWF reinforced specimens tended to border the values reached for the C-Grid in a similar fashion as they did for shear capacity. As can be seen in Figure 5-9 the only C-Grid specimen whose peak load occurred at a slip past the heavy gauge WWF was one of the 1.6x1.8 C-Grids (B19), but it was not by much. The remaining C-Grid reinforced specimens did not slip as much when peak capacity was reached, however they all reached slip values larger than that of the light gauge WWF.

These findings suggest that the C-Grids tested behave similarly to WWF in terms of longitudinal shear behavior. Consider that 6x6 WWF with intermediate gauge sizes in between that of the two used in this research exist (such as W2.1/W2.1, W2.5/W2.5, W2.9/W2.9, and W3.4/W3.4). It is reasonable to assume these would have shear-slip responses that fall within the range of the two that were tested (W1.7/W1.7 and W4.0/W4.0), which is where the C-Grid reinforced specimen longitudinal shear-slip responses' lie.

Therefore, this presents further evidence that C-Grid is a suitable reinforcement material. Like WWF, C-Grid can be selected to a size appropriate for the design needs and longitudinal shear strength on par with existing WWF reinforced toppings can be obtained. These results also provide the motivation to consider using existing shear-friction models to predict the longitudinal shear strength of C-Grid reinforced concrete.

5.4.3 Other Observations

In the first series of shear tests, 2.9x2.9 C-Grid in the two possible orientations (perpendicular and diagonal) were compared in Section 4.4.2 and it was found that the diagonal orientation had a slightly higher shear capacity than the perpendicularly oriented C-Grid. In this series of shear tests, 2.2x2.2 C-Grid was oriented in those directions and, again, a slight increase in shear capacity was observed, in this case 8% as seen in Figure 5-11. Therefore, it appears that orienting the C-Grid diagonally does not result in a large longitudinal shear capacity increase.

With respect to the C150 2.4 C-Grid, this was the best performing C-Grid used in this research, partly because it contains a large reinforcement ratio with 150,000 carbon fibers per strand, as opposed 50,000 carbon fibers per strand in all the other C-Grids. However, this unusual type of C-Grid, which is intended to take loads in only one direction, would not be a good selection for crack control. As was discussed in Section 2.2, crack control is one of the reasons for reinforcing cast-in-place toppings.

One final observation is made by comparing the shear-slip response of all the C50 1.6x1.8 strong direction oriented C-Grid reinforced specimens in both series of shear tests; of which there were three in total (one in the first series from Chapter 4, and two in this Chapter's second series). Since the first series of tests used a different concrete batch than the second, the first series specimen's shear-slip must be normalized to the second series. In order to do so, the shear per unit length q is normalized by the ratio of the square root of the compressive strengths of concrete (from Appendix C), as seen in Eq. [5-1]. This normalized q is plotted as B3 in Figure 5-12 along with the other 1.6x1.8 strong oriented C-Grids.

$$q_{\text{1st series normalized to 2nd series}} = q_{\text{1st series}} \left(\frac{\sqrt{f_c'}_{\text{2nd series}}}{\sqrt{f_c'}_{\text{1st series}}} \right) \quad [5\text{-}1]$$

As can be seen in that graph, the specimen from the first series of tests (B3) is considerably weaker (32% on average) than the specimens from the second series of tests (B14 and B19). The slip at peak load was also lower. Recall that specimen B3 suffered from premature debonding (so much so that it was the weakest C-Grid reinforced specimen from the first series of tests), whilst the specimens from the second series had no debonding issues. This observation further cements the idea that premature debonding must be avoided as it is detrimental to the overall shear capacity a C-Grid reinforced specimen can obtain.

Since the premature debonding of the cold joint (interface) problem has been resolved in this Chapter, it is now necessary to devise a mathematical model to predict the longitudinal shear capacity of C-Grid reinforced concrete. Since it has been shown in this Chapter that, within the scope of this research, C-Grid and WWF behave similarly (Section 5.4.2), Chapter 6 studies several shear-friction models from the literature and current practice that were developed for steel reinforcement and alters them to work with C-Grid reinforcement

CHAPTER 6 MODELING C-GRID REINFORCED CONCRETE SHEAR CAPACITY

6.1 OVERVIEW

As discussed in Section 2.5, the longitudinal shear strength of reinforced concrete elements can be modeled using shear-friction models. Since results from Chapter 5 showed that Carbon Fiber Grid (C-Grid) and Welded Wire Fabric (WWF) reinforced concrete specimens exhibit similar shear-slip behavior it is reasonable to believe that existing shear-friction models can be applied to C-Grid reinforced concrete. In this Chapter, the shear specimen's experimental data from Sections 4.3 and 5.3 are compared against such shear-friction models, despite the fact they were derived for steel reinforced concrete.

Each model from Section 2.5 considers the quantity of and yield strength of the reinforcement. Therefore, all graphs and data presented in this Chapter will plot along the ordinate the longitudinal shear capacity per unit length q and the reinforcement stiffness af_u along the abscissa; where a is the reinforcement area per unit length and f_u is the ultimate stress of the reinforcing material. For WWF, the ultimate stress will be considered the yield stress f_y and for C-Grid, the ultimate stress will be considered the rupture stress f_r. The term af_u is expressed in units of kip/ft or kN/m where 1 kip/ft is equal to 14.5939 kN/m. In addition, q will be expressed in units of kip/ft or kN/m.

For WWF, the term af_u is determined by taking the cross-sectional area of an individual wire times the number of wires per unit length (a), then multiplying by the yield stress (f_y) as determined through the tension tests of Appendix E. This is illustrated in the following equation:

$$af_u = (\text{Yield Stress})(\text{Wire Cross Sectional Area})\left(\frac{\text{No. Wires}}{\text{Unit Length}}\right) \qquad [6\text{-}1]$$

For C-Grid, it is necessary to use the rupture strength (f_r) since C-Grid does not have a yield plateau since it is a linear-elastic material. Additionally, C-Grid, unlike WWF, does not have a measurable cross-sectional area because C-Grid is a composite material of carbon

fibers and epoxy resin resulting in an irregular and varying cross-sectional shape. This makes the determination of the individual terms of the reinforcement stiffness impractical, however the combined term af_u can be indirectly calculated by taking the number of strands per unit length (units: L^{-1}) and multiplying by the rupture load of an individual C-Grid strand (units: F) as determined in Appendix D. This indirectly results in the term af_u (units: FL^{-1}). This is acceptable given that the cross-sectional area per strand cancels out as illustrated by the following equation:

$$af_u = \left(\cancel{\text{Cross Section Area}} \times \frac{\text{No. Strands}}{\text{Unit Length}} \right) \left(\frac{\text{Strand Rupture Load}}{\cancel{\text{Cross Section Area}}} \right) \qquad [6\text{-}2]$$

Appendix D and Appendix E also calculate af_u for each C-Grid and WWF reinforced single-shear specimen, respectively. The values for q come from the calculated Peak Shear per unit length as determined in Table 4-2 and Table 5-3. These values are concisely presented in Table 6-1. Recall from the previous two Chapters that some specimens were discarded (B4, B5, and B16) and therefore are not used in this Chapter. Also not used are the control specimens (B1, B2, B11, B12, and B13) as they are not representative of the shear-friction mechanism.

Table 6-1 Summary of experimental data

Series No.	Specimen No.	Specimen Details: reinforcement type, size, orientation of strands/wires, reinforcement placement (chairing-surface roughness)	q		af_u	
			(kN/m)	(kip/ft)	(kN/m)	(kip/ft)
1	**B3**	C-Grid, C50 1.6 x 1.8, Strong, NR-CSP-4	172.9	11.8	102.7	7.04
	B6	C-Grid, C50 2.9 x 2.9, Perpendicular, NR-CSP-4	215.6	14.8	54.3	3.72
	B7	C-Grid, C50 3.5 x 4.0, Strong, NR-CSP-4	253.8	17.4	47.2	3.23
	B8	C-Grid, C50 3.5 x 4.0, Weak, NR-CSP-4	212.4	14.6	50.6	3.47
	B9	C-Grid, C50 2.2 x 2.2, Diagonal, NR-CSP-4	253.0	17.3	76.8	5.26
	B10	C-Grid, C50 2.9 x 2.9, Diagonal, NR-CSP-4	237.2	16.3	57.6	3.95
2	**B14**	C-Grid, C50 1.6x1.8, Strong, FC-CSP-4	231.6	15.9	102.7	7.04
	B15	C-Grid, C50 2.2x2.2, Perpendicular, FC-CSP-4	216.3	14.8	72.4	4.96
	B17	WWF, 6x6 W1.7/W1.7, Perpendicular, WC-CSP-4	157.6	10.8	38.5	2.64
	B18	WWF, 6x6, W4.0/W4.0, Perpendicular, WC-CSP-4	254.9	17.5	104.2	7.14
	B19	C-Grid, C50 1.6x1.8, Strong, NR-CSP-8	213.8	14.6	102.7	7.04
	B20	C-Grid, C50 2.2x2.2, perpendicular, NR-CSP-8	166.0	11.4	72.4	4.96
	B21	C-Grid, C50 2.2x2.2, Diagonal, NR-CSP-8	178.7	12.2	76.8	5.26
	B22	C-Grid, C150 2.4, Perpendicular, NR-CSP-8	243.3	16.7	203.0	13.90

6.2 LONGITUDINAL SHEAR-FRICTION MODELS

This section will briefly re-introduce and modify the models derived from the literature (Chapter 2). The models are modified for two reasons. The first is to be applicable to this specific research. The second is so that the nomenclature introduced in Section 6.1 is used, thus the models predict a shear flow q and terms for the quantity and strength of reinforcement is inputted in terms of reinforcement stiffness af_u. Therefore, the terms are consistent throughout this Chapter.

6.2.1 ACI 318-08

Recall from Section 2.5.1 the "shear-friction design method" from ACI 318-08 §11.7.4 gives the shear capacity in pounds of a reinforced concrete element as:

$$V_n = A_{vf}\, f_y \mu \qquad [6\text{-}3]$$

Equation [6-3] is modified to use terms of shear flow q and reinforcement area per unit length a by dividing both sides by the length of the shear plane L. In addition, the term f_u – which in turn is interpreted as f_y for WWF and f_r for C-Grid – is substituted for f_y. Since this research used normalweight concrete and concrete cast monolithically at the shear plane the values for λ and μ are 1.0 and 1.4, respectively. This results in the equation:

$$q = 1.4 a f_u$$

where

$$q = \frac{V_n}{L} \qquad [6\text{-}4]$$

$$a = \frac{A_{vf}}{L}$$

Recall that ACI 318-08 also gives the following upper bounds to the shear strength:

$$V_n = \min\begin{Bmatrix} 800 A_c \\ 0.2 f_c' A_c \end{Bmatrix} \qquad [6\text{-}5]$$

Note that Eq. [6-5] is not dimensionally correct and is meant to be used with in and lb units only.

Consider that the concrete strengths for the first and second series of tests are f_c' = 26.54 MPa (3849 psi) and f_c' = 20.55 MPa (2981 psi), respectively (Appendix C). Also consider that the nominal depth and length of the layer of concrete resisting shear with both series of tests is d = 69.85 mm (2.75 in) and L = 457.2 mm (18 in), respectively. Given this, the upper bound limits from Eq. [6-5] can be calculated as 169.50 kN (38105 lb) and 131.28 kN (29512 lb) for the first and second series, respectively. Note that the limit of $800A_c$, or 176.15 kN (39600 lb), does not govern for either series. In terms of shear flow q, the upper bounds are 370.7 kN/m (25.4 kip/ft) and 287.2 kN/m (19.68 kip/ft) for the first and second series, respectively. Another consideration is the application of the strength reduction factor φ. In this case φ should be taken as 0.65 for design or otherwise as 1.0.

Combining equations [6-4] and [6-5] as well as adding the term φ results in the following model, in SI metric:

$$q = 1.4\phi a f_u$$
$$q_{1st\ series} \le 370.7\phi \text{ kN/m} \qquad [6\text{-}6]a$$
$$q_{2nd\ series} \le 287.2\phi \text{ kN/m}$$

or the following in U.S. customary:

$$q = 1.4\phi a f_u$$
$$q_{1st\ series} \le 25.4\phi \text{ kip/ft} \qquad [6\text{-}6]b$$
$$q_{2nd\ series} \le 19.68\phi \text{ kN/m}$$

6.2.2 6th Edition of the PCI Design Handbook

Recall from Section 2.5.2 that the sixth edition of the Precast Concrete Institute Design Handbook §4.3.6 contains a model for Shear-Friction resistance as follows:

$$A_{vf} = \frac{V_u}{\phi f_y \mu_e}$$

where [6-7]

$$\mu_e = \frac{1000 \lambda A_{cr} \mu}{V_u}$$

In this equation, φ is the strength reduction factor (which in this case would be 0.75 for design or 1.0 otherwise). In addition, V_u is the applied ***factored*** shear force in lb.

Equation [6-7] can be simplified specifically for the purposes of this research by substituting μ_e and rearranging the equation to solve for V_u. It can also be simplified by using the appropriate values for μ, λ, and A_{cr} for this research. As the concrete used was normalweight, λ = 1.0. The concrete crack interface condition was concrete-to-concrete, cast monolithically, therefore μ = 1.4 and μ_e is limited to 3.4. Also, given that the depth and length of the shear plane is 69.85 mm (2.75 in) and 457.2 mm (18 in), respectively, A_{cr} = 3.19 x 10^5 mm^2 (49.5 in^2), and Eq. [6-7] can be rewritten as:

$$V_u = \begin{cases} \sqrt{69300 \phi f_y A_{vf}} & \text{if } V_u \geq 20382 \text{ lb} \\ 3.4 \phi f_y A_{vf} & \text{if } V_u < 20382 \text{ lb} \end{cases} \quad [6\text{-}8]$$

Note that Eq. [6-7] and [6-8] are empirical (i.e. not dimensionally correct) and require the use of in and lb units.

Before expressing Eq. [6-8] in terms of shear flow, the fact that V_u is a ***factored*** shear force must be addressed. In order to utilize the nominal shear force (V_n, as was used in Section 6.2.1 with the ACI model) it will be necessary to derive a factor based on expected loading conditions. Given the scope of this research, wind and earthquake loads are likely to dominate; therefore, a load factor of 1.6 is appropriate, resulting in:

$$V_u = 1.6 V_n \quad [6\text{-}9]$$

Substituting Eq. [6-9] into Eq. [6-8] results in:

$$V_n = \begin{Bmatrix} \sqrt{27070\phi f_y A_{vf}} & \text{if } V_n \geq 12739 \text{ lb} \\ 2.125\phi f_y A_{vf} & \text{if } V_n < 12739 \text{ lb} \end{Bmatrix} \quad [6\text{-}10]$$

Equation [6-10] can now be altered to use the variables of this Chapter (q and af_u) as well as the units of this chapter (kip/ft or kN/m). For SI metric, this results in:

$$q = \begin{Bmatrix} \sqrt{263.3\phi a f_u} & \text{if } q \geq 123.9 \text{ kN/m} \\ 2.125\phi a f_u & \text{if } q < 123.9 \text{ kN/m} \end{Bmatrix} \quad [6\text{-}11]a$$

or the following in US customary:

$$q = \begin{Bmatrix} \sqrt{18.05\phi a f_u} & \text{if } q \geq 8.493 \text{ kip/ft} \\ 2.125\phi a f_u & \text{if } q < 8.493 \text{ kip/ft} \end{Bmatrix} \quad [6\text{-}11]b$$

6.2.3 Oehlers & Bradford (Modified Mattock Model)

Recall from Section 2.5.3 the model originally developed by the combined work of Mattock & Hawkins (1972) and Mattock et al (1975). The model was then further developed and modified by Oehlers & Bradford (1995) and Oehlers & Bradford (1999) as seen in Section 2.5.4. This modified model is given as:

$$Q_{ch} = v_{lock} + v_{dow} + v_{fric} \quad [6\text{-}12]$$

where v_{lock} is defined as:

$$v_{lock} = \Gamma f_{ct} L_p$$

where

$$\Gamma = \begin{Bmatrix} 0.66 \text{ cracked concrete, characteristic strength} \\ 1.1 \text{ cracked concrete, mean strength} \\ 1.6 \text{ un-cracked concrete, mean strength} \end{Bmatrix} \quad [6\text{-}13]$$

$$f_{ct} = 0.4\sqrt{f_c'}$$

where v_{dow} is defined as:

$$v_{dow} = 0.8 A_{tr} f_{yr} \quad [6\text{-}14]$$

and where v_{fric} is defined as:

$$v_{fric} = 0.8F_{nf} \quad [6\text{-}15]$$

In this form, equations [6-12] through [6-15] are already in terms of shear flow. In addition, the units of equations [6-12] through [6-15] use units of N and mm. Thus, the terms q and af_u can be substituted directly for Q_{ch} and $A_{tr}f_{yr}$, respectively. In addition, since no applied active normal forces were applied to the shear specimens in this research, Eq. [6-15] can be eliminated. Equation [6-12] can be simplified and the nomenclature of this Chapter substituted to give the following:

$$q = \frac{2L_p\Gamma\sqrt{f_c'} + 4af_u}{5} \quad [6\text{-}16]$$

It should be noted that this equation is not dimensionally correct, and only units of N and mm may be used.

Also, recall from Section 2.5.4 the lower bound limit placed on the value of v_{dow}:

$$A_{tr} f_{yr} \geq 0.66 f_{ct} L_p \quad [6\text{-}17]$$

which can be rewritten as:

$$af_u \geq 0.66 f_{ct} L_p \quad [6\text{-}18]$$

As was discussed in Section 2.5.3 and 2.5.4, the reason for this limit is the need for a minimum dowel force (v_{dow}) to completely develop the concrete interlock force (v_{lock}). When this limit is violated, the contribution of v_{lock} was shown to decrease in a parabolic manner to the point where v_{lock} is zero when v_{dow} is zero. This is logical, as it would be impossible for a cracked concrete section to resist any shear without transverse reinforcement to tie the crack together. Because the parabolic equations are not given, they will be derived in this Section. The parabolic equation can be derived since the end-points of the parabola are known (points 0 and B of Figure 2-8) as well as the slope of the parabola at point B (which is 0.8, as seen in Figure 2-8).

First, a ratio Ξ is defined from Eq. [6-18]:

$$\Xi = \frac{af_u}{0.66 f_{ct} L_p} \qquad [6\text{-}19]$$

such that, if $\Xi \geq 1$, then v_{dow} is above the lower bound of Eq. [6-18] and the full value of v_{lock} is used with the original concrete/statistical coefficient Γ of Eq. [6-13].

However, in the case when $\Xi < 1$ (i.e. v_{dow} is insufficient to use the full value of v_{lock}) then Γ is determined by the following parabolic equation:

$$\Gamma = c_2 \Xi^2 + c_1 \Xi \qquad [6\text{-}20]$$

where the constants c_1 and c_2 are presented in Table 6-2 which vary according to the original value of Γ. Note again that these equations are not dimensionally correct and only units of N and mm may be used.

Table 6-2 Constants c_1 and c_2

Constant	Γ=0.66	Γ =1.1	Γ =1.6
c_1	1.32	2.2	3.2
c_2	-0.66	-1.1	-1.6

As an alternative to the use of Eq. [6-20], one could simply use a conservative idealized linear equation, again related to Γ. It can be derived by fitting a straight-line segment from the point where $\Xi = 1$ (where v_{dow} is at its minimum in order to sustain the full value of the v_{lock}), to the point where $\Xi = 0$ (when $af_u = 0$, $v_{dow} = 0$, and therefore $q = 0$). This again is point B and 0 of Figure 2-8, respectively. This results in:

$$q = \begin{Bmatrix} 1.8af_u & \text{if } \Gamma = 0.66 \\ 2.465af_u & \text{if } \Gamma = 1.1 \\ 3.224af_u & \text{if } \Gamma = 1.6 \end{Bmatrix} \qquad [6\text{-}21]$$

Finally, recall there is an upper bound to the permissible shear strength using this model, which is rewritten in the nomenclature of this Chapter as:

$$q \leq 0.3 f_c^{'} L_p \qquad [6\text{-}22]$$

Using the values of the concrete compressive strengths from Appendix C, the limits from for the first and second series of shear tests are 556.0 kN/m (38.01 kip/ft) and 430.6 kN/m (29.51 kip/ft), respectively. Given that the largest shear flow strength obtained experimentally was 254.9 kN/m (17.47 kip/ft), the upper bound limit does not control the predictions and thus can be ignored.

The model can be used in one of two forms, differing by the two approaches taken to model the region $0 \leq \Xi \leq 1$. The first is termed the *parabolic* Oehlers & Bradford model:

$$q = \frac{2L_p \Gamma \sqrt{f_c'} + 4af_u}{5}$$

where

$$\Gamma = \begin{Bmatrix} \begin{Bmatrix} 0.66 & \Xi > 1 \\ -0.66\Xi^2 + 1.32\Xi & 0 \leq \Xi \leq 1 \end{Bmatrix} & \text{cracked characteristic} \\ \begin{Bmatrix} 1.1 & \Xi > 1 \\ -1.1\Xi^2 + 2.2\Xi & 0 \leq \Xi \leq 1 \end{Bmatrix} & \text{cracked mean} \\ \begin{Bmatrix} 1.6 & \Xi > 1 \\ -1.6\Xi^2 + 3.2\Xi & 0 \leq \Xi \leq 1 \end{Bmatrix} & \text{uncracked mean} \end{Bmatrix} \quad [6\text{-}23]$$

$$\Xi = \frac{af_u}{0.66 f_{ct} L_p}$$

The second is termed the *simplified* (linear) Oehlers & Bradford model:

$$q = \frac{2L_p \Gamma \sqrt{f_c'} + 4af_u}{5} \quad \text{if } \Xi = \frac{af_u}{0.66 f_{ct} L_p} > 1$$

else

$$q = \begin{Bmatrix} 1.8af_u & \text{cracked characteristic} \\ 2.465af_u & \text{cracked mean} \\ 3.224af_u & \text{uncracked mean} \end{Bmatrix} \quad [6\text{-}24]$$

6.3 COMPARISON OF SHEAR-FRICTION MODELS TO EXPERIMENTAL DATA

6.3.1 General

When plotting the shear flow strength q against the reinforcement stiffness af_u for just the experimental data by itself in Figure 6-1, a couple of data points stand out as outliers. From the first series, (denoted by circles) specimen B3 (C50 1.6x1.8, strong, flat, smooth) has a shear capacity considerably lower than the rest of the group as it failed prematurely by interface debonding, as described in Section 4.4.3. This further illustrates the negative effects of premature debonding, as looking at this graph alone shows the sub-standard performance of specimen B3. The second series (denoted by triangles) specimen that appears as an outlier from its group is B22 (C150 2.4). Specimen B22 has a much higher reinforcement stiffness than any other specimen tested in this experimental program.

Also, note that within the second series of tests, WWF reinforced specimens are denoted by hollow triangles. Recall from Figure 5-9 that the WWF reinforced specimens appeared to bracket all of the C-Grid reinforced specimens in terms of shear flow strength q. In Figure 6-1, it is clearly seen that the WWF specimens also bracket the C-Grid specimens in terms of reinforcement stiffness, with the exception of the B22 outlier. This is further evidence that WWF and C-Grid behave similarly in longitudinal shear, as discussed in Chapter 5.

When comparing one series of shear tests to another, it is clear that the first series was stronger than the second series. This is likely due to the fact that the concrete strength for the second series was slightly lower at 26.53 MPa (3848 psi) versus 20.55 MPa (2980 psi) for the first series, a difference of about 25%.

Appendix F contains all of the calculated ($q_{predicted}$) maximum shear flow values from each specimen using each shear-friction model in addition to the experimental data ($q_{measured}$). In Table 6-3, the Average Under-Prediction is the amount each model under predicts the experimental data with larger values indicating a more conservative model and negative

values reflecting an un-conservative over-prediction. The Most Conservative and Least Conservative columns reflect each shear-friction models' most or least extreme under-prediction of the strength of an individual test specimen, respectively. If a particular model over-predicts any of the individual test specimen's strength, then the Least Conservative column will contain a negative value. Also, note that in these calculations Table 6-3 excludes the previously discussed "outlier" specimens B3 and B22. These calculations are meant to determine if the models are suitable for design purposes within the scope of this research (i.e. a model that is conservative) as well as to determine the relative efficiency of the models (i.e. a model whose conservatism is not extreme, which would result in excessive over-design).

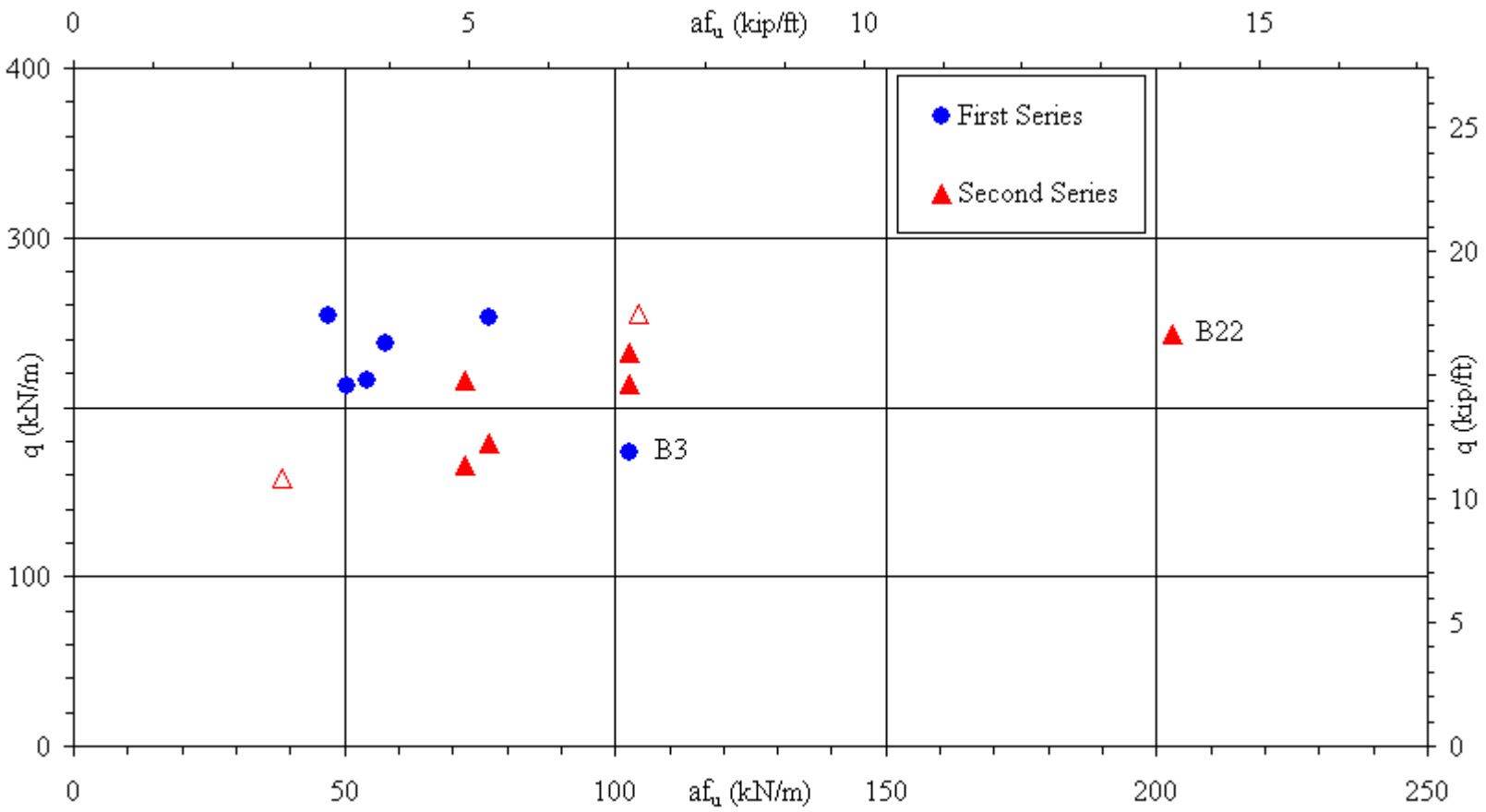

Figure 6-1 Experimental data

Table 6-3 Summary of conservativeness of the shear-friction models

Model Name	φ or Γ	Equation	Average Under-Prediction	Most Conservative	Least Conservative
ACI	φ = 1.0	[6-6]	76.2 %	86.7 %	65.7 %
ACI	φ = 0.65	[6-6]	84.5 %	91.4 %	77.7 %
PCI	φ = 1.0	[6-11]	35.0 %	60.5 %	7.30 %
PCI	φ = 0.75	[6-11]	49.2 %	70.4 %	30.5 %
Oehlers & Bradford	Γ = 0.66	[6-23]	36.0 %	57.2 %	15.7 %
Oehlers & Bradford	Γ = 1.1	[6-23]	11.1 %	38.5 %	-17.3 %
Oehlers & Bradford	Γ = 1.6	[6-23]	-17.2 %	17.4 %	-54.8 %
Simplified Oehlers & Bradford	Γ = 0.66	[6-24]	42.1 %	66.5 %	21.5 %
Simplified Oehlers & Bradford	Γ = 1.1	[6-24]	21.3 %	54.1 %	-7.60 %
Simplified Oehlers & Bradford	Γ = 1.6	[6-24]	-2.40 %	40.0 %	-40.6 %

6.3.2 Comparison of ACI 318-08 to Experimental Data

Figure 6-2 compares the experimental data with Eq. [6-6] which was derived from the ACI 318-08 shear-friction model. Because of the use of two different concrete strengths and two potential values for φ, four lines are shown. For lines with the same strength reduction factor, the slope of the lines is the same but, because of the different concrete strengths, the upper bounds are different.

Compared to the experimental data, the ACI model is extremely conservative. So much so that for design, when φ = 0.65, the model under-predicts the strength of both outliers. Of the non-outlier specimens from Table 6-3, the average under-prediction was 84.5% with a range of 77.7% to 91.4%. In other words, the ACI model under-predicts the strength by a factor of about 6.5 with a range from a factor of 4.5 to a factor of 11.6. Even without the use of the strength reduction factor φ the model under-predicts the strength by a factor of 4.2 on average.

This model is certainly safe for use in design within the scope of this research. However, the amount of overdesign as a result of using this model would make said design inefficient. It is again interesting to note that the model does not consider the concrete strength. This is contrary to the results of this research that suggest a difference in concrete strength has an impact on the overall shear strength.

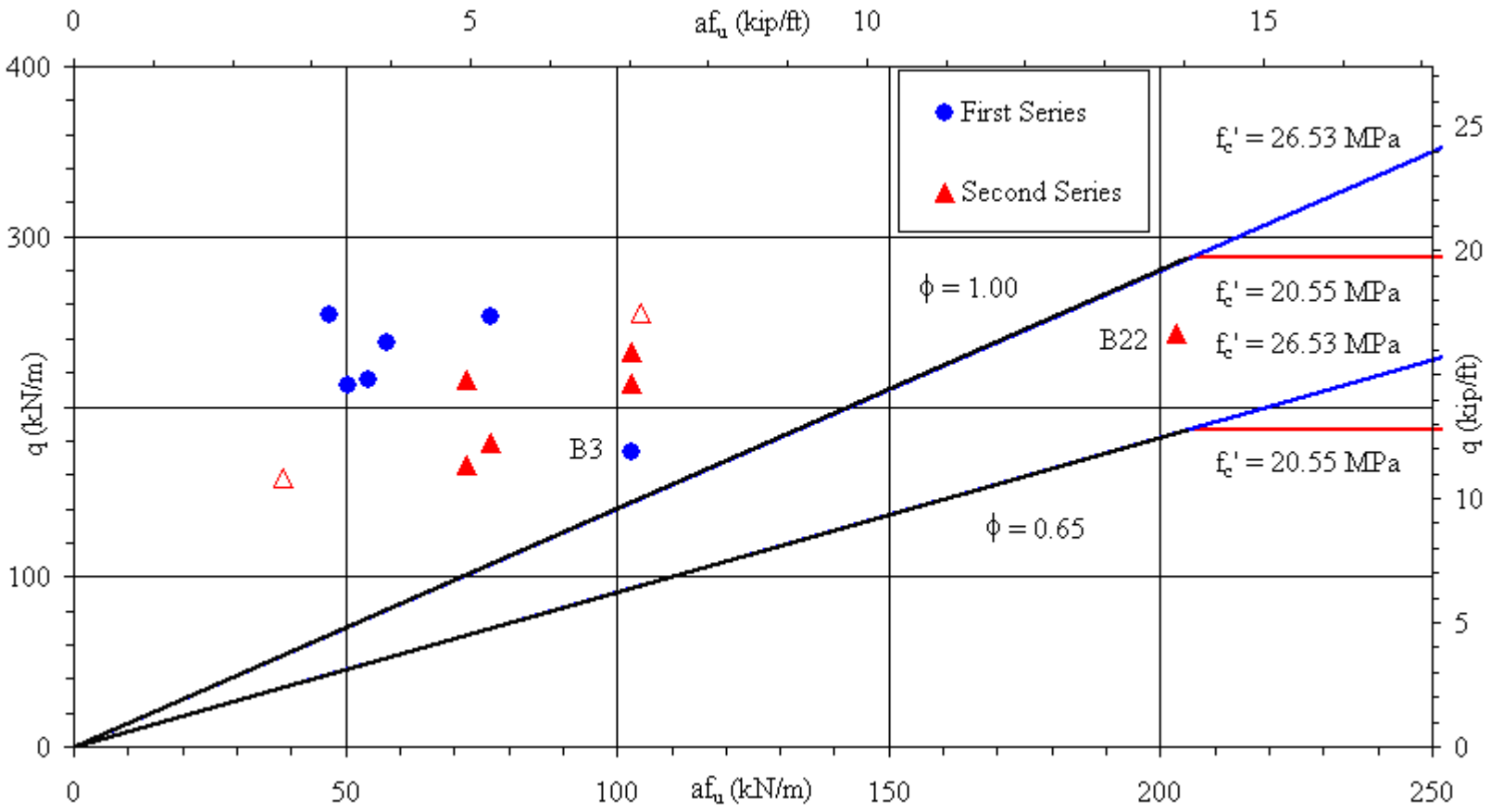

Figure 6-2 Comparison of ACI 318-08 shear-friction model

6.3.3 Comparison of 6th Edition of PCI Design Handbook to Experimental Data

Figure 6-3 compares the experimental data with Eq. [6-11], which was derived from the PCI shear-friction model. Because of the two possible values for φ (0.75 in design and 1.0 otherwise), there are two curves.

Compared to the experimental data, the PCI model is moderately conservative. The model under-predicts the strength of all specimens including both of the outliers, even when the strength reduction factor φ is taken as 1.0. From Table 6-3, using φ of 0.75 the under-prediction was on average 49.2% with a range of 30.5% to 70.4%. In other words, the PCI model under-predicts the strength by a factor of about 2.0 with a range from a factor of 1.7 to 3.4. Without the use of the strength reduction factor φ the model under-predicts the strength by a factor of 1.5 on average with a range of 1.1 to 2.5.

This model is also safe for use in design. The amount of overdesign using the PCI model is not excessive. It is again worth noting that the model, like the ACI shear-friction model discussed previously, does not consider the concrete strength.

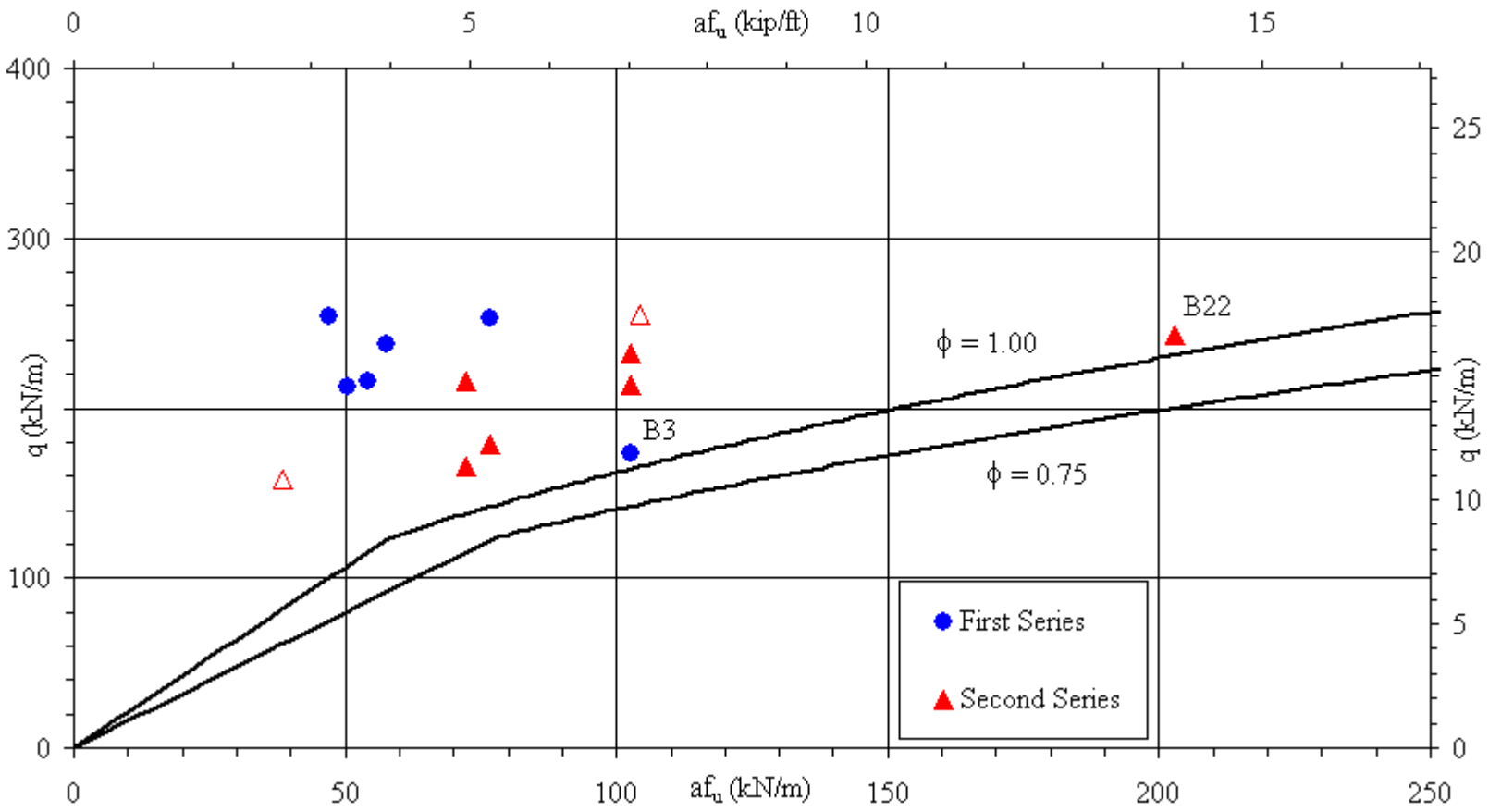

Figure 6-3 Comparison of PCI 6th ed. design handbook shear-friction model

6.3.4 Comparison of Oehlers & Bradford to Experimental Data

In the design of concrete for shear and shear-friction, it is generally assumed that the concrete is fully cracked. It general it cannot be assumed that a concrete section will remain uncracked, due to many factors such as long-term effects, handling, and construction. Therefore, the assumption of an always fully cracked concrete plane is conservative. Most design equations do not even include an option to model the uncracked concrete condition; however the Oehlers & Bradford model does thanks to the concrete/statistical coefficient Γ. Consider for example the value of $\Gamma = 1.1$ for a cracked shear plane and $\Gamma = 1.6$ for an uncracked shear plane, both representing the mean strength (as opposed to characteristic or design strength). They are expected to represent the bounds of the shear capacity with the experimental data points falling in between. Although there were no visible cracks along the line of shear, it is likely that there was some micro-cracking present.

Figure 6-4 and Figure 6-5 plot the modified Oehlers & Bradford model, Eq. [6-23] from Section 2.5.4, with $\Gamma = 1.1$ and $\Gamma = 1.6$ along with each set of data from each test series (with varying f_c' for clarity), the former being for the first series of tests (B1-B10) and the latter for the second series of tests (B11-B22). These curves are most useful when the objective is to get an accurate prediction (rather than a lower bound design prediction) of the shear capacity. There is recognition that the overall shear strength can vary considerably depending on whether the concrete is cracked along the line of shear, as discussed previously.

Indeed, most of the measured values do fall in between or near the two curves. The only points that diverge significantly are the outliers discussed in Section 6.3.1. The debonded specimen (B3), being considerably below the $\Gamma = 1.1$ curve is obvious, however it is not clear why the C150 2.4 C-Grid (B22) specimen appears to lie so far outside this mean lower bound. With only one specimen using this unique C-Grid with a very high reinforcement ratio, it is not possible to make any conclusions. It is also interesting to note that the first series of shear tests, with the higher concrete strength, were nearer to the curve

representing the uncracked condition (Figure 6-4). The second series of tests, with the lower concrete strength, were nearer to the curve representing the cracked condition (Figure 6-5).

For design, the Oehlers & Bradford model uses $\Gamma = 0.66$ to represent the characteristic, cracked condition. In this form, the model predicts the lower bound design (characteristic) shear capacity instead of the mean shear capacity. The parabolic model, given by Eq. [6-23], is plotted in Figure 6-6 and the simplified (linear) model, given by Eq. [6-24], is plotted in Figure 6-7.

The characteristic equation is reasonably conservative for all data points, including the outlier specimens. The simplified model is also shown to be a safe and reasonable idealization. As seen in Table 6-3, the average under-prediction of the parabolic and simplified model is 36.0% and 42.1%, respectively. This means the parabolic and simplified Oehlers & Bradford models, in design mode, under-predict the shear capacity by a factor of approximately 1.6 and 1.7, respectively. The simplified model will always be slightly more conservative due to the nature of the idealization. The simplified model may be more desirable for design due to its ease of implementation.

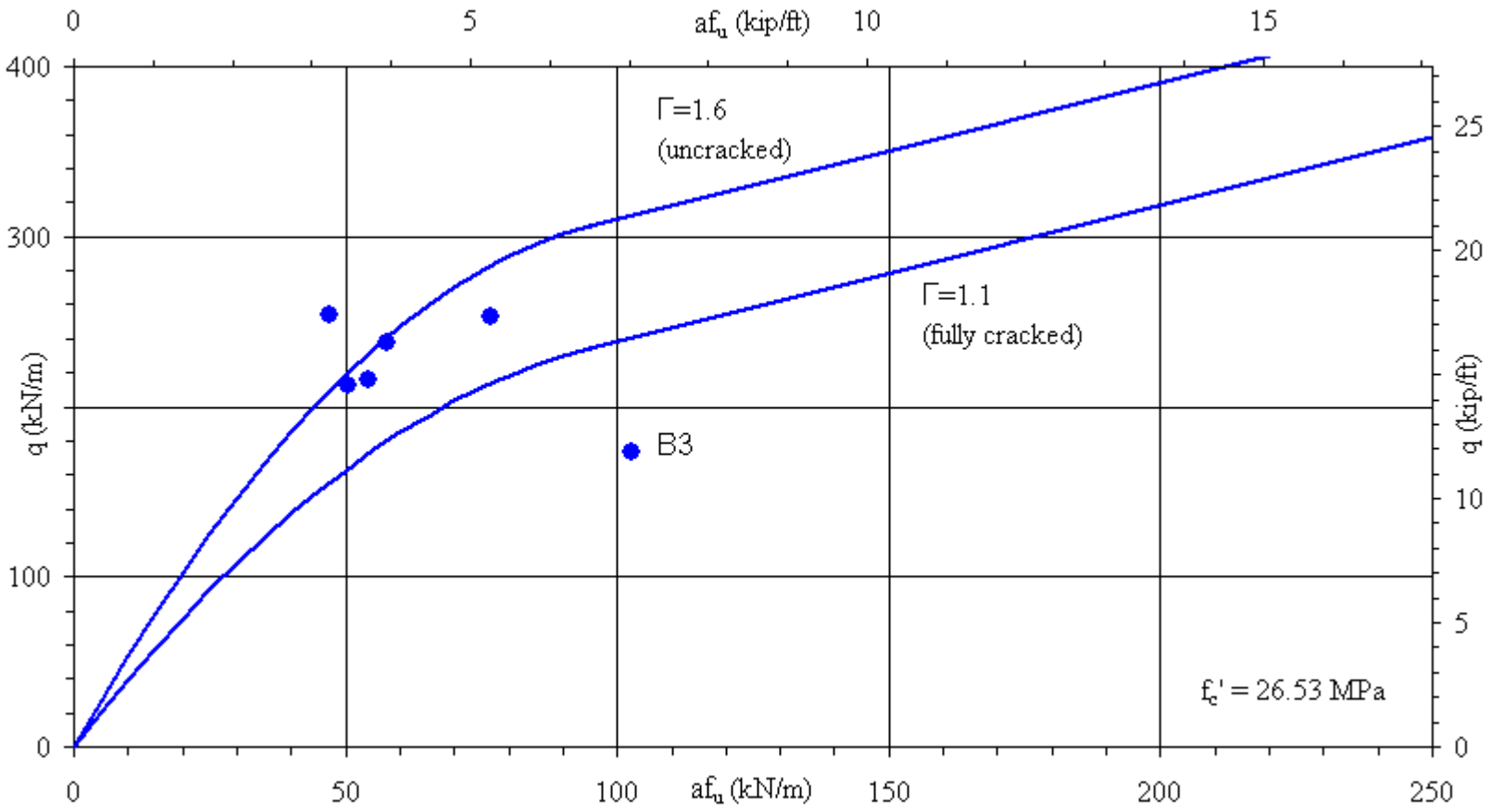

Figure 6-4 Comparison of Oehlers & Bradford mean shear-friction model (first series)

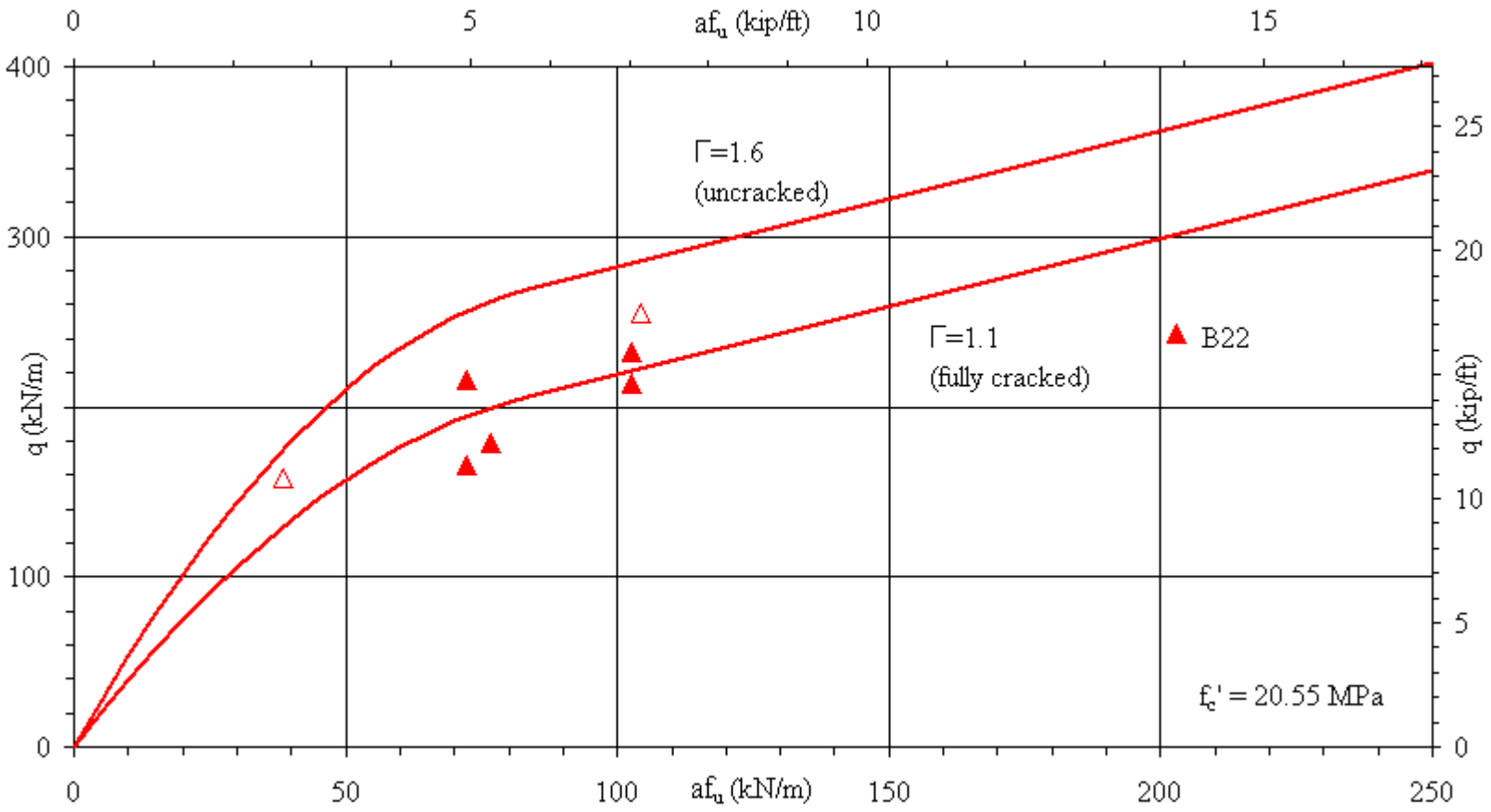

Figure 6-5 Comparison of Oehlers & Bradford mean shear-friction model (second series)

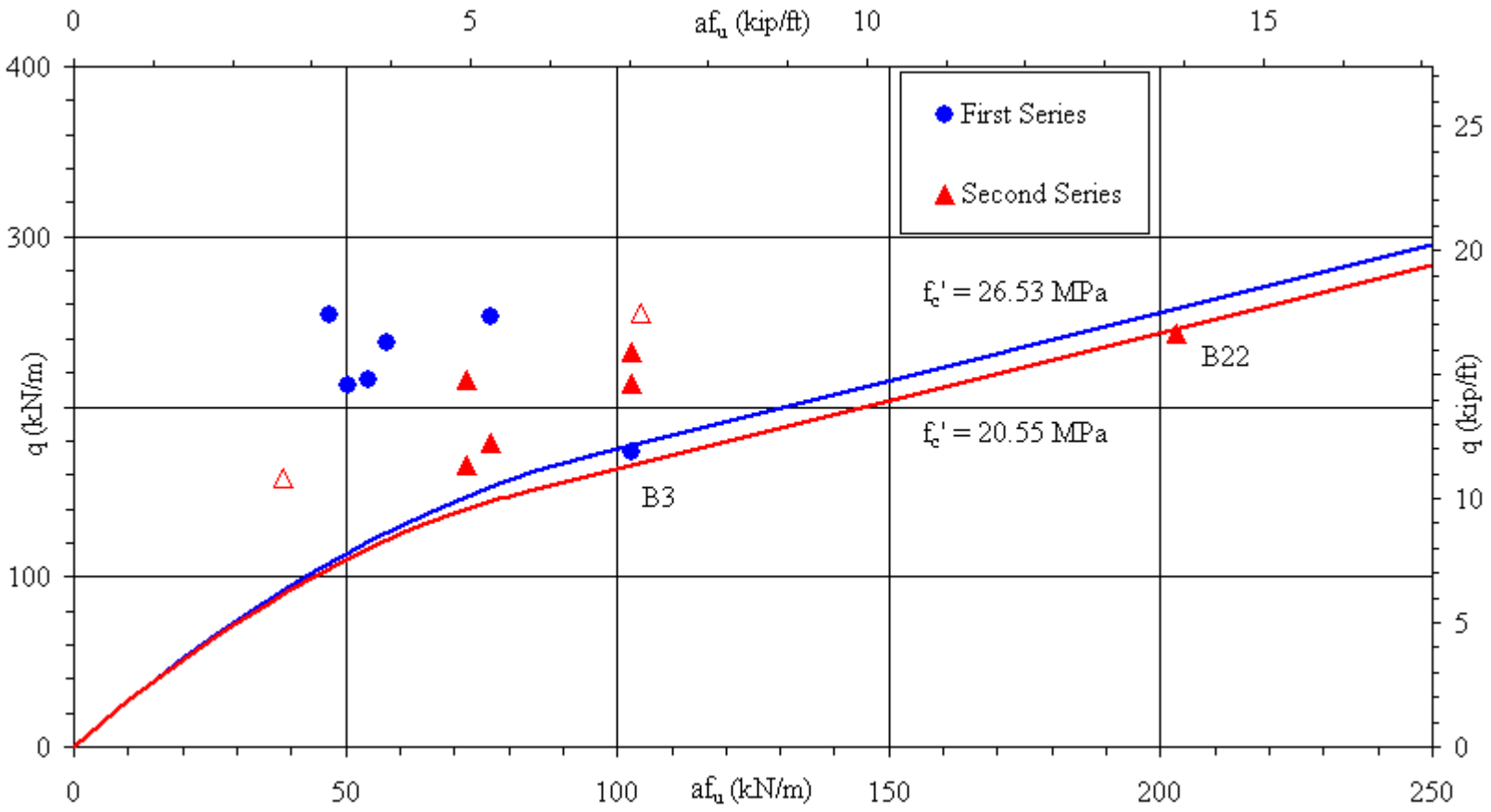

Figure 6-6 Comparison of Oehlers & Bradford design shear-friction model

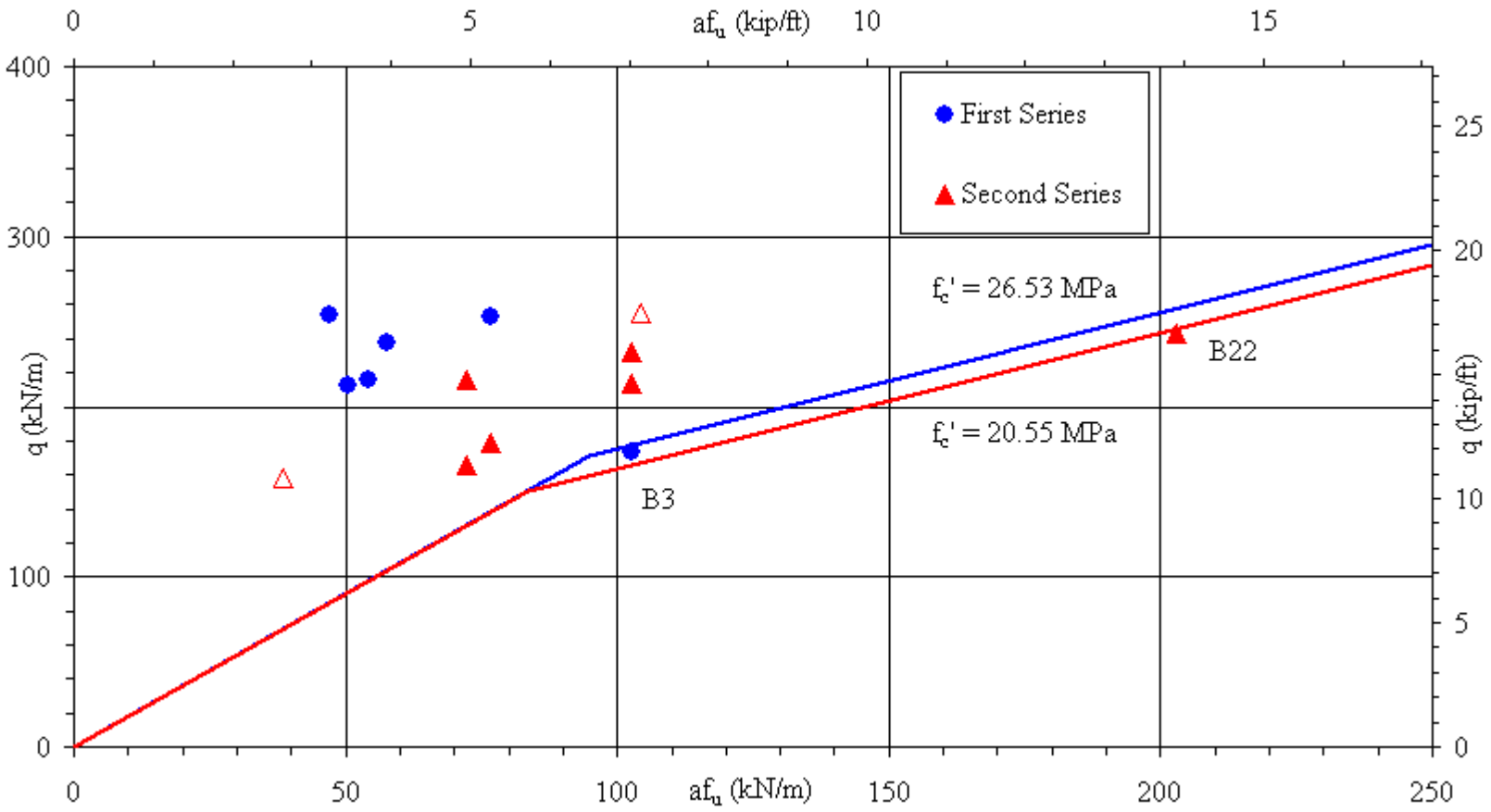

Figure 6-7 Comparison of Oehlers & Bradford simplified design shear-friction model

6.4 DISCUSSION

For design with normal strength concrete and within the parameters considered in this research, any of the three models would be acceptable for use. Each model was conservative, and did not overestimate the shear capacity of any of the specimens, including the two outlier specimens. Because the ACI and PCI models do not factor in the strength of the concrete, it may not be advisable to use them in applications where the concrete compressive strength is considerably higher or lower than normal strength.

Overall the ACI model ($\varphi = 0.65$) was the most conservative with an average under-prediction of the experimental data of 84.5 %. The Oehlers & Bradford model, in design (characteristic) mode, was the least conservative with an average under-prediction of the experimental data of 36.0 % or 42.1% for the parabolic and simplified version, respectively. The PCI model ($\varphi = 0.75$) fell between the two with an average under-prediction of 49.2 %. With regard to simplicity of calculation, the ACI model is the simplest, while Oehlers & Bradford was the least. It could be said that, in the case of the models considered in this research, the more complex the model the more accurate the predictions. Of course, none of these models are too complicated to implement, especially if using a spreadsheet analysis.

It would seem that the Oehlers & Bradford shear-friction model is the most robust model of those considered, for design purposes as well as research purposes. The model can be readily adapted to calculate the mean strength of an uncracked and (completely) cracked shear plane, representing the range of possible shear plane conditions.

Nevertheless, it would still be appropriate, for design, to use the conservative and simple ACI model or the PCI model. However, they would not be well suited for research or predictive purposes as they are intentionally designed to model the lower bound shear capacity value. They also do not consider the concrete strength. Even when neglecting the strength reduction factor φ, the models are still very conservative.

Finally, one aspect that all of these models have in common is that they are all based on research, and intended for design, using steel reinforcement. As the primary focus of this

research is to study the use of C-Grid reinforcement, the models are being used beyond their original scope and intent. Despite this, based on the results of this Chapter, the applicability of existing shear-friction models, with minor modification, has been demonstrated. This compatibility provides more evidence that C-Grid is a suitable replacement for WWF, within the range of parameters considered in this research.

CHAPTER 7 CONCLUSIONS

7.1 OVERVIEW

The goal of this research was to determine the longitudinal shear behavior and suitability of Carbon Fiber Grid (C-Grid), as a replacement of Welded Wire Fabric (WWF), to act as reinforcement for cast-in-place toppings of Precast/Prestressed Double Tee (Precast DT) systems.

The investigation focused in large part on the shear-slip behavior of the C-Grid reinforced topping with different parameters such as the reinforcement ratio/stiffness (af_u) and orientation of the C-Grid strands. Also of importance was if the shear-slip response of a C-Grid reinforced topping was similar to that of a WWF reinforced topping. In addition, various longitudinal shear-friction models were modified and analyzed to determine if they could be used to accurately predict or be used to conservatively design for the longitudinal shear capacity. Other parameters considered were construction and placement issues of the C-Grid, namely whether the C-Grid would move excessively during casting and if it would interfere with the cold joint bond between the topping and precast deck.

From the tension tests presented in Chapter 3 it was determined that C-Grid will not excessively deflect from its placed position against the top surface of a precast deck (the flange of the Precast DT), regardless of the size of C-Grid used or the use (if any) of a method to restrain the C-Grid from moving.

With regard to cold joint debonding, the tension tests of Chapter 3 showed a significant deterioration of the bond strength between the two layers of concrete when C-Grid was not chaired and the single-shear tests of Chapter 4 showed this could result in the premature debonding of the two layers of concrete. Chapter 5 derived and implemented two methods for avoiding this. The methods were to either suitably chair the C-Grid 10 mm (0.4 in) above the surface which it is placed against or to instead apply a suitably rough finish to said surface (CSP-8). It was shown that both methods worked, therefore either one can be implemented.

The shear-slip response of C-Grid, as obtained by the single-shear tests of Chapter 4 and Chapter 5, shows a relatively stiff shear-slip response until peak shear capacity and brittle failure of the specimen by shear cracking along the line of shear. Using C-Grid with a higher reinforcement ratio or orienting the C-Grid strands diagonal to the line of shear resulted in modest strength gain but no appreciable ductility was obtained in any specimen, including the WWF specimens.

Chapter 5 also showed that the shear-slip response of C-Grid reinforced specimens to be similar to that of WWF specimens. The shear capacity of the two WWF specimens of this Chapter effectively served as upper and lower bounds to that of the C-Grid specimens, indicating that C-Grid is a suitable reinforcement material with respect to shear capacity.

Finally, Chapter 6 demonstrated that it was possible to, with modification, adapt several shear-friction models originally intended for use with steel reinforcement to be used with C-Grid reinforcement. The ACI and PCI models worked well for design purposes, with the ACI model being the simplest but also very conservative. The Oehlers & Bradford model was the most robust model, allowing for use in a design mode (lower bound, conservative) or for prediction of actual shear capacity by assuming either fully cracked or uncracked initial concrete condition.

The end result of this research is, that with some extra attention to detail, C-Grid is a suitable replacement for WWF as reinforcement of cast-in-place concrete topping of Precast DT systems. It is recommended that, until further research investigates the matter more closely, that premature debonding of the cold joint between the two layers of concrete should be deliberately avoided. The two methods that prevented premature debonding in Chapter 5 can easily be applied to full-scale projects. Recall the two methods consist of chairing of the C-Grid as little as 10 mm (0.4 in) above the surface, accomplished by the affixing of small rubberized chairs as described in Chapter 3, or by finishing the Precast DT element to a surface roughness grade of CSP-8. It is also recommended, as it appears to be standard

practice, to ensure the surface of hardened concrete which is about to have another layer cast on top of it is not excessively dry or wet.

7.2 FURTHER RESEARCH

In order to more accurately understand the effect of premature debonding in precast concrete systems with C-Grid reinforced topping, it would be of interest to construct full scale specimens using two or three (for either single or double shear) typical sized Double Tee precast elements with a full 50 to 75 mm (2 to 3 in) thick concrete topping. It would determine if the effect of premature debonding observed in this research was the result of the use of small-scale specimens, where localized areas of weakness in the cold joint may have exacerbated this observation.

It also would be of interest to conduct a cost-benefit analysis of the use of C-Grid versus the use of WWF as cast-in-place topping reinforcement. This would quantify the money saved both in the short term due to a reduced concrete cover requirement as well as over the long term due to reduced maintenance and repair costs. If it is found in future full scale testing that extra money must be spent to implement one of the two methods outlined in this research to prevent premature debonding at the cold joint interface, then the cost-benefit analysis could also determine which of the two methods would be cheaper to implement.

REFERENCES

ACI 318, 2008, Building Code Requirements for Structural Concrete (318-08), American Concrete Institute, Farmington Hills, MI.

Abu-Tair, A. I., Lavery, D., Nadjai, A., Rigden, S. R., Ahmed, T. M.A. (2000). A New Method for Evaluating the Surface Roughness of Concrete Cut for Repair or Strengthening. *Construction and Building Materials 14*(3), 171-176.

Austin, S., Robins, P., Pan, Y. (1995). Tensile Bond Testing of Concrete Repairs. *Materials and Structures, 28*(179), 249-259.

Chorinsky, E. G.F. (1986). *Repair of Concrete Floors with Polymer Modified Cement Mortars.* Abstatt, W. Germany: Chapman & Hall, 230-234.

Cleland, D. J., & Long, A. E. (1997). The Pull-off Test for Concrete Patch Repairs. *Proceedings of the Institution of Civil Engineers: Structures and Buildings, 122*(4), 451-460.

Emmons, P. H. (1993). *Concrete Repair and Maintenance, Part Three: Surface Repair, Section 6: Bonding Repair Materials to Existing Concrete*. Kingston, MA: R. S. Means Company.

Hofbeck, J. A., Ibrahim, I. O., & Mattock, A. H. (1969). Shear Transfer in Reinforced Concrete. *Journal of the American Concrete Institute, 66*(2), 119-128.

Júlio, E. N.B.S., Branco, F. A.B., & Silva, V. D. (2004). Concrete-to-Concrete Bond Strength. Influence of the Roughness of the Substrate Surface. *Construction and Building Materials, 18*(9), 675-681.

Hindo, K. R. (1990). In-Place Bond Testing and Surface Preparation of Concrete. *Concrete International, 12*(4), 46-48.

ICRI, 1997, Selecting and Specifying concrete surface preparation for sealers, coating, and polymer overlays, Technical guideline No. 03732. International Concrete Repair Institute, Des Plaines, IL.

PCI Design Handbook, 2004, Design Handbook Precast & Prestressed Concrete 6th edition (MNL 120-04), Precast/Prestressed Concrete Institute, Chicago, IL.

Maerz, N. H., Chepur, P., Myers, J., & Linz, J. J. (2001). Concrete Roughness Characterization Using Laser Profilimetry for Fiber-Reinforced Polymer Sheet Application. *Transportation Research Record, 1775*, 132-139.

Matana, M., Galecki, G., Maerz, N. H., Nanni, A. (2005). Concrete Substrate Preparation and Characterization Prior to Adhesion of Externally Bonded Reinforcement. *Proceedings of the International Symposium on Bond Behaviour of FRP in Structures*, International Institute for FRP in Construction, Hong Kong, China, 133-139.

Mattock, A. H. & Hawkins, N. M. (1972). Shear Transfer in Reinforced Concrete – Recent Research. *Journal of the Prestressed Concrete Institute, 17*(2), 55-75.

Mattock, A. H., Johal, L., & Chow, H. C. (1975). Shear Transfer in Reinforced Concrete with Moment or Tension Acting Across the Shear Plane. *Journal of the Prestressed Concrete Institute*, *20*(4), 76-93.

Oehlers, D. J., & Bradford, M. A. (1995). *Composite Steel and Concrete Structural Members*. Kidlington, Oxford, U.K.: Elsevier Science, Ltd.

Oehlers, D. J., & Bradford, M. A. (1999). *Elementary Behaviour of Composite Steel & Concrete Structural Members*. Woburn, MA: Butterworth-Heinemann.

Santos, P. M.D., Júlio, E. N.B.S., & Silva, V. D. (2007). Correlation between concrete-to-concrete bond strength and the roughness of the substrate surface. *Construction & Building Materials, 21*(8), 1688-1695.

Shao, Y. & Mirmiran, A. (2007). Control of Plastic Shrinkage Cracking of Concrete with Carbon Fiber-Reinforced Polymer Grids. *Journal of Materials in Civil Engineering 19*(5), 441-444.

Silfwerbrand, J. (1990). Improving Concrete Bond in Repaired Bridge Decks. *Concrete International, 12*(9), 61-66.

Stuart, A. (2006). Contraction of in-situ concrete toppings. *Concrete (London), 40*(4), 45-46.

Talbot, C., Pigeon, M., Beaupré, D., & Morgan, D. R. (1994). Influence of Surface Preparation on Long-Term Bonding of Shotcrete. *ACI Materials Journal, 91*(6), 560-566.

Wall, J. S., Shrive N. G., & Gamble, B. R (1986). *Testing of Bond Strength Between Fresh and Hardened Concrete*. Calgary, AL: Chapman & Hall, 335-344.

APPENDICES

Appendix A: C-Grid Float Raw Data

Table A-1 C-Grid float

Sample Set	No.†	Final Location 0º, mm	Final Location 90º, mm	Final Location 180º, mm	Final Location 270º, mm	Final Location Specimen Avg., mm	Final Location Sample Avg., mm	Initial Height, mm	Specimen Float, mm	Sample Float Avg., mm
2.9x2.9 WC	A1	7.5	10	9	8	8.625	12.25	25	- 16.375	- 12.75
2.9x2.9 WC	A2	8	7.5	17.5	22	13.75		25	- 11.25	
2.9x2.9 WC	A3	16	11	10	20.5	14.375		25	- 10.625	
3.5x4.0 FC	A4	17	29	21	7.5	18.625	9.17 4.44*	10	8.625	- 0.83 - 5.56*
3.5x4.0 FC	A5	3	3.5	7.5	7.5	5.375		10	- 4.625*	
3.5x4.0 FC	A6	5	2	4	3	3.5		10	- 6.5	
3.5x4.0 RC	A7	4	3	3	4.5	3.625	4.25	10	-6.375	- 5.75
3.5x4.0 RC	A8	6	9	5	3	5.75		10	- 4.25	
3.5x4.0 RC	A9	3.5	3	4	3	3.375		10	- 6.625	
2.9x2.9 HG	A10	1	1	2.5	0.5	1.25	1.38	0	1.25	1.38
2.9x2.9 HG	A11	2	1.5	1.5	1	1.5		0	1.5	
2.9x2.9 HG	A12	1	2	1.5	1	1.375		0	1.375	
3.5x4.0 HG	A13	3	2	5.5	6	4.125	4.21	0	4.125	4.21
3.5x4.0 HG	A14	4	3	2.5	4	3.375		0	3.375	
3.5x4.0 HG	A15	4	6	7	3.5	5.125		0	5.125	

* Calculation excluded specimen A4 from average.

† Specimens A16 - A21 are omitted, they are control specimens with no C-Grid.

Table A-1 Continued

Sample Set	No.†	Final Location 0º, mm	Final Location 90º, mm	Final Location 180º, mm	Final Location 270º, mm	Final Location Specimen Avg., mm	Final Location Sample Avg., mm	Initial Height, mm	Specimen Float, mm	Sample Float Avg., mm
1.6x1.8 NR	A22	3	3	2	2	2.5	3.08	0	2.5	3.08
1.6x1.8 NR	A23	3	3	1.5	1.5	2.25		0	2.25	
1.6x1.8 NR	A24	4	4	4	6	4.5		0	4.5	
2.2x2.2 NR	A25	4	5	4	5.5	4.625	5.08	0	4.625	5.08
2.2x2.2 NR	A26	4	6	6.5	4.5	5.25		0	5.25	
2.2x2.2 NR	A27	5	7.5	4	5	5.375		0	5.375	
2.9x2.9 NR	A28	6.5	4.5	5	5.5	5.375	4.54	0	5.375	4.54
2.9x2.9 NR	A29	4	6.5	5	4	4.875		0	4.875	
2.9x2.9 NR	A30	4	4	1.5	4	3.375		0	3.375	
3.5x4.0 NR	A31	2	2	1.5	2	1.875	1.50	0	1.875	1.50
3.5x4.0 NR	A32	2	0.5	1	1	1.125		0	1.125	
3.5x4.0 NR	A33	2	1	2	1	1.5		0	1.5	
1.6x1.8 HG	A34	2.5	2.5	3.5	4	3.125	2.92	0	3.125	2.92
1.6x1.8 HG	A35	3	1.5	3	3	2.625		0	2.625	
1.6x1.8 HG	A36	2	3	3.5	3.5	3		0	3	
2.2x2.2 HG	A37	1	2	2	2	1.75	1.96	0	1.75	1.96
2.2x2.2 HG	A38	1.5	1.5	2	3	2		0	2	
2.2x2.2 HG	A39	2	3	2	1.5	2.125		0	2.125	

† Specimens A16 - A21 are omitted, they are control specimens with no C-Grid.

Appendix B: Tension Test Raw Data

Table B-1 Tension test data

Specimen Set†	No.	Max Load (lb)	Max Stress (psi)	Avg. Stress (psi)	Avg. as % of control stress
2.9x2.9 WC	A2	4628	163.68	181.53	73.1%
2.9x2.9 WC	A3	5637	199.37		
3.5x4.0 FC	A4	4308	152.36	169.86	68.4%
3.5x4.0 FC	A5	4016	142.04		
3.5x4.0 FC	A6	6084	215.18		
3.5x4.0 RC	A7	8767	310.07	229.75	92.5%
3.5x4.0 RC	A8	6228	220.27		
3.5x4.0 RC	A9	4493	158.91		
3.5x4.0 HG	A10	2141	75.72	106.61	42.9%
3.5x4.0 HG	A11	5252	185.75		
3.5x4.0 HG	A12	1650	58.36		
2.9x2.9 HG	A13	7122	251.89	167.65	67.5%
2.9x2.9 HG	A14	3479	123.04		
2.9x2.9 HG	A15	3620	128.03		
none (ctrl)	A16	7157	253.13	248.49	100.0%
none (ctrl)	A17	5855	207.08		
none (ctrl)	A18	8996	318.17		
none (ctrl)	A21	6096	215.60		

Specimen Set	No.	Max Load (lb)	Max Stress (psi)	Avg. Stress (psi)	Avg. as % of control stress
1.6x1.8 NR	A22	3089	109.25	80.70	32.5%
1.6x1.8 NR	A23	1056	37.35		
1.6x1.8 NR	A24	2700	95.49		
2.2x2.2 NR	A25	5229	184.94	119.07	47.9%
2.2x2.2 NR	A26	2555	90.36		
2.2x2.2 NR	A27	2316	81.91		
2.9x2.9 NR	A28	2797	98.92	126.49	50.9%
2.9x2.9 NR	A29	3867	136.77		
2.9x2.9 NR	A30	4065	143.77		
3.5x4.0 NR	A31	3137	110.95	103.96	41.8%
3.5x4.0 NR	A32	2720	96.20		
3.5x4.0 NR	A33	2961	104.72		
1.6x1.8 HG	A34	4653	164.57	171.91	69.2%
1.6x1.8 HG	A35	5073	179.42		
1.6x1.8 HG	A36	4856	171.75		
2.2x2.2 HG	A37	3711	131.25	131.07	52.7%
2.2x2.2 HG	A38	3848	136.10		
2.2x2.2 HG	A39	3559	125.87		

† Specimens A1, A19, and A20 are omitted as they were not tested.

Appendix C: Concrete Compressive Strength

For this research, whenever concrete was cast - either for the slabs from which the tensile test series (specimens A1-A39) were cored (Slabs 1 and 2) or for the two series of single-shear tests (specimens B1-B10 and specimens B11-B22) - standard compressive cylinders were cast alongside and kept in the same environmental conditions as that of the specimens (field curing). When a particular series of tests were conducted, three cylinders were tested before the start of the tests. When the tests were completed, three more cylinders were tested. This was deemed sufficient since the single-shear series of tests each only took no more than two months to finish. However, the tension test series took considerably longer to compete (four months); therefore, three cylinders were tested when this test series was halfway completed. One will notice that the values for the end of the tension test series of tests are equal to the start of the first single-shear test series; which is due to the fact they were started after the tension test series was finished.

The cylinders were all tested in a Forney testing machine and loaded at an ASTM C39 standard load rate of 35 ± 7 psi/s (0.25 ± 0.05 MPa/s), see Figure C-1. The results of all of the cylinder tests are summarized in Table C-1. The values for the compressive strength of the concrete (f_c') from the top layer of concrete were used when considering the shear strength since the bottom layer of concrete did not resist any shear.

(a) Specimen setup (b) Typical failure

Figure C-1 Testing of compressive cylinders

Table C-1 Concrete compressive strength

Specimens:	A1-A39	A1-A39	B1-B10	B1-B10	B11-B22	B11-B22
Concrete Layer:	Bottom	Top	Bottom	Top	Bottom	Top
Start of Tests:						
Cylinder 1 (lb)	86575	56718	100345	47668	28783	34183
Cylinder 2 (lb)	91099	40460	88413	57509	30112	27143*
Cylinder 3 (lb)	96556	51515	88159	48971	26634	37633
Middle of Tests:						
Cylinder 4 (lb)	92541	49847				
Cylinder 5 (lb)	91863	53777				
Cylinder 6 (lb)	91655	53099				
End of Tests:						
Cylinder 7 (lb)	100345	47668	92287	44475	31384	37322
Cylinder 8 (lb)	88413	57509	96302	45012	28107	38453
Cylinder 9 (lb)	88159	48971	91806	46596	30649	39697
Average (lb):	91912	51063	92885	48372	29278	37458
f_c' (psi):	7312	4062	7389	3848	2329	2980
f_c' (MPa)	50.41	28.01	50.95	26.53	16.06	20.55
Variance (%):	4.7%	10.2%	5.1%	9.9%	6.0%	5.5%

* Excluded

Appendix D: Carbon Fiber Grid Tensile Strength

For the Carbon Fiber Grid (C-Grid), it is necessary to determine the rupture strength of the individual strands that make up C-Grid. The rupture load values are necessary in order to calculate the reinforcement stiffness af_u (see Section 6.1).

In order to do this, six strands of C-Grid were cut from the same batch of C-Grid used in the single-shear tests of Chapter 4 and Chapter 5. In order to properly test the C-Grid strands it was necessary to build up the ends of the strands so that, when the machine gripped the specimens, they would not break prematurely at the ends. Tabs were built up on each side of each end of the C-Grid strand using two strips of glass fiber cloth that were cut to approximately 50 by 100 mm (2 by 4 in). The process of constructing the C-Grid coupons is illustrated from left to right in Figure D-1. Weight was then placed on top of the tabs and they were allowed to cure for 72 hours before testing.

After that time, the resulting C-Grid coupons were loaded in direct tension in a Q-Test machine at the ASTM D3039 standard rate of 1.25 millimeter per minute (0.05 inches per minute). A data acquisition computer recorded the load from the machine's load cell. See Figure D-2 for an illustration of a typical coupon test setup and failure.

Due to the fact that the cross-sectional area of C-Grid strands cannot be measured with sufficient accuracy as a result of the manufacturing method of the C-Grid, only the rupture load, not stress, can be recorded. Also, since Carbon Fibers by their nature do not yield, (that is, they are linear-elastic until sudden rupture) there is no yield strength of the material.

There was some concern that the values for rupture strength might vary depending on which direction the C-Grid strands were cut from (longitudinal or transverse). Of the six specimens cut, the first three (a-c) were cut from the longitudinal direction and the last three (d-f) were cut from the transverse direction. It was found that those C-Grids which were square (having an equal spacing of strands in both directions) had no appreciable difference in strength between the two directions. This is contrary to the rectangular C-Grids (having a

more dense spacing in the transverse direction than the longitudinal) in which the strands in the "strong" (named because the closer spacing results in more strands per unit length) direction were considerably weaker than that in the "weak" direction.

The results of these tensile tests are presented in Table D-1. In addition to calculating the rupture load the term af_u, as described in Section 6.1, is calculated for each set of specimens. Since this calculation requires knowing the number of strands per unit length, that is also determined in Table D-1 based off the number of strands in the line of shear from Table 4-1 and Table 5-1.

Finally, note that for C-Grids oriented diagonally, a separate calculation of af_u is performed. Orienting the C-Grids diagonally places more strands over the shear line (and subsequently per unit length). Furthermore, because the orientation of the strands is ±45º from the perpendicular of the line of shear the rupture tensile load must be multiplied by 0.707 (sin 45 º). This results in a different value of af_u for diagonally oriented C-Grid. Since the diagonally oriented strands will contribute to the passive internal shear-friction resistance whether they are at a +45º or -45º angle, both are counted in the Strands Crossing Shear Line column, (see discussion of shear-friction in Section 2.5) as was done in Table 4-1 and Table 5-1.

With this in mind, for the C-Grids that had a diagonal orientation within the experimental program of this research, af_u is recalculated in a separate section of columns. Note that there is not much difference between the diagonal and perpendicular values, the diagonals being only 6.1% larger.

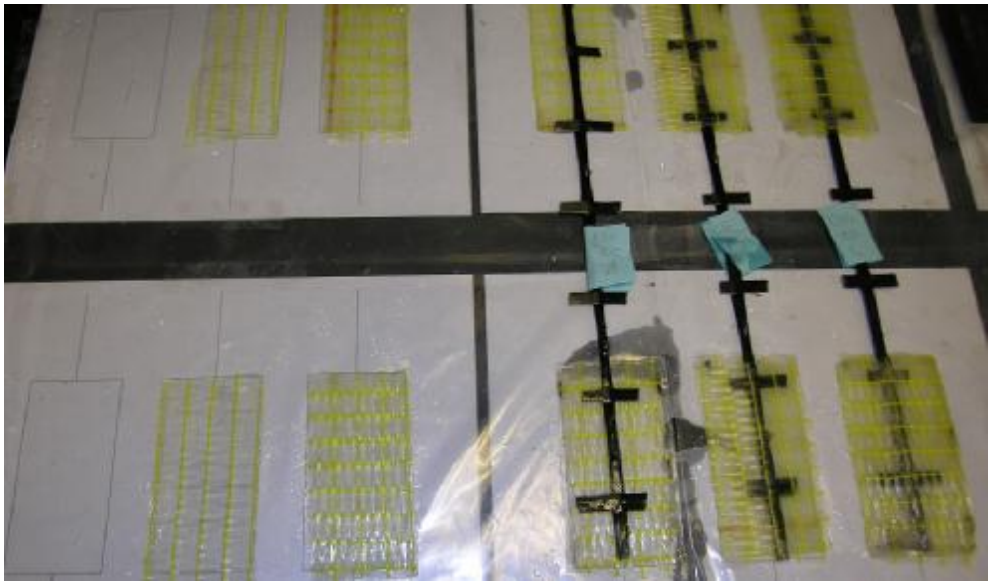

Figure D-1 Preparation of C-Grid coupons

(a) Specimen setup

(b) Typical failure

Figure D-2 Testing of C-Grid coupons

Table D-1 C-Grid strengths

Specimen	Strand Orientation	Rupture Load (lb)	Strands Crossing Shear Line	Strands per unit Length, (ft^{-1})	af_u, (kip/ft) [kN/m]
C50 1.6x1.8 a	Strong	949			
C50 1.6x1.8 b	Strong	895			
C50 1.6x1.8 c	Strong	1034			
C50 1.6x1.8 d	Weak	1574			
C50 1.6x1.8 e	Weak	1457			
C50 1.6x1.8 f	Weak	1323			
C50 1.6x1.8 Average:	Strong	959	11	7.333	7.04 [102.7]
C50 1.6x1.8 Average:	Weak	1451	10	6.667	9.67 [141.1]
C50 2.2x2.2 a	Transverse	875			
C50 2.2x2.2 b	Transverse	923			
C50 2.2x2.2 c	Transverse	858			
C50 2.2x2.2 d	Longitudinal	1035			
C50 2.2x2.2 e	Longitudinal	954			
C50 2.2x2.2 f	Longitudinal	946			
C50 2.2x2.2 Average	Perpendicular	932	8	5.333	4.96 [72.4]
C50 2.2x2.2 Average	Diagonal	932	12	8	5.26 [76.8]
C50 2.9x2.9 a	Transverse	946			
C50 2.9x2.9 b	Transverse	857			
C50 2.9x2.9 c	Transverse	868			
C50 2.9x2.9 d	Longitudinal	966			
C50 2.9x2.9 e	Longitudinal	799			
C50 2.9x2.9 f	Longitudinal	1126			

Table D-1 Continued

Specimen	Strand Orientation	Rupture Load (lb)	Strands Crossing Shear Line	Strands per unit Length, (ft^{-1})	af_u, (kip/ft) [kN/m]
C50 2.9x2.9 Average	Perpendicular	927	6	4	3.72 [54.3]
C50 2.9x2.9 Average	Diagonal	927	9	6	3.95 [57.6]
C50 3.5x4.0 a	Strong	840			
C50 3.5x4.0 b	Strong	1025			
C50 3.5x4.0 c	Strong	1054			
C50 3.5x4.0 d	Weak	1330			
C50 3.5x4.0 e	Weak	1276			
C50 3.5x4.0 f †	Weak				
C50 3.5x4.0 Average:	Strong	973	5	3.333	3.23 [47.2]
C50 3.5x4.0 Average:	Weak	1303	4	2.667	3.47 [50.6]
C150 2.4 a	Transverse	875			
C150 2.4 b	Transverse	923			
C150 2.4 c	Transverse	858			
C150 2.4 d	Transverse	1035			
C150 2.4 e	Transverse	954			
C150 2.4 f	Transverse	946			
C150 2.4 Average	Perpendicular	932	7	4.667	13.91 [203.0]

† Excluded as it was damaged before testing.

Appendix E: Welded Wire Fabric Tensile Strength

For the welded wire fabric (WWF), it was deemed necessary to have an accurate yield stress of the wires composing the fabric. In order to do this, six coupons were cut from the same source as was used for reinforcement in the shear tests conducted in this research. The coupons were fourteen inches long and were loaded in direct tension in a Q-Test machine at a rate of 1.25 millimeters per minute (0.05 inches per minute), which is within the range of load rates allowed by ASTM A370. It is also the same loading rate specified for the C-Grid (see Appendix D). A data acquisition computer recorded the load from the machine's load cell and the strain was determined from an attached extensionometer.

It was found that the WWF specimens could be placed within the machine directly without any preparation with regard to the ends gripped in the machine. The specimens typically failed at or near at the location of a weld (connecting it to a perpendicular wire) or near the middle of the wire.

The ultimate stress of each specimen was determined by taking the maximum load recorded and dividing by the average measured cross-sectional area of each specimen. The yield stress was determined from the stress-strain curves of each specimen, in which a line with a slope equal to that of the stress-strain curve in the elastic region is drawn from a strain of 0.002 (at zero load) until it intersects the actual stress strain curve. This intersection is observed visually and is considered the yield stress of the specimen. This "0.2% offset rule" was used because there was no clear yield plateau; see Figure E-2 for an illustration.

In order to calculate the reinforcement stiffness af_u as described in Section 6.1, the cross-sectional area (in^2) of an individual strand is multiplied by the number of strands per unit length (ft^{-1}), giving a; and then multiplying by the yield stress f_y (ksi) giving the quantity af_u in kip/ft. The number of stands per unit length is found by taking the number of wires crossing the 1½ ft shear line (from Table 5-1) and dividing by the length of the shear line. Finally, af_u can be converted to kN/m by multiplying by 14.5939 (1 kip/ft = 14.5939 kN/m). The results are presented in Table E-1.

(a) Specimen setup

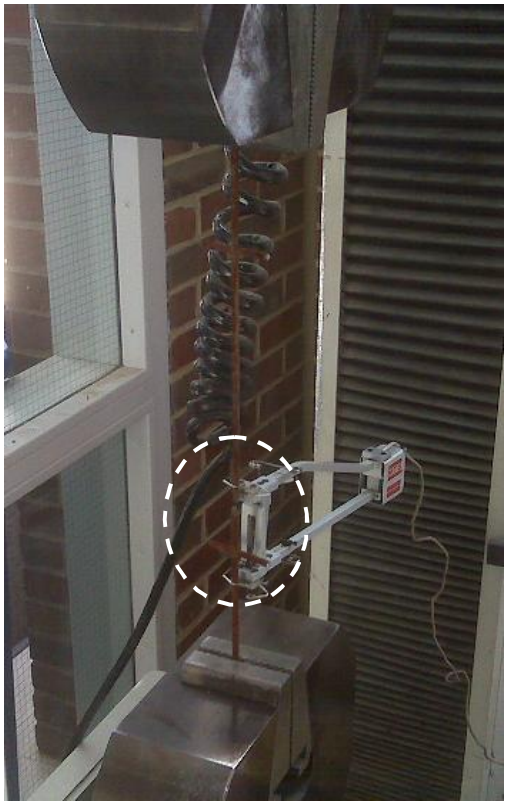

(b) Typical failure

Figure E-1 Testing of WWF coupons

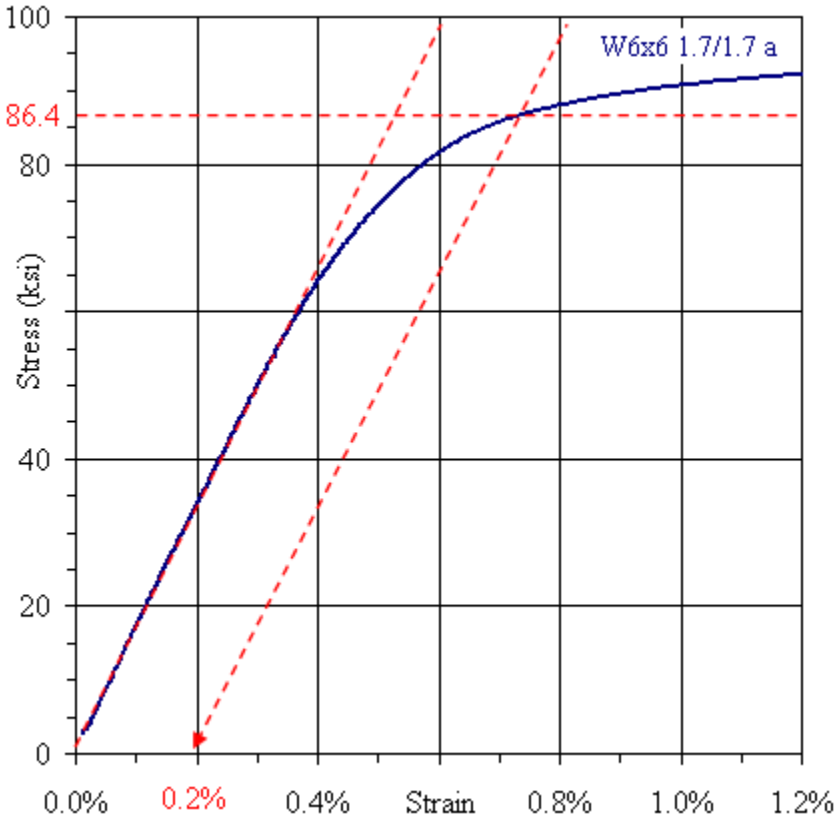

Figure E-2 Typical stress-strain response and yield stress

Table E-1 WWF strengths

Specimen:	Cross-Sectional Area (in^2)	Ultimate Load (kip)	Yield Load (kip)†	Yield Stress f_y (ksi)	Wires Crossing the Shear Line	Number of Wires per Unit Length (ft^{-1})	Area per unit length, a (in^2/ft)	af_u (kip/ft) [kN/m]
W6x6 1.7/1.7 a	0.016	1.46	1.34	86.4				
W6x6 1.7/1.7 b	0.015	1.38	1.30	84.8				
W6x6 1.7/1.7 c	0.015	1.40	1.32	87.0				
W6x6 1.7/1.7 d	0.015	1.36	1.31	89.2				
W6x6 1.7/1.7 e	0.015	1.41	1.34	89.5				
W6x6 1.7/1.7 f	0.015	1.39	1.29	87.8				
W6x6 1.7x1.7 average:	0.015	1.40	1.32	87.5	3	2	0.030	2.64 [38.5]
W6x6 4.0/4.0 a	0.042	3.90	3.73	89.3				
W6x6 4.0/4.0 b	0.041	3.66	3.55	85.7				
W6x6 4.0/4.0 c	0.041	3.76	3.71	89.9				
W6x6 4.0/4.0 d	0.042	3.73	3.66	87.9				
W6x6 4.0/4.0 e	0.041	3.22	3.22	78.2				
W6x6 4.0/4.0 f	0.040	3.13	3.09	77.6				
W6x6 4.0x4.0 average:	0.041	3.57	3.49	84.7	3	2	0.082	7.14 [104.2]

† From 0.2% offset rule

Appendix F: Calculation of Difference between Measured and Predicted Shear Flow

This Appendix calculates the difference between the measured shear flow capacity q and the predicted shear flow of each of the three shear-friction models discussed in Chapter 6. For a given model, it is first necessary to – for each specimen considered in that Chapter – compute the predicted q. These are presented in Table F-1.

For a given model, Table F-2 then calculates the percentage difference between the measured and predicted values by the means of the following equation:

$$\text{difference } (\%) = \left(\frac{q_{\text{measured}} - q_{\text{predicted}}}{q_{\text{actual}}} \right) \times 100 \qquad \text{[F-1]}$$

This results in values that are negative when the model is over-predicting the strength and positive when it is under-predicting the actual strength (i.e. conservative). Therefore, this can be thought of as a "Percent Under-Prediction". In addition, Table F-2 calculates the Average Under-Prediction for an individual model using each specimen, with the exception of the outlier specimens B3 and B22 (as discussed in Section 6.3.1). The Most Conservative and Least Conservative value is also tabulated which is, for each individual model, the highest and lowest under-prediction made (again, excluding the outliers). If a particular model did not over-predict the strength of any specimen, then both of these quantities will be positive.

Table F-1 Calculated shear capacities

Specimen	$q_{measured}$	$q_{predicted}$									
	Table 6-1 (kN/m)	ACI (6.2.1)		PCI (6.2.2)		Parabolic O&B (6.2.3)			Simplified O&B (6.2.3)		
		φ=0.65 (kN/m)	φ=1.0 (kN/m)	φ=0.75 (kN/m)	φ=1.0 (kN/m)	Γ=0.66 (kN/m)	Γ=1.1 (kN/m)	Γ=1.6 (kN/m)	Γ=0.66 (kN/m)	Γ=1.1 (kN/m)	Γ=1.6 (kN/m)
B3	172.9	47.7	73.4	142.4	164.4	177.1	240.5	312.4	177.1	240.5	312.4
B6	215.6	25.2	38.8	86.5	115.4	121.0	172.7	231.4	97.7	133.9	175.1
B7	253.8	21.9	33.7	75.2	100.3	108.7	156.0	209.7	85.0	116.4	152.2
B8	212.4	23.5	36.1	80.6	107.5	114.7	164.2	220.4	91.1	124.8	163.1
B9	253	35.7	54.9	122.4	163.2	152.9	213.9	283.2	138.2	189.4	247.6
B10	237.2	26.7	41.1	91.8	122.4	126.4	179.9	240.6	103.7	142.1	185.7
B14	231.6	47.7	73.4	142.4	164.4	165.7	221.5	284.8	165.7	221.5	284.8
B15	216.3	33.6	51.7	115.4	153.9	140.0	194.7	256.9	130.3	178.6	233.4
B17	157.6	17.9	27.5	61.4	81.8	90.1	129.6	174.5	69.3	95.0	124.1
B18	254.9	48.4	74.4	143.4	165.6	166.9	222.7	286.0	166.9	222.7	286.0
B19	102.7	47.7	213.8	142.4	164.4	165.7	221.5	284.8	165.7	221.5	284.8
B20	72.4	33.6	166	115.4	153.9	140.0	194.7	256.9	130.3	178.6	233.4
B21	76.8	35.7	178.7	122.4	163.2	144.5	199.8	262.7	138.2	189.4	247.6
B22	203	94.3	243.3	200.2	231.2	246.0	301.7	365.0	246.0	301.7	365.0

Table F-2 Tabulation of Under-Prediction for each single-shear specimen

Specimen	ACI (6.2.1)		PCI (6.2.2)		Parabolic O&B (6.2.3)			Simple O&B (6.2.3)		
	φ=0.65	φ=1.0	φ=0.75	φ=1.0	Γ=0.66	Γ=1.1	Γ=1.6	Γ=0.66	Γ=1.1	Γ=1.6
B3	72.4 %	57.6 %	17.6 %	4.9 %	-2.5 %	-39.1 %	-80.7 %	-2.5 %	-39.1 %	-80.7 %
B6	88.3 %	82.0 %	59.9 %	46.5 %	43.9 %	19.9 %	-7.3 %	54.7 %	37.9 %	18.8 %
B7	91.4 %	86.7 %	70.4 %	60.5 %	57.2 %	38.5 %	17.4 %	66.5 %	54.1 %	40.0 %
B8	88.9 %	83.0 %	62.0 %	49.4 %	46.0 %	22.7 %	-3.8 %	57.1 %	41.2 %	23.2 %
B9	85.9 %	78.3 %	51.6 %	35.5 %	39.5 %	15.4 %	-11.9 %	45.4 %	25.1 %	2.1 %
B10	88.7 %	82.7 %	61.3 %	48.4 %	46.7 %	24.2 %	-1.5 %	56.3 %	40.1 %	21.7 %
B14	79.4 %	68.3 %	38.5 %	29.0 %	28.4 %	4.4 %	-23.0 %	28.4 %	4.4 %	-23.0 %
B15	84.5 %	76.1 %	46.7 %	28.9 %	35.3 %	10.0 %	-18.8 %	39.8 %	17.4 %	-7.9 %
B17	88.7 %	82.6 %	61.1 %	48.1 %	42.9 %	17.8 %	-10.7 %	56.0 %	39.7 %	21.2 %
B18	81.0 %	70.8 %	43.7 %	35.0 %	34.5 %	12.6 %	-12.2 %	34.5 %	12.6 %	-12.2 %
B19	77.7 %	65.7 %	33.4 %	23.1 %	22.5 %	-3.6 %	-33.2 %	22.5 %	-3.6 %	-33.2 %
B20	79.8 %	68.8 %	30.5 %	7.3 %	15.7 %	-17.3 %	-54.8 %	21.5 %	-7.6 %	-40.6 %
B21	80.0 %	69.3 %	31.5 %	8.7 %	19.2 %	-11.8 %	-47.0 %	22.6 %	-6.0 %	-38.6 %
B22	61.3 %	40.4 %	17.7 %	5.0 %	-1.1 %	-24.0 %	-50.0 %	-1.1 %	-24.0 %	-50.0 %
Average Under-Prediction:	84.5 %	76.2 %	49.2 %	35.0 %	36.0 %	11.1 %	-17.2 %	42.1 %	21.3 %	-2.40 %
Least Conservative:	77.7 %	65.7 %	30.5 %	7.30 %	15.7 %	-17.3 %	-54.8 %	21.5 %	-7.60 %	-40.6 %
Most Conservative:	91.4 %	86.7 %	70.4 %	60.5 %	57.2 %	38.5 %	17.4 %	66.5 %	54.1 %	40.0 %